

QC852
.C6
no. 435
ATSL

**SURFACE PRESSURE FEATURES
ASSOCIATED WITH A MIDLATITUDE
MESOSCALE CONVECTIVE SYSTEM
IN OK PRE-STORM**

LIBRARIES
JAN 13 1989
COLORADO STATE UNIVERSITY

GREGORY J. STUMPF

**Colorado
State
University**

**DEPARTMENT OF
ATMOSPHERIC SCIENCE**

PAPER NO.

435

**SURFACE PRESSURE FEATURES ASSOCIATED WITH A MIDLATITUDE
MESOSCALE CONVECTIVE SYSTEM IN OK PRE-STORM**

by

Gregory J. Stumpf

Department of Atmospheric Science
Colorado State University
Fort Collins, CO 80523

This research was supported by the National Science Foundation
under Grant No. ATM-8711649

Atmospheric Science Paper No. 435

December 1988

QC859
.C6
no. 435
ATSL

ABSTRACT

SURFACE PRESSURE FEATURES ASSOCIATED WITH A MIDLATITUDE MESOSCALE CONVECTIVE SYSTEM IN O.K. PRE-STORM

A midlatitude mesoscale convective system (MCS) passed through the domain of the Oklahoma-Kansas Preliminary Regional Experiment for STORM-Central (OK PRE-STORM) during the period 3-4 June 1985. Radar and satellite data are presented to provide an overview of the life cycle of the MCS. Observations from the OK PRE-STORM mesonet network are used to document the surface pressure features associated with this MCS. Also, upper air sounding data, wind profiler data, and dual-Doppler data are presented to detail the upper level structure of this MCS.

The MCS initially developed as a random pattern of convection. As the MCS matured, it developed a surface precipitation structure resembling an occluded wave cyclone but on a much smaller scale. The southern part of the system was comprised of a north-south intense convective line while the northern part contained significant stratiform rain. Finally, after a few hours of maturity, the MCS began to dissipate leaving behind a slowly decaying stratiform anvil.

During the mature phase of the MCS, a broad surface mesohigh was observed over the northern stratiform rain area. At the rear edge of this rain area was an intense surface wake low. Local pressure gradients between the wake low and the mesohigh were as strong as 2 mb per 10 km. A strong wake low was not observed following the southern portion of the MCS.

The upper level storm structure revealed a complex relative flow pattern. A stratiform anvil was observed north and northeast of the southern convective line. A small portion

of the stratiform anvil trailed the northern rain area. The southern part of the MCS was devoid of a trailing stratiform rain region.

The absence of a trailing stratiform rain region and surface wake low in the southern part of the MCS suggest that mesoscale circulations within and below the stratiform anvil in the northern segment were important in producing a surface wake low there.

Gregory J. Stumpf
Department of Atmospheric Science
Colorado State University
Fort Collins, Colorado 80523

ACKNOWLEDGEMENTS

The author expresses his gratitude to adviser Dr. Richard Johnson for his endless guidance and thoughtful criticism of the research. Committee members Wayne Schubert and V. Bringi also offered their comments and suggestions.

Dr. Bradley Smull of the Mesoscale Research Division of the National Severe Storms Laboratory (NSSL) in Boulder Colorado prepared the Doppler data used in the paper. José Meitín of the Mesoscale Research Division of NSSL provided the radar composites and some sounding data.

Much appreciation is given to Dr. James Toth of the Naval Environmental Prediction Research Facility in Monterey California for his assistance with computer programming and data retrieval. Michael Fortune assisted in obtaining wind profiler plots, and additional radar data was provided by Ray McAnelly. Thanks also go to Paul Hamilton, William Gallus, Michael Vescio, and Sue Chen for their assistance.

The final manuscript was prepared by Gail Cordova. This research was supported by the National Science Foundation Grant No. ATM-8711649.

TABLE OF CONTENTS

1 INTRODUCTION	1
2 BACKGROUND	3
2.1 Observations of mesohighs and mesolows	3
2.2 MCS wake structure observations	8
3 THE DATA SET	12
3.1 PRE-STORM	12
3.2 Data used for the analyses	14
3.2.1 Surface data	14
3.2.2 Upper air data	17
3.2.3 Radar and satellite data	17
4 SYNOPTIC OVERVIEW	19
4.1 Initial synoptic conditions and MCS1	19
4.2 Radar and satellite overview	28
5 THREE-DIMENSIONAL MESOSCALE STRUCTURE OF THE STORM AND ITS ENVIRONMENT: COMPARISON WITH LINEAR MESOSCALE CONVECTIVE SYSTEMS	43
5.1 Surface observations	43
5.1.1 Pressure and wind analyses	44
5.1.2 Time series of surface pressure	60
5.1.3 Rainfall characteristics	64
5.2 Horizontal upper air analyses	69
6 STORM CIRCULATION CHARACTERISTICS LEADING TO OB- SERVED PRESSURE FEATURES	93
6.1 Vertical flow structure along the plane of motion	93
6.2 Internal flow structure of the mature MCS	113
6.3 Variations between wake low and mesohigh structure and north-south varia- tions in wake low structure	121
7 SUMMARY	125
REFERENCES	130
APPENDIX A	136
APPENDIX B	138
APPENDIX C	144

LIST OF FIGURES

2.1	Schematic of surface pressure, wind field, and precipitation during the mature stage of a squall line with a trailing stratiform rain region (after Johnson and Hamilton, 1988).	7
2.2	Schematic cross section of stratiform anvil region in a squall line (after Johnson and Hamilton, 1988).	9
3.1	The O K PRE-STORM observational mesonetnetwork (after Cuning, 1986).	13
3.2	The PRE-STORM Portable Automated Mesonetnetwork (PAM) and Surface Automated Mesonetnetwork (SAM) surface array.	15
3.3	National Weather Service (NWS) Standard Aviation Observation (SAO) sites.	16
3.4	The PRE-STORM upper air mesonetnetwork.	18
4.1	Tracks of the three MCSs which occurred in the 3-4 June 1985 period (adapted from Hamilton and Johnson, 1987).	20
4.2	Surface mesoanalysis at 1200 GMT 3 June 1985.	21
4.3	Surface PAM/SAM mesoanalysis at 1100 GMT 3 June 1985.	22
4.4	1200 GMT 3 June 1985 NMC upper air analyses: a) 850 mb; b) 700 mb; c) 500 mb; d) 500 mb; e) 300 mb; f) 200 mb.	24
4.4	Continued.	25
4.4	Continued.	26
4.5	1300 GMT 3 June 1985 infrared (IR) satellite image.	27
4.6	0900 GMT 3 June 1985 Dodge City KS (DDC) vertical sounding of temperature, dewpoint, and actual winds.	29
4.7	Same as Fig. 4.5 except for 1600 GMT 3 June 1985.	30
4.8	Same as Fig. 4.2 except for 1800 GMT 3 June 1985.	31
4.9	Same as Fig. 4.5 except for: a) 1900 GMT 3 June 1985, b) 2000 GMT 3 June 1985, c) 2100 GMT 3 June 1985, d) 2200 GMT 3 June 1985, e) 2300 GMT 3 June 1985, f) 0000 GMT 4 June 1985, g) 0100 GMT 4 June 1985, h) 0200 GMT 4 June 1985, i) 0300 GMT 4 June 1985, j) 0400 GMT 4 June 1985.	32
4.9	Continued.	33
4.9	Continued.	34
4.9	Continued.	35
4.10	Radar composites of RADAP-II digitized data.	37
4.10	Continued.	38
4.10	Continued.	39
4.10	Continued.	40
4.11	Same as Fig. 4.2 except for 0000 GMT 4 June 1985.	41
5.1	Surface analysis of: a) adjusted pressure; and b) streamlines, at 2000 GMT 3 June 1985 for PAM and SAM.	45

5.2	Same as 5.1 except for 2100 GMT 3 June 1985.	47
5.3	Same as 5.1 except for 2200 GMT 3 June 1985.	49
5.4	Same as 5.1 except for 2300 GMT 3 June 1985.	51
5.5	Same as 5.1 except for 0020 GMT 4 June 1985.	53
5.6	Same as 5.1 except for 0120 GMT 4 June 1985.	55
5.7	Time series plot of adjusted pressure for station P12.	56
5.8	Same as 5.1 except for 0150 GMT 4 June 1985.	58
5.9	Same as 5.1 except for 0300 GMT 4 June 1985.	59
5.10	Time series plots of adjusted pressure for each mesonetstation (base figure is Fig. 5.7).	61
5.11	Isochrones of the mesohigh axis.	62
5.12	Same as 5.11 except for pre-squall mesolow.	65
5.13	Same as 5.11 except for wake low.	66
5.14	Total rainfall measured during MCS2 passage in mm.	67
5.15	Same as 5.7 except for rainfall in mm: a) station P41; b) station P21.	70
5.16	Isochrones of axis of mesohigh (solid line), rear edge of stratiform rain (dashed line), and axis of maximum stratiform rain rate (dotted line).	72
5.17	Mesoanalysis of storm-relative winds for 700 mb at 2100 GMT 3 June 1985.	74
5.18	Same as 5.17 except for 500 mb at 2100 GMT 3 June 1985.	75
5.19	Liberal KS profiler time series.	76
5.20	Same as 5.17 except for 300 mb at 2100 GMT 3 June 1985.	77
5.21	Thermodynamic profiles at 2100 GMT.	78
5.22	a) Same as 5.17 except for 700 mb at 0000 GMT 4 June 1985; b) Mesoanalysis of geopotential height, temperature, and actual winds for 700 mb at 0000 GMT 4 June 1985.	80
5.22	Continued.	81
5.23	Same as 5.22 except for 500 mb at 0000 GMT 4 June 1985.	82
5.23	Continued.	84
5.24	Same as 5.17 except for 300 mb at 0000 GMT 4 June 1985.	85
5.25	a) Same as 5.17 except for 700 mb at 0130 GMT 4 June 1985; b) Relative humidity in % for 700 mb at 0130 GMT 4 June 1985.	86
5.25	Continued.	88
5.26	Same as 5.17 except for 500 mb at 0130 GMT 4 June 1985.	89
5.27	Same as 5.17 except for 700 mb at 0300 GMT 4 June 1985.	90
5.28	Same as 5.17 except for 500 mb at 0300 GMT 4 June 1985.	91
6.1	Time-height vertical cross section at Russell KS (RSL): a) storm-relative winds; b) relative humidity.	95
6.1	Continued.	97
6.2	Same as 6.1 except for Wichita KS (IAB).	99
6.2	Continued.	100
6.3	Same as 6.1 except for Pratt KS (PTT).	101
6.3	Continued.	103
6.4	Thermodynamic profile at 0130 GMT 4 June 1985 for Pratt KS (PTT).	104
6.5	Same as 6.1a except for Enid OK (END).	105
6.6	Same as 5.19 except for McPherson KS.	107

6.7	Time-height vertical cross section of potential temperature at: a) Russell KS (RSL); b) Enid OK (END).	108
6.7	Continued.	109
6.8	Time height vertical cross section of geopotential height perturbation for: a) Russell KS (RSL); b) Enid OK (END).	111
6.8	Continued.	112
6.9	SW and NE analysis domains of the CP3 and CP4 dual-Doppler pair.	114
6.10	East-west vertical cross section of Doppler winds and reflectivity.	115
6.11	Dual-Doppler horizontal wind fields of storm-relative motion in the SW analysis domain for: a) 0110 GMT 4 June 1985 at 0.5 km AGL (above ground level for CP4.); b) 3.5 km AGL; c) 9.5 km AGL.	118
6.11	Continued.	119
6.11	Continued.	120
6.12	Same as 6.4 except for: a) 0000 GMT 4 June 1985 at Fort Riley KS (FRI); b) 0130 GMT 4 June 1985 at Russell KS (RSL); c) 0130 GMT 4 June 1985 at Wichita KS (IAB).	122
A.1	The diurnal tide curve.	137
B.1	Non-smoothed analysis of average pressure with first corrections.	140
B.2	Smoothed analysis of average pressure in mb with final corrections.	141
B.3	Surface pressure traces at P41 and S38.	143
C.1	Time series plots of temperature (T), dewpoint (D), station pressure (p), and wind speed and gust (W) during heat burst at station P19.	145
C.2	Same as 6.4 except at 0000 GMT 4 June 1985 for Pratt KS (PTT).	146
C.3	Schematic of heat burst mechanism (after Johnson <i>et al.</i> , 1988).	148

LIST OF TABLES

5.1	Summary of radar reflectivity coverage as percentage of total rain.	68
6.1	Calculations of hydrostatic surface pressure change.	123
B.1	PAM and SAM pressure corrections.	142

Chapter 1

INTRODUCTION

The O K PRE-STORM (Oklahoma-Kansas Preliminary Regional Experiment for STORM-Central) experiment conducted in the south-central United States in May and June of 1985 offered scientists the opportunity to collect and analyze high resolution sets of meteorological data gathered during MCS evolution across the field experiment area. The data collection period was blessed by a frequent number of MCS excursions through the PRE-STORM domain (Augustine and Howard, 1988). These included a variety of linear (squall line) and non-linear MCSs. Since the completion of the field phase, many studies of the more significant systems have been conducted or are currently underway.

One such system travelled across the PRE-STORM domain during the afternoon and evening of 3-4 June 1985. This was a very active convective period with three MCSs progressing through the southern Great Plains region. The system of study was the second of the three and fell into the category of an MCS with an attached region of stratiform rain. This MCS had characteristics of both linear and non-linear MCSs. An unusual feature of this MCS was its "occluded" (Blanchard and Watson, 1987) appearance with a convective line to the south and a stratiform region to the north.

It is the purpose of this paper to document the life cycle of the MCS, with a primary emphasis on the surface pressure features. In addition, the structure of the other surface features and upper air characteristics will be detailed to study the possible mechanisms controlling the development, location, strength, and evolution of the observed pressure features. Also, this paper proposes to contrast the complex three-dimensional structure of the mature MCS with features observed in conjunction with linear MCSs having attendant stratiform rain regions. The MCS studied in this paper exhibited surface pressure features that were typically observed with squall lines that had trailing anvils.

Chapter 2 of this paper will provide some research background of surface pressure observations with MCSs. Chapter 2 will also detail the research history of MCSs with stratiform rain regions including theories on observed airflow structure within these systems and their relationship to observed surface pressure perturbations. Chapter 3 gives attention to the data sets used in the analyses. Chapter 4 provides a synoptic overview and a radar and satellite sequence of the MCS. Chapter 5 details the mesoscale surface and upper air features observed with the passage of the MCS through the PRE-STORM mesonet network. These observations will be contrasted to features typically observed with linear MCSs. Chapter 6 further details the mature storm circulation structure and attempts to provide some answers for the observed pressure features. Finally, Chapter 7 summarizes the work.

Chapter 2

BACKGROUND

2.1 Observations of mesohighs and mesolows

Analyses of surface pressure features in relation to MCSs have been carried out by a number of authors [e.g., Williams (1948, 1953, 1954, 1963), Brunk (1949), Byers and Braham (1949), Tepper (1950), Fujita (1955, 1959, 1963), Pedgley (1962), Hoxit *et al.* (1976), Fritsch and Chappell (1980), Ogura and Liou (1980), Koch and McCarthy (1982), Wakimoto (1982), Johnson and Nicholls (1983; tropical squall line), Garratt and Physick (1983), Cuning and DeMaria (1986), Hamilton and Johnson (1987), Johnson and Hamilton (1988), and Johnson *et al.* (1988)]. Prominent features noted in these studies included mesolows (both preceding and following the system), and mesohighs (normally within the system). Similar pressure features were identified with the second MCS of 3-4 June 1985.

Mesohighs are probably the best-documented mesoscale feature accompanying MCSs [e.g., Williams (1948, 1953), Brunk (1949), Byers and Braham (1949), Tepper (1950), Fujita (1955, 1959, 1963), Pedgley (1962), Fritsch and Chappell (1980), Wakimoto (1982), Johnson and Nicholls (1983), Hamilton and Johnson (1987), Johnson and Hamilton (1988), and Johnson *et al.* (1988)]. They usually follow the leading edge of the convection. Williams (1948) and Pedgley (1962) have shown that up to 8 mb pressure rises can occur with the passage of a mesohigh. The causes of the mesohigh have been attributed to evaporational cooling by precipitation, rain loading, and dynamic effects (e.g., the impact of the precipitation laden air on the ground).

A number of early studies have documented the evolution of the mesohigh. Some early terminology included "pressure pulsation" (Brunk, 1949), "pressure jump line" (Tepper, 1950), "elevation type waves" (Williams, 1953), and "pressure surge lines" (Fujita, 1955)

to characterize the progression of the leading edge of the mesohigh. Tepper (1950) argued that the pressure jump lines were the cause of the convection, but this has been shown to be untrue (mesohighs usually appear after the thunderstorms have formed). Byers and Braham (1949) and Fujita (1955) suggested that the mesohigh is the result of high-momentum air aloft being evaporatively cooled by rain and brought down to the surface by downdrafts, spreading out over the ground. The downdraft within the precipitation is caused by the frictional drag of falling precipitation (Pedgley, 1962) and evaporation of rain into the saturated downdraft (Zipser, 1977). The area affected by cooling at the surface is found to be greater than the area over which rain occurs (Byers and Braham, 1949). Fujita (1955) observed the peak in pressure associated with the mesohigh coincided with the convective rain maximum.

Fujita (1959) found that the mesohigh is about 1000-1500m deep at the ground and 10 to 100 km across. Winds with the mesohigh are found to be strongly divergent as the air spreads across the ground. As the mesohigh spreads out, part of the cold air gets fed into the gust front ahead of the system (Wakimoto, 1982) and part of it spreads to the rear of the system leaving a low-level cold pool in the wake [Zipser (1977), Johnson and Nicholls (1983), Smull and Houze (1985, 1987a, 1987b), and Johnson and Hamilton (1988)]. Fritsch and Chappell (1980) have shown numerically that subsidence occurs as the mesohigh cold dome spreads out and weakens.

The non-hydrostatic effects of the mesohigh have been discussed by Wakimoto (1982). He found that the non-hydrostatic contribution is greater at the leading pressure rise at the gust front whereas in the stratiform rain area, hydrostatic effects dominate.

Mesolows can also accompany MCSs. Although they have been observed by a number of authors [e.g., Williams (1953, 1954, 1963), Fujita (1955, 1963), Pedgley (1962), Hoxit *et al.* (1976), Fritsch and Chappell (1980), Ogura and Liou (1980), Koch and McCarthy (1982), Johnson and Nicholls (1983), Cuning and DeMaria (1986), Johnson and Hamilton (1988), and Johnson *et al.* (1988)], their causes have only recently been studied. They can be found preceding the mesohigh [e.g., Pedgley (1962), Fujita (1963), Hoxit *et al.* (1976), Fritsch and Chappell (1980), Ogura and Liou (1980), Koch and McCarthy (1982), Johnson and Hamilton (1988)] or following in the mesohigh's wake [e.g.,

Fujita (1955), Pedgely (1962), Williams (1963), Fritsch and Chappell (1980), Johnson and Nicholls (1983), Johnson and Hamilton (1988), and Johnson *et al.* (1988)].

Williams (1953, 1954) studied what he called "depression type waves" associated with convective systems. He observed that they are not accompanied by severe weather. He did note, however, that any rain which had been falling ceased as the lowest pressure passed. It had been found that the wake low developed a few hours after the development of the mesohigh [Fujita (1955, 1963), Pedgely (1962), Johnson and Hamilton (1988)] and that it is usually strongest during the MCS's dissipating stage [Fujita (1963), Williams (1963), Johnson and Hamilton (1988)]. Fujita (1955) called the trailing mesolow of a squall line a "wake depression". He originally had attributed it to a sort of "barrier flow blocking" effect of the mesohigh, but he later discounted this (Fujita, 1963).

Williams (1963) speculated that the wake depression was caused by hydrostatic pressure falls accompanying subsidence aloft trailing a thunderstorm. Hoxit *et al.* (1976) studied the formation of a mesolow in advance of convective systems and suggested they are due in part by subsidence in the mid and upper troposphere (near the anvil region). They said that this subsidence heating dominates over latent heat release, warm air advection, and radiation absorption. Upper level subsidence was also observed by Fankhauser (1974) and Ogura and Liou (1980). In a modeling study, Fritsch and Chappell (1980) found that subsidence occurs not only ahead of convective systems, but all around them. With certain configurations of convective activity, the strongest subsidence would be focused in certain areas. They hypothesize that deep convective systems force circulations which cause a mass imbalance. This in turn leads to thickness changes, accelerations, and vertical motions within a column, consequently leading to surface pressure changes. The subsidence warming must be focused and continue for a long enough period of time and extend over a deep layer to necessitate mesolow formation. They listed several variables which could influence the timing, location, and intensity of mesocyclogenesis [c.f., Fritsch and Chappell (1980), Table 1]. They also documented this in their modeling study. This same subsidence warming idea was discussed by Cuning and DeMaria (1986) in relation to airmass thunderstorms over Florida.

Johnson and Hamilton (1988) have studied the wake low trailing a squall line case. They showed that the wake low is well correlated with mesoscale circulations found in the trailing anvil of a squall line (this will be discussed in the next section). The maximum amplitude of the wake low is found at the rear edge of the trailing stratiform precipitation.

Another mechanism for mesolow formation was modeled by Johnson *et al.* (1988). They showed that a collapsing cold pool or spreading density current can cause mesolow formation in dissipating MCSs.

The surface airflow in the vicinity of surface pressure features accompanying MCSs is highly ageostrophic [e.g., Tepper (1950), Williams (1954), Fujita (1955), Koch and McCarthy (1982), Leary and Rappaport (1987), and Johnson and Hamilton (1988)]. Due to the highly transient nature of these pressure features, the air does not have enough time to come into geostrophic balance. This was studied quantitatively by Garratt and Physick (1983). Winds are observed to blow forward through mesohighs and backward through trailing wake lows. These winds are found to blow perpendicular to the isobars. Divergence is found at the rear edge of the mesohigh with convergence being observed to the rear of the trailing wake low. Occasionally, convergence in the wake of MCSs will trigger future convection [Pedgley (1962), Williams (1963), Smull and Houze (1985), Stumpf and Gallus (1989)]. If the atmosphere is not convectively unstable, new convection will be suppressed [Koch and McCarthy (1982), Johnson and Nicholls (1983), Johnson and Hamilton (1988)].

Figure 2.1 represents a schematic of the surface pressure features and airflow structure with a mature midlatitude squall line with a trailing stratiform precipitation area (Johnson and Hamilton, 1988). Note the airflow is highly ageostrophic with respect to the isobars. Bear in mind that this figure depicts surface parameters observed with linear MCSs (squall lines). It will be shown that surface pressure and wind features associated with the second MCS of 3-4 June 1985 bear striking resemblances to those shown in Fig. 2.1, especially in the northern stratiform rain area of the MCS.

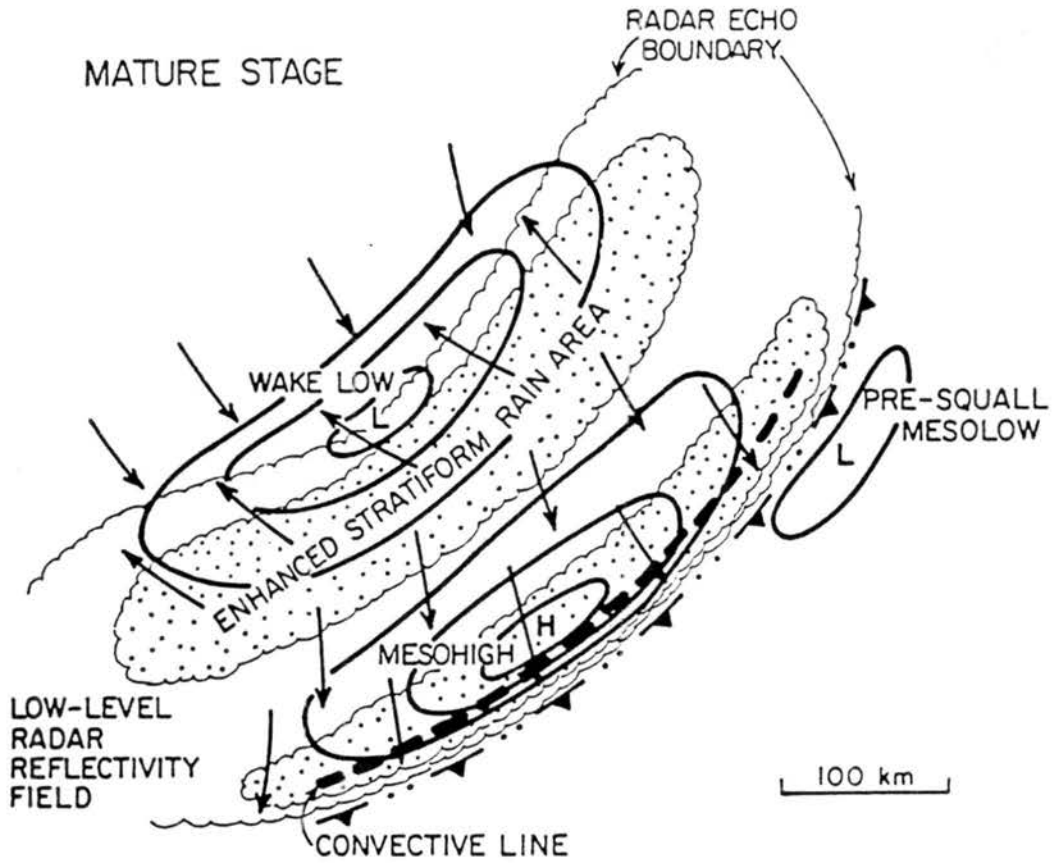


Figure 2.1: Schematic of surface pressure, wind field, and precipitation during the mature stage of a squall line with a trailing stratiform rain region (after Johnson and Hamilton, 1988).

2.2 MCS wake structure observations

Mesoscale upper air circulations in the vicinity of MCS stratiform rain regions appear to be a contributing factor in the development of a surface wake low. The stratiform rain region is associated with a thick anvil-like structure (hereafter referred to as the *anvil*, *trailing anvil*, or *stratiform anvil*) which forms next to active convective towers in MCSs. The environmental wind shear about the MCS determines the location of the stratiform anvil. In many midlatitude and tropical squall lines, it has been observed to the rear of the system, however occasionally it has been found leaning forward from the convective towers [see Johnson and Hamilton (1988) for a full list of references regarding stratiform anvil locations in MCSs]. As will be shown with this case, the stratiform anvil had a unique structure due to the complex nature of the upper level winds.

Figure 2.2 depicts a schematic cross-section through the rear portion of a midlatitude squall line on 10-11 June 1985 (Johnson and Hamilton, 1988). Airflow depicted on this figure represents the storm-relative flow. This particular squall line was accompanied by a trailing stratiform rain region following directly behind a leading convective line. The front-to-rear (FTR) storm-relative flow originating at the storm's low levels ahead of the leading convective line was pronounced. This was also the case with the mid-level rear-to-front (RTF) inflow and low-level FTR outflow found at the rear of the system. FTR flow began as low-level inflow of high θ_e air and rose in the convective updrafts at the leading edge of the squall lines [Ogura and Liou (1980) also observed this]. This flow continued rearward in a sloping fashion and was responsible for the rearward transport of hydrometeors from the convective towers into the trailing anvil [Smull and Houze (1985, 1987a), Rutledge and Houze (1987)]. Above the convective towers, divergent outflow was observed with the spreading of the anvil at the tropopause [Gamache and Houze (1982), Smull and Houze (1987a)].

The stratiform anvil has also been found to be partially sustained by mesoscale ascent at and above the freezing level in the trailing anvil [Brown (1979), Ogura and Liou (1980), Gamache and Houze (1982), Srivastava *et al.* (1986), Smull and Houze (1987a, 1987b),

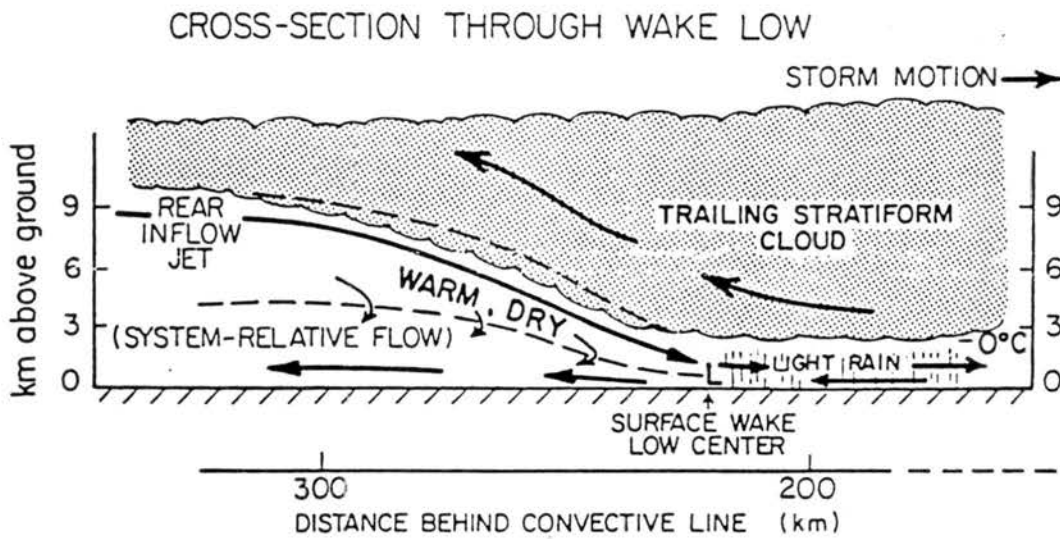


Figure 2.2: Schematic cross section of stratiform anvil region in a squall line (after Johnson and Hamilton, 1988). Arrows represent system relative airflow.

Rutledge and Houze (1987)]. This mesoscale ascent has been observed to keep stratiform anvils active long after the dissipation of cumulonimbus towers (Srivastava *et al.*, 1986).

Evaporative cooling beneath the stratiform anvil results in a mesoscale downdraft (Zipser, 1977). The downdraft air descends in a subsaturated environment, and some warming and drying will occur. The amount of this warming is dependent on the amount of stratiform rain falling in the downdraft because evaporative cooling by the precipitation will offset the warming. If all of the precipitation evaporates upon descent, then the air will warm dry adiabatically at a greater rate than if the parcel contained precipitation. This subsidence warming will hydrostatically produce surface pressure reductions. These pressure falls should be maximized where the warming is the greatest, for example, just outside the surface rain area. Johnson and Hamilton (1988) observed the maximum of the wake low "hugging" back edge of the surface stratiform rain.

Latent heat release accompanying the mesoscale updraft and evaporative cooling in the downdraft has been shown to produce a midlevel mesolow in the anvil (Brown, 1979). The resulting pressure gradients may be responsible for driving a rear inflow jet (Smull and Houze, 1987b) which has been observed in a number of MCS cases (see Smull and Houze, 1987b, Table 1). Johnson and Hamilton (1988) felt that the wake low is a surface manifestation of the rear inflow jet. This jet is depicted on Fig. 2.2.

Near the mesoscale updraft/downdraft interface in the trailing anvil, convergence is found between the rear inflow and the opposing FTR flow emanating from the convective towers. Midlevel convergence has been found in several studies of MCSs [Brown (1979); Ogura and Liou (1980), Srivastava *et al.* (1986), Johnson and Gallus (1988), Rutledge *et al.* (1988)]. Melting of snow at the freezing level also provides additional horizontal convergence [Leary and Houze (1979), Szeto *et al.* (1988)]. Smull and Houze (1987b) felt that this convergence is a factor in forcing the mesoscale updraft/downdraft in the stratiform anvil region.

It will be shown with the second MCS of 3-4 June 1985 that a complex three-dimensional airflow transported hydrometeors away from the convective towers in a different fashion than commonly observed with squall lines having trailing stratiform rain

regions. A stratiform anvil-like structure was present in the northern segment of the MCS, north of the heavy convective cells. The mesoscale circulations in and below the relatively short trailing stratiform anvil appear to have played a primary role in the development of a strong wake low on the rear edge of the stratiform rain area.

Chapter 3

THE DATA SET

3.1 PRE-STORM

A major field experiment known as the Oklahoma-Kansas Preliminary Regional Experiment for STORM¹-Central (OK PRE-STORM; hereafter called PRE-STORM) was conducted during the period 1 May to 30 June 1985 over the southern Great Plains of the United States. Some goals of the project were to assure the quality of an observing system to research MCSs, to collect the necessary data to begin preliminary investigation into the development, evolution, and structure of midlatitude MCSs, and to gain some forecasting insight of these phenomena. PRE-STORM also served to sharpen and focus the scientific objectives for the proposed STORM-Central project slated for the 1990s (NCAR, 1984).

A large number of MCSs affected the PRE-STORM operations area during the May-June 1985 period. In fact, more MCSs occurred during 1985 than in previous years since routine accounting of MCSs began in 1978 (Augustine and Howard, 1988). The PRE-STORM observing network offered scientists the opportunity to collect data on a highly compact spatial grid of meteorological instruments with time intervals much shorter than conventional daily operations of the current synoptic data network. The data collected during this experiment consisted of surface, upper air, radar, satellite, aircraft, and lightning data. A summary of the surface, upper air, radar, and lightning networks are shown in Figure 3.1. A comprehensive overview of the project goals and data systems is discussed by Cuning (1986). In addition, Meitin and Cuning (1986) summarize the daily operations conducted during the experiment. This summary includes daily synoptic overviews

¹STORM: STormscale Operational and Research Meteorology

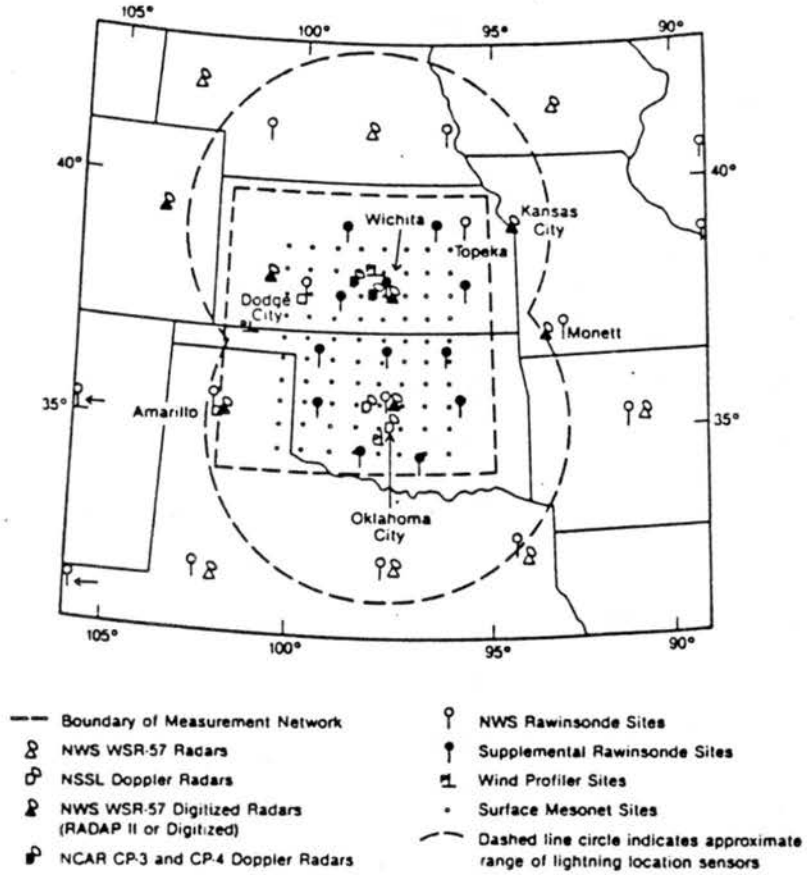


Figure 3.1: The OK PRE-STORM observational mesonet (after Cuning, 1986).

for each day of the experiment, and summarizes the data collected during each operational mission.

3.2 Data used for the analyses

3.2.1 Surface data

Surface data used consisted of the mesonet network of 84 automated observing platforms deployed for the PRE-STORM project. These stations were arranged in a semi-rectangular grid with a station spacing of about 50 km (Fig. 3.2). The northern half of the mesonet network was comprised of 40 NCAR/FOF² Portable Automated Mesonet-II (PAM-II; hereafter called PAM) stations. The southern half was comprised of 40 NSSL³ Surface Automated Mesonet (SAM) stations. Two additional PAM stations were collocated with two of the SAM stations for comparison purposes. These automated observing platforms measured station (surface) pressure, dry-bulb temperature, wet-bulb temperature, u- and v-wind components, and rainfall. Data were collected in most cases at 5-minute intervals. Except for rainfall accumulation and wind gust, data values represented the 5-minute averages for the period ending at the reported time. National Weather Service (NWS) Standard Aviation Observations (SAO) hourly data were also used to supplement the analyses (Fig. 3.3).

To minimize topographic effects, station pressure data from the PAM and SAM were adjusted hydrostatically for the mean elevation of the stations (480 m) using the surface virtual temperature (\bar{T}_{vs}) as an approximation to the mean virtual temperature in the column with the following formula,

$$p_{480} = p_s \exp \left[\frac{g(480 - z_s)}{R_d \bar{T}_{vs}} \right]. \quad (3.1)$$

Gravity $g = 9.8 \text{ m s}^{-2}$ and the gas constant for dry air $R_d = 287 \text{ J kg}^{-1} \text{ K}^{-1}$. Station elevation in m and surface pressure in mb are given as z_s and p_s respectively. Since the

²NCAR/FOF: National Center for Atmospheric Research/Field Observing Facility

³NSSL: National Severe Storms Laboratory

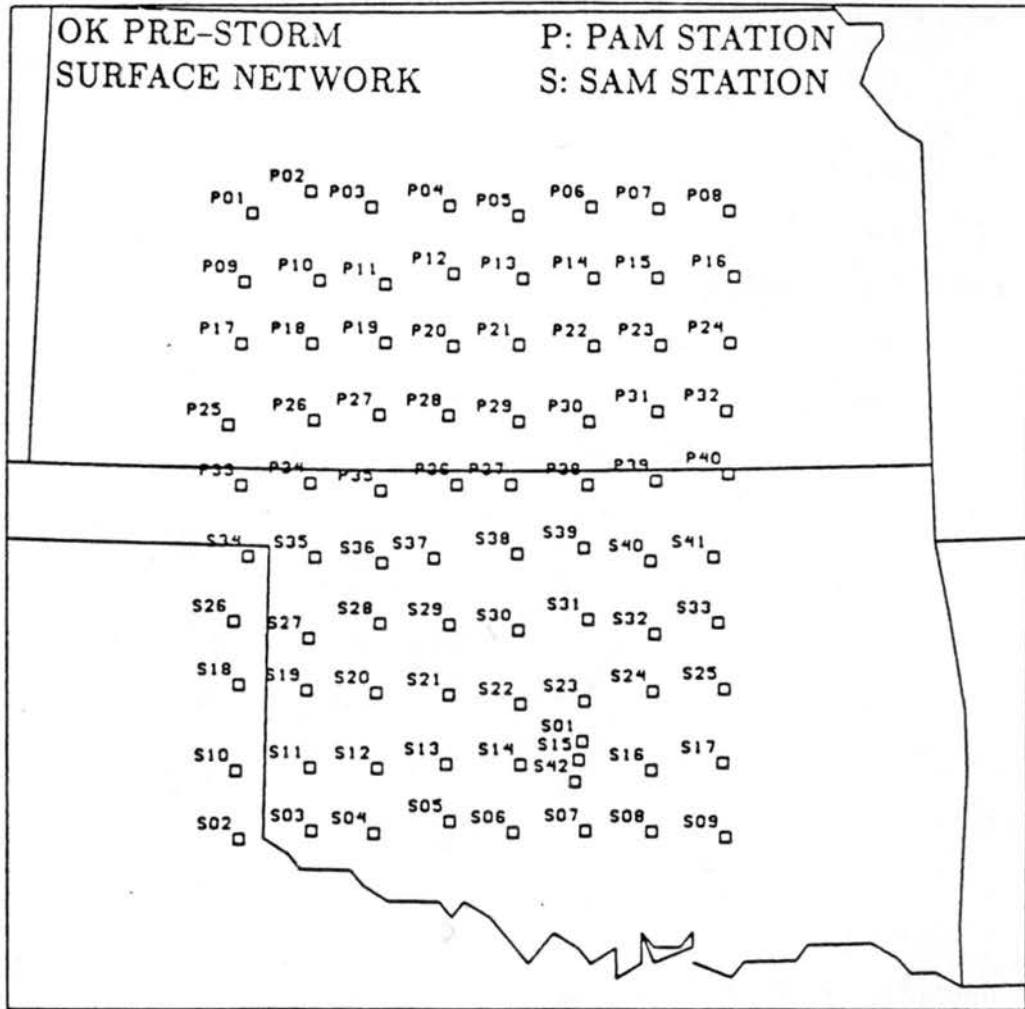


Figure 3.2: The PRE-STORM Portable Automated Mesonetwork (PAM) and Surface Automated Mesonetwork (SAM) surface array.

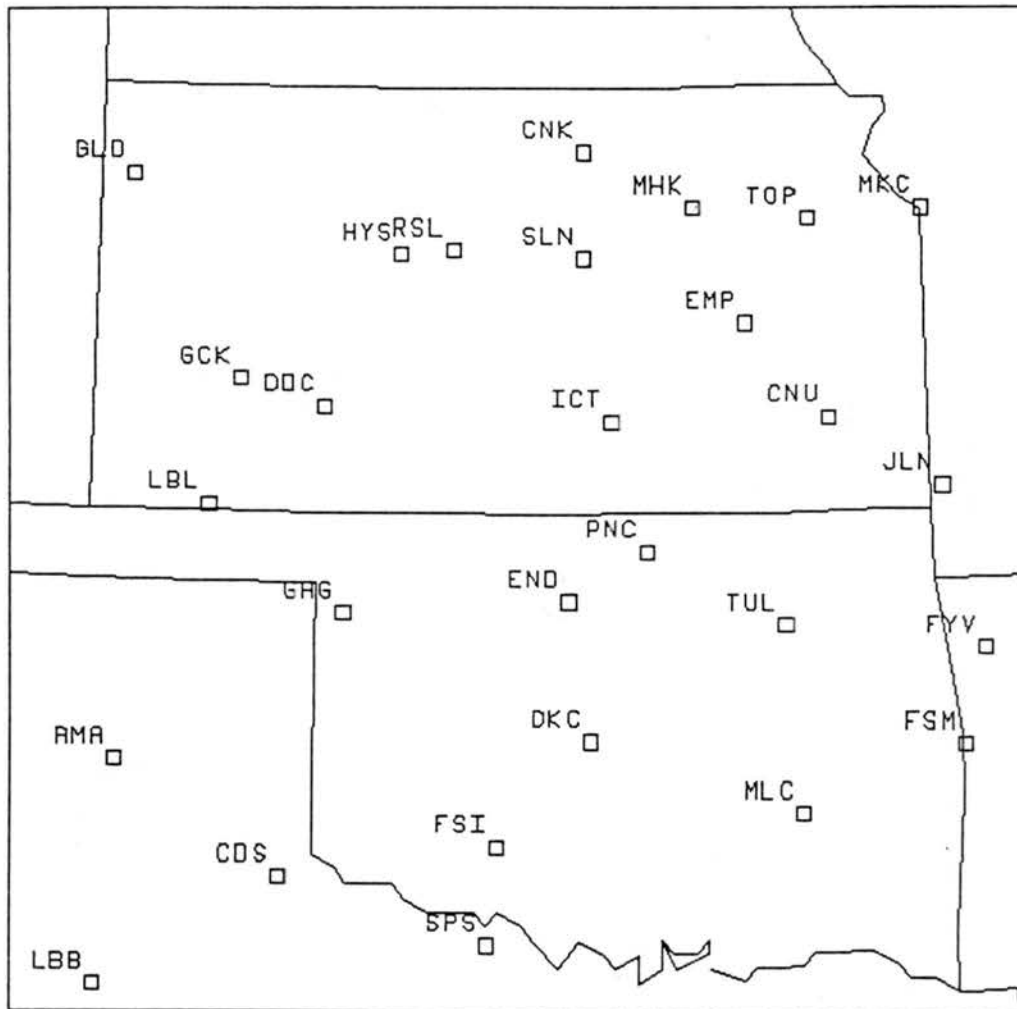


Figure 3.3: National Weather Service (NWS) Standard Aviation Observation (SAO) sites.

depth of the column is minimized by using the 480 m level, the mean virtual temperature approximation used in this equation is more accurate than if surface pressures were reduced to sea-level. Next, corrections were applied to the data to remove the diurnal solar tide oscillation. This procedure is described in detail in Appendix A. Finally, errors resulting from instrument calibration bias were removed from the data. This procedure is fully described in Appendix B, with the adjustments listed in Table B.1. Given that $tide(t)$ is the tidal correction at time t and $bias(n)$ is the bias correction for mesonet station n ,

$$p_{adj} = p_{480} - tide(t) + bias(n) \quad (3.2)$$

is the final value obtained, the adjusted pressure.

3.2.2 Upper air data

The upper air network consisted of NWS sites and twelve supplemental sounding sites (Fig. 3.4). Soundings were taken at approximately 90-minute intervals during selected operational periods. Data included temperature, moisture, wind, pressure, height, and balloon displacement measurements. Also, three 50 MHz wind profiling systems collected wind data at Liberal KS, McPherson KS, and Norman OK. An acoustic sounding system at McPherson KS provided additional wind data in the lowest 1 km of the atmosphere.

3.2.3 Radar and satellite data

The radar data used included NWS WSR-57 radars located at Amarillo TX, Oklahoma City OK, Garden City KS, Wichita KS, and Monett MO. Volume scan radar data were digitized by the NWS's second generation RADAR DATA Processor (RADAP-II). Composites of radar images from several radar sites were prepared using the digitized data. Low-level reflectivity (base scans at 0.5° elevation angle) were used for the analyses. Also available were data from the NCAR/FOF CP-3 and CP-4 5cm Doppler radars located at Cheney Reservoir KS and Nickerson KS.

The satellite data used were from GOES-West, which was situated at 105°W during the experiment.

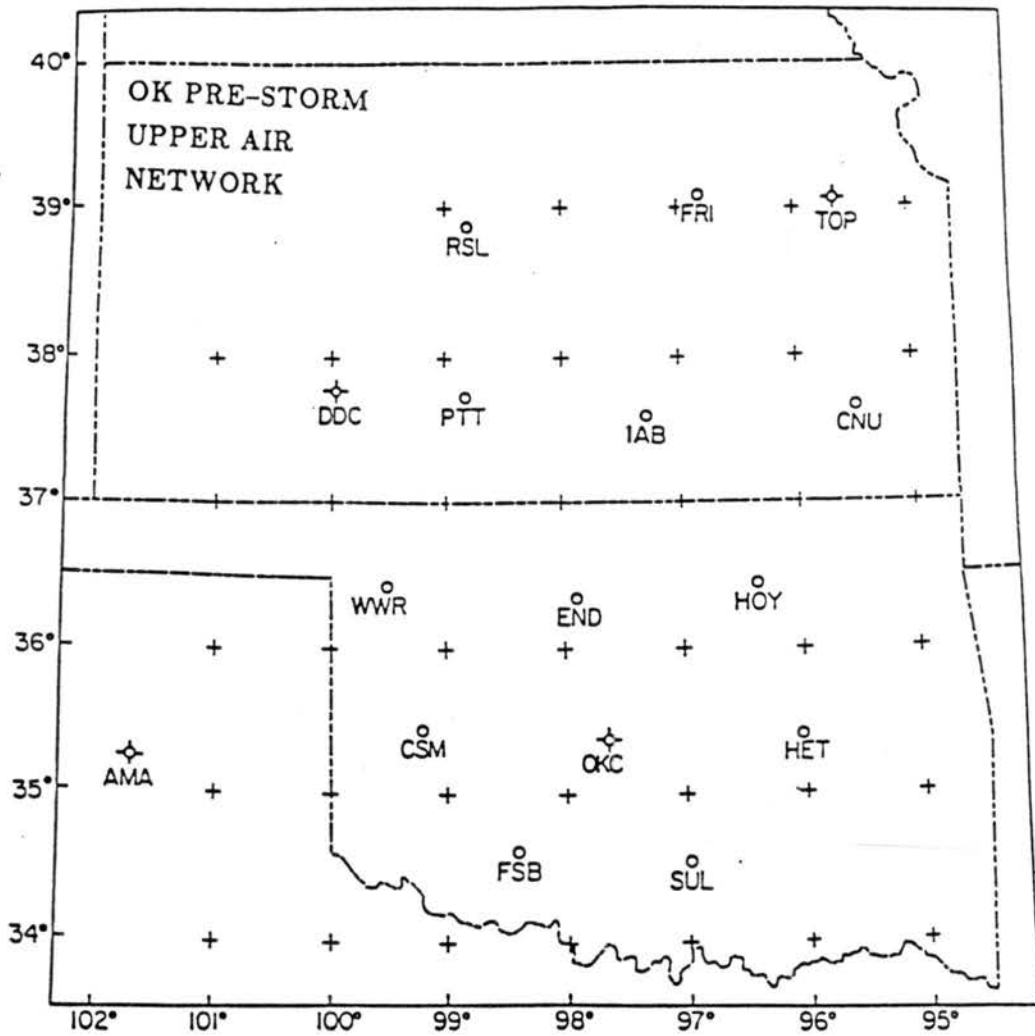


Figure 3.4: The PRE-STORM upper air mesonet. Crossed circles indicate NWS sites. Plain circles indicate supplemental sites.

Chapter 4

SYNOPTIC OVERVIEW

The period 3-4 June 1985 was an active period for PRE-STORM operations as a series of three MCSs passed through the project domain. The life cycles of these systems were generally similar, originating in the Texas Panhandle and moving along an anticyclonically curved track to the east-northeast, into and through the state of Kansas (Fig. 4.1). Each system apparently influenced to some degree the subsequent formation and tracking of successive MCSs by some sort of boundary layer modification. Hereafter, the three systems will be referred to as MCS1, MCS2 (the case study of the paper), and MCS3 respectively¹.

4.1 Initial synoptic conditions and MCS1

Conditions at 1200 GMT 3 June prior to MCS2 are presented here to examine the environment leading up to the formation of the MCSs during the 3-4 June 1985 period. Analysis of surface conditions using NWS SAOs at 1200 GMT 3 June (Fig. 4.2) shows a warm² front from northeast Oklahoma west-southwestward into the Northern Texas Panhandle. The front was characterized at the surface by a windshift, pressure trough, and a weak temperature gradient. South of the front was a warm moist airmass. Dewpoints were about 18-20°C in Oklahoma, and the winds were mainly southerly. The area north of the front was slightly cooler but still somewhat moist with dewpoints a few degrees cooler. The flow here was basically northeast. Fig. 4.3 shows a surface analysis of PAM

¹MCS1 affected the PRE-STORM domain from approximately 1300 - 2100 GMT 3 June 1985. MCS2 affected the domain from about 1900 GMT 3 June - 0400 GMT 4 June. MCS3 affected the domain from about 0200 - 1400 GMT on 4 June.

²A warm front was analyzed rather than a stationary front as depicted on NMC analysis. This frontal boundary was slowly moving to the north.

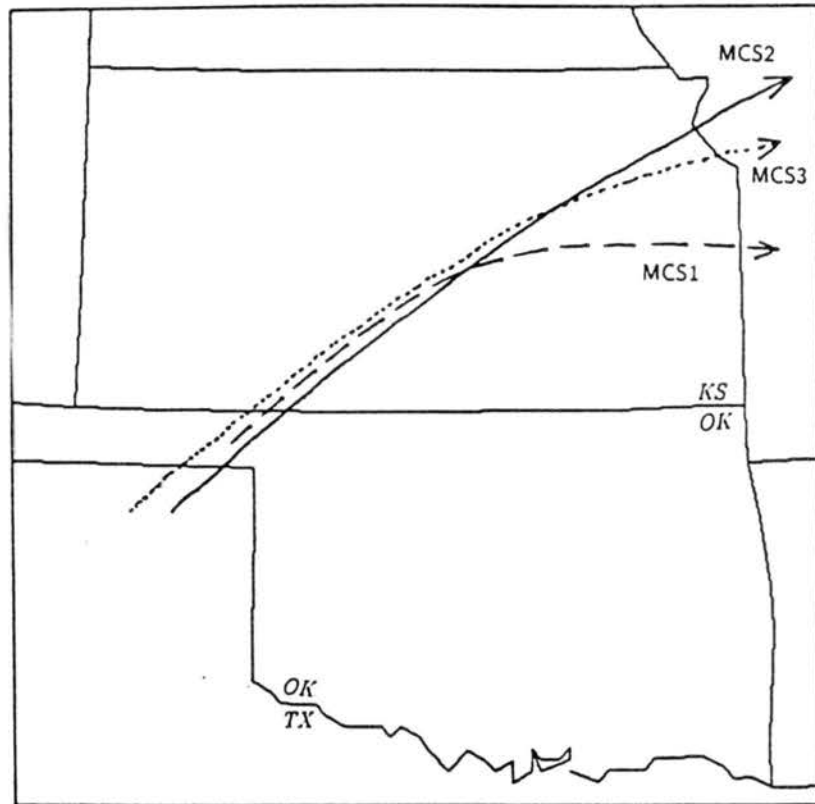


Figure 4.1: Tracks of the three MCSs which occurred in the 3-4 June 1985 period (adapted from Hamilton and Johnson, 1987). The dashed line represents MCS1. The solid line represents MCS2. The dotted line represents MCS3.

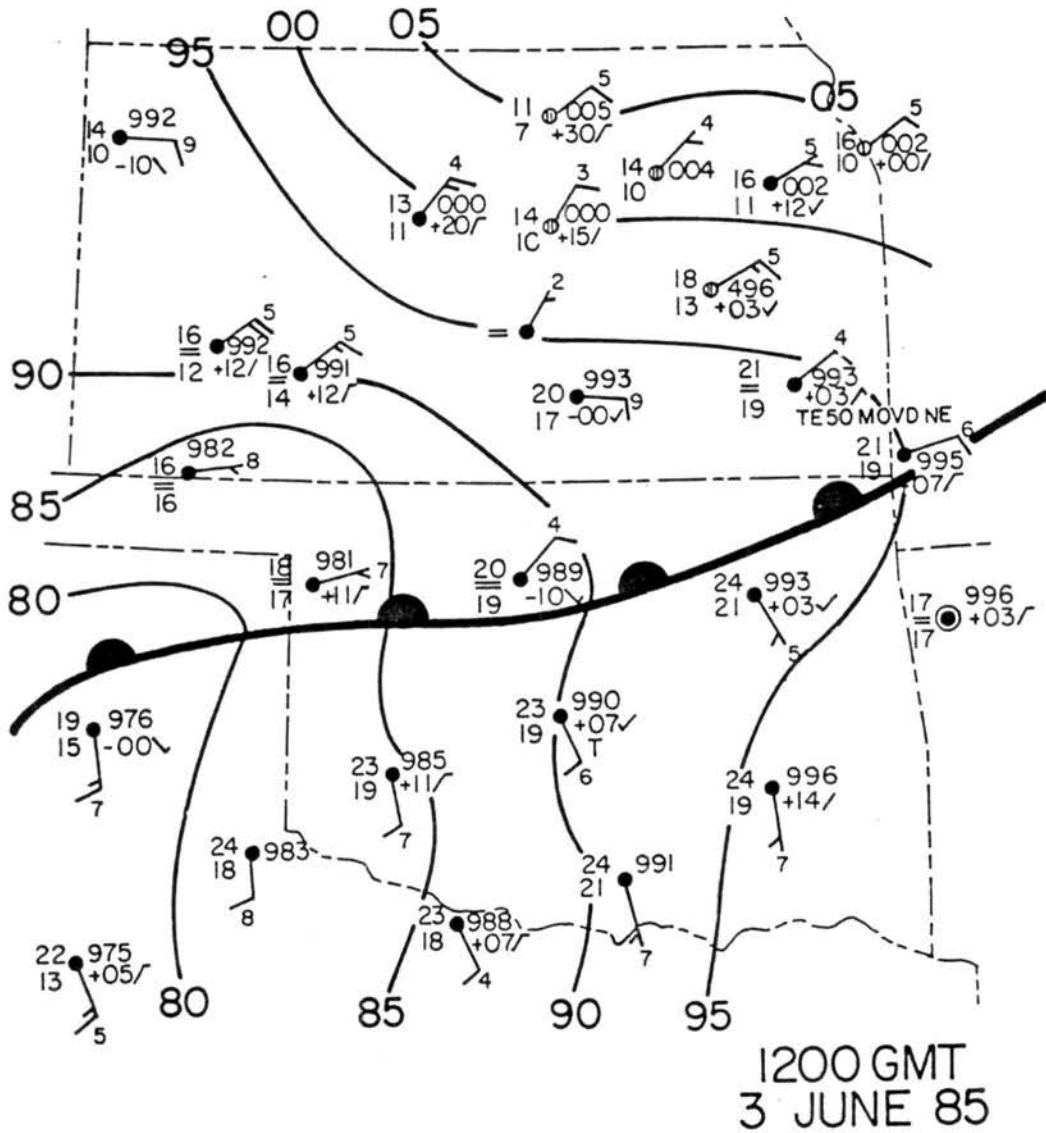


Figure 4.2: Surface mesoanalysis at 1200 GMT 3 June 1985. Plotted stations are NWS SAOs. Contours represent altimeter settings adjusted to 480 m using a modification of the procedure by Sangster (1987), in units of inches Hg (e.g., 90 = 29.90 inches Hg).

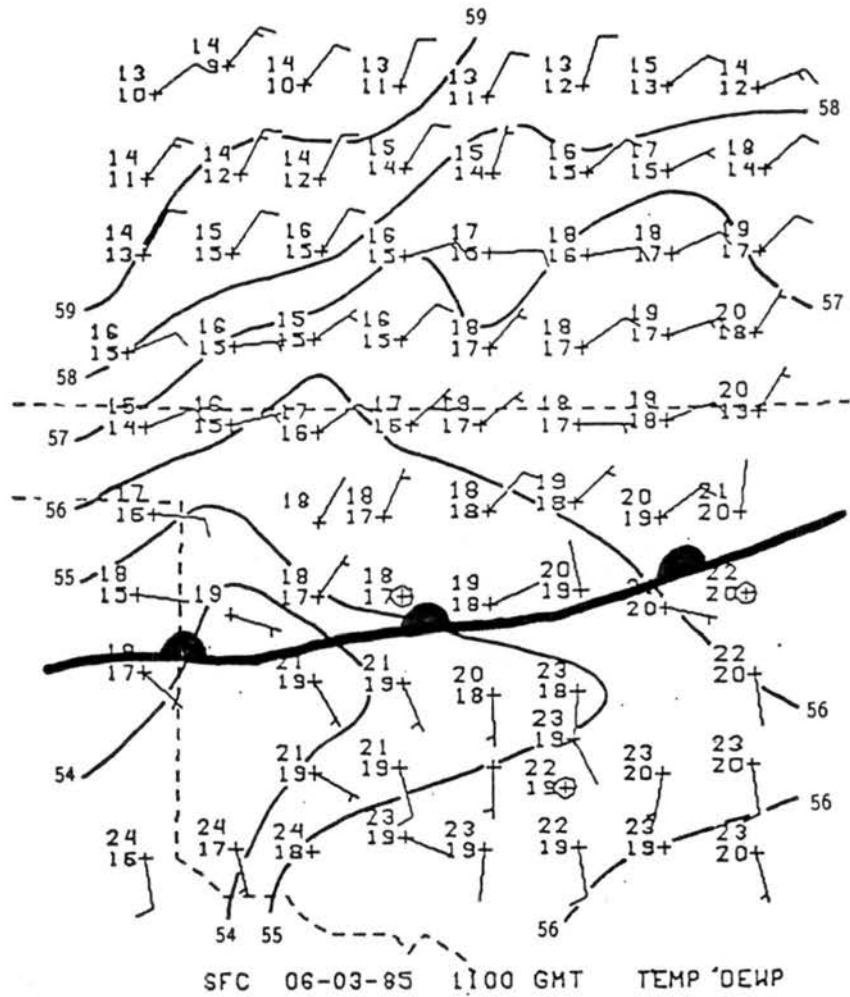


Figure 4.3: Surface PAM/SAM mesoanalysis at 1100 GMT 3 June 1985. Contours represent adjusted pressure (p_{adj}) in mb (e.g., 59 = 959 mb). Temperature and dewpoint are plotted at the left of each station in $^{\circ}\text{C}$. One wind barb equals 5 m s^{-1} .

and SAM data at 1100 GMT. Note the location of the windshift along the front on this analysis. On both surface analyses (Figs. 4.2 and 4.3), lower pressure was evident in Western Oklahoma.

The upper air features at 1200 GMT 3 June are presented in Fig. 4.4. At 850 mb (Fig. 4.4a), the flow was southerly from Texas to the Dakotas. A moist pocket ($T_d \geq 12^\circ\text{C}$) was centered over northwest Oklahoma, and a wind maximum was evident at Dodge City KS (DDC; 25 knots), indicating that overrunning north of the warm front was occurring. From 700 mb to 200 mb (Figs. 4.4b-f), the winds veered to an anticyclonically southwesterly curved flow. This mid to upper tropospheric flow was representative of the tracks of the three MCSs (see Fig. 4.1). There was an absence of any significant positive vorticity advection (PVA) at 500 mb (Fig. 4.4c), an indicator of upward vertical motion forcing. It is possible that short waves responsible for convective triggering may have passed through without being resolved on NMC analysis grids. The advection of vorticity by the thermal wind may have forced upward vertical motion [Hoskins *et al.* (1978), Trenberth (1978)]. Figure 4.4d shows the 500 mb vorticity field superimposed on the 1000-500 mb thickness field. Since the thermal wind blows parallel to thickness contours, this figure serves to show areas of PVA by the thermal wind. Positive vorticity advection by the thermal wind is present at 1200 GMT 3 June (to the west of the heavy dashed line on Fig. 4.4d). A jet core maximum of wind speed of 100 knots was located over Dodge City KS at the 200 mb level (Fig. 4.4f). This could have provided some upper-level divergence to aid in convective development.

An overview of the conditions associated with MCS1 are included now because it is felt that this system influenced to a large degree the development and movement of MCS2, the case study in this paper. Convection from MCS1 initially developed in southwest Kansas. A satellite picture (Fig. 4.5) depicts this area as a small region of cold cloud tops. Interestingly, this convection developed in a region which was experiencing no surface convergence, and was north of the surface warm front by about 150 km. However, the convection was at the southwest end of a surface mesoscale pressure trough which was clearly evident on the 1100 GMT mesonet network analysis (Fig. 4.3). Stumpf and Johnson

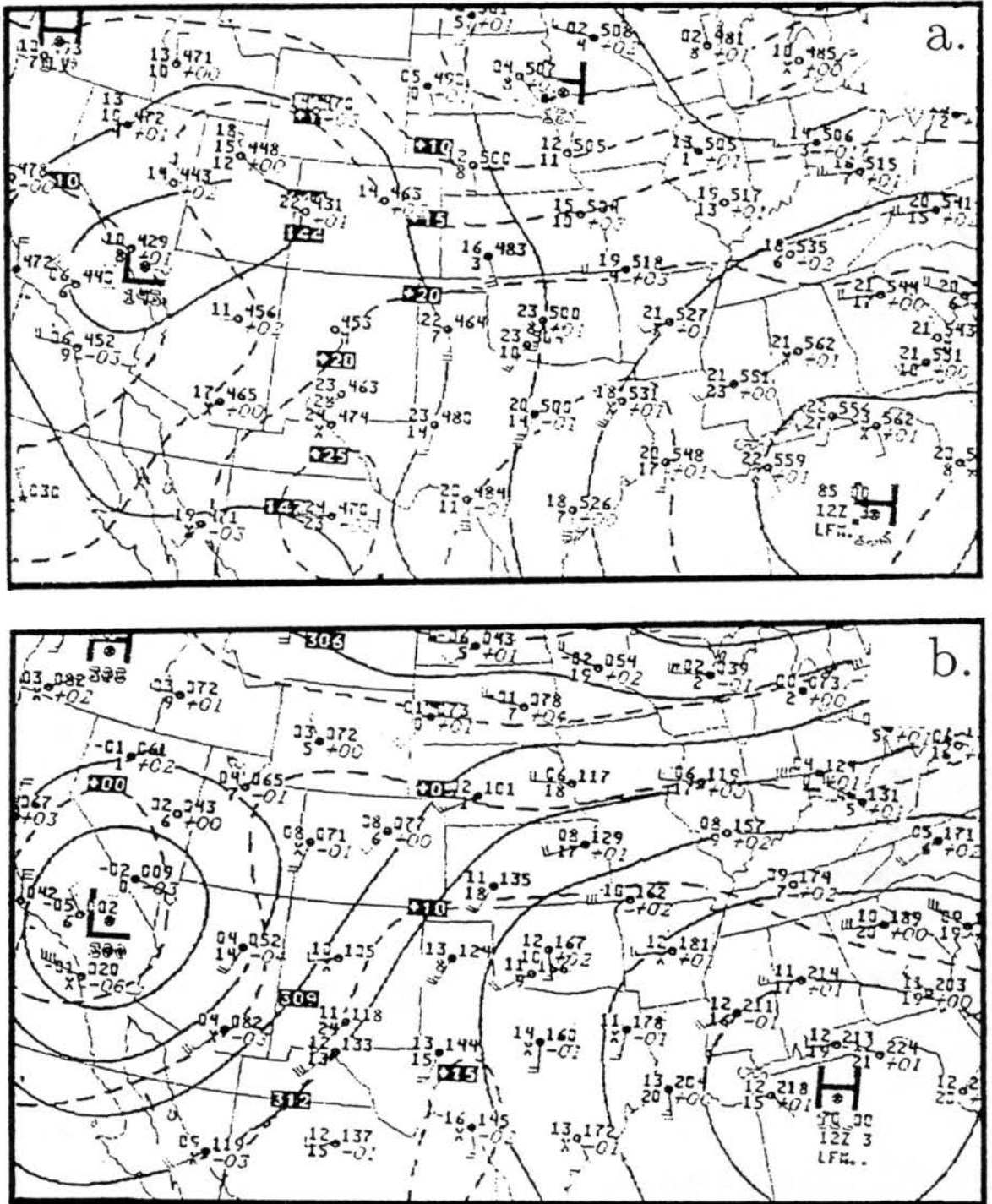


Figure 4.4: 1200 GMT 3 June 1985 NMC upper air analyses: a) 850 mb; b) 700 mb; c) 500 mb; d) 500 mb; e) 300 mb; f) 200 mb. Solid contours represent geopotential height in meters on all figures except d. where it represents the 1000 - 500 mb thickness field in Dm. Dashed contours represent temperature in $^{\circ}\text{C}$ on figures a. and b. Dashed contours represent vorticity on figures c. and d. Dashed contours represent wind speed in knots on figures e. and f. Heavy dashed line in d. marks axis of neutral vorticity advection by thermal wind.

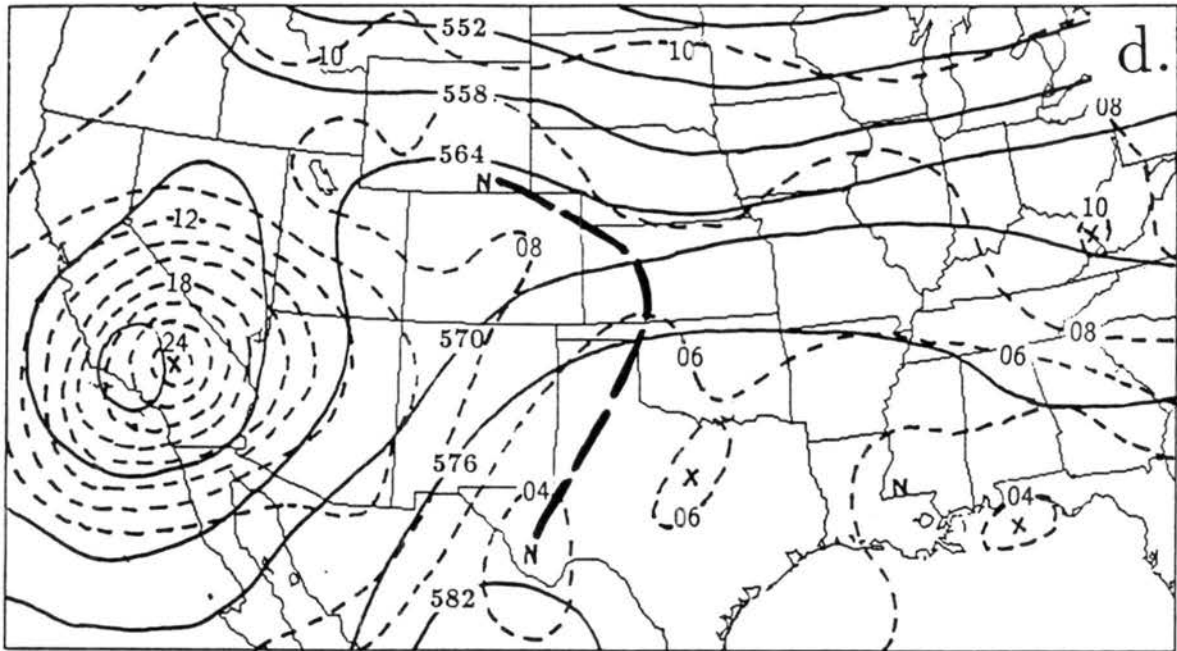
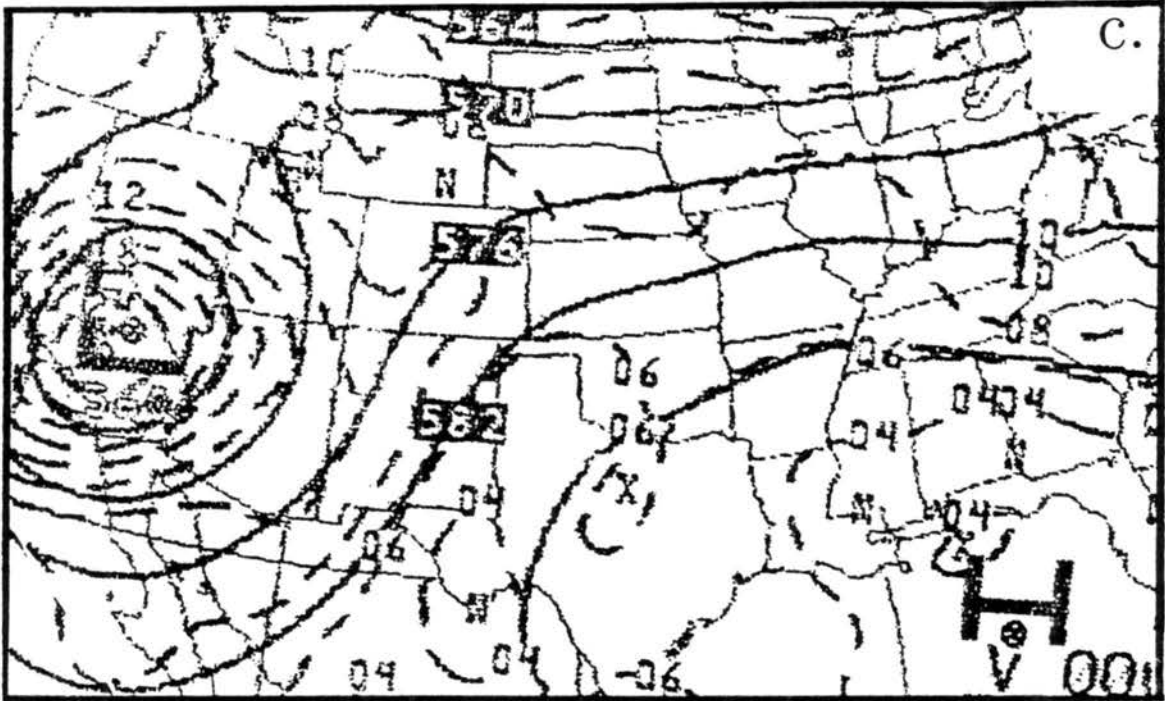


Figure 4.4: Continued.

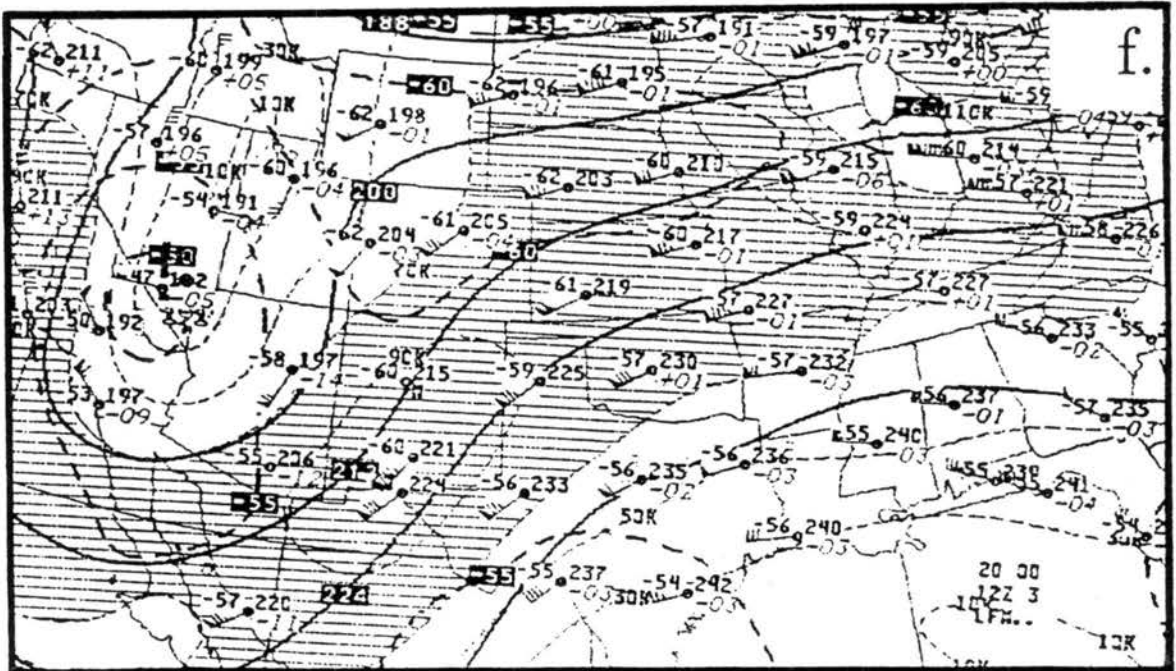
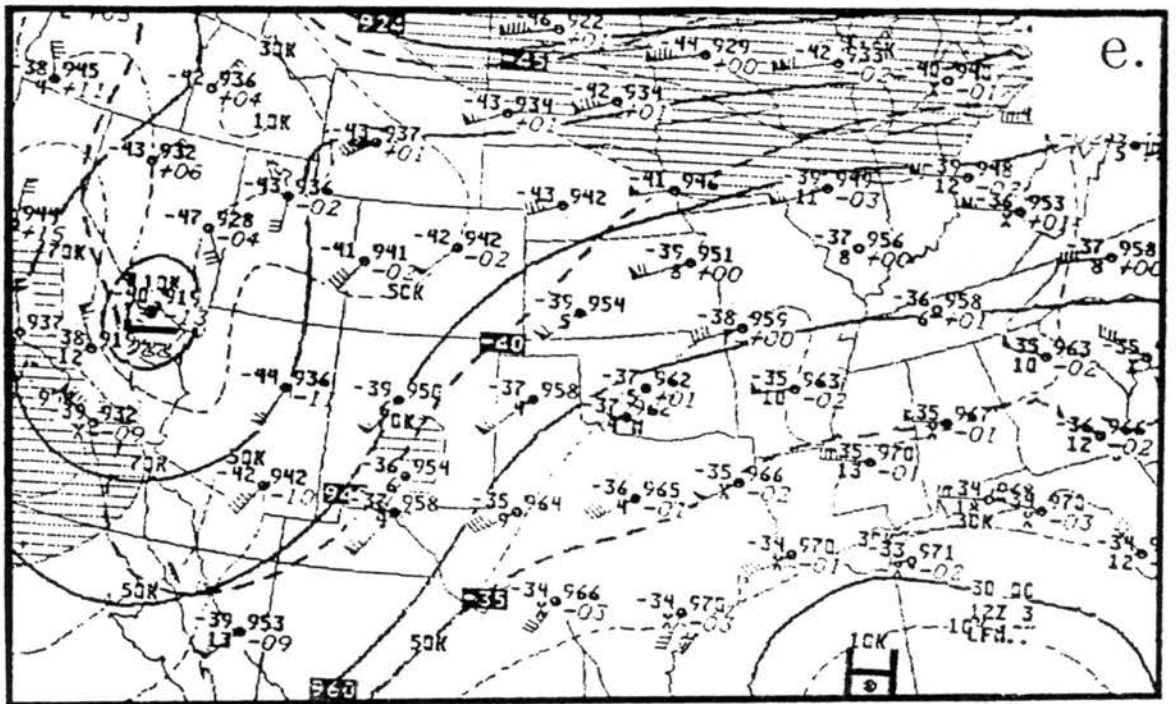


Figure 4.4: Continued.

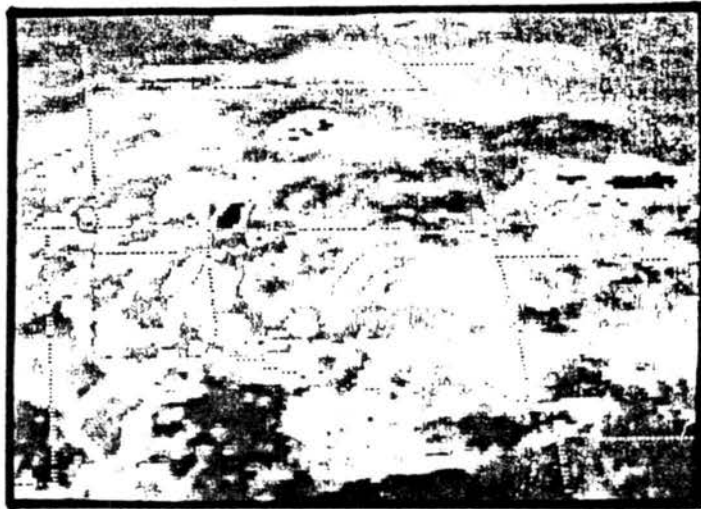


Fig. 4.5: 1300 GMT 3 June 1985 infrared (IR) satellite image.

(1988) speculated that this surface pressure trough may have represented a deformation in the frontal surface which lied about 1 to 2 km above the ground. An upper air sounding launched at 0900 GMT 3 June at Dodge City KS (Fig. 4.6) shows a frontal inversion and windshift at about 800 mb. A frontal inversion was not present on the Oklahoma City OK sounding at 1200 GMT (figure not shown). The lack of significant lower-tropospheric data in the vicinity of the convective development associated with MCS1 posed an interesting forecast problem for this case. This forecasting problem is beyond the scope of this research and is not studied in this paper.

In time, the convection associated with MCS1 developed a very large cloud shield (Fig. 4.7) and tracked east-northeastward through Kansas. The warm front which was in central Oklahoma at 1200 GMT had slowly moved north in the past seven hours and was now situated along the Kansas-Oklahoma border at 1800 GMT (Fig. 4.8). Oklahoma was still dominated by warm southerly flow at the surface. At this time, the front was not too well defined as it had been partially washed out by outflow from MCS1 in northeast Kansas. Note the cooler temperatures there. The role that MCS1 had in influencing MCS2 is not clear, but surface data show that the atmospheric boundary layer in the wake of MCS1 was modified to some extent. Low-level convergence boundaries were evident in Kansas (to be shown in the mesoscale overview in the next chapter), and these may have enhanced the new convective development associated with MCS2.

4.2 Radar and satellite overview

A radar and satellite overview of MCS2 is presented now to illustrate the larger scale life cycle of this system. A full mesoscale surface and upper air overview will be presented in the next chapter.

The satellite sequence (Figs. 4.9a-j) shows the development and movement of the cloud shield associated with MCS2. Note the general path of the MCS—northeastward in a slight anticyclonically curved manner.

Referring to Fig. 4.9a, one can see that the large cloud shield associated with MCS1 had moved into northeast Kansas, and a new area of cold cloud tops was developing in

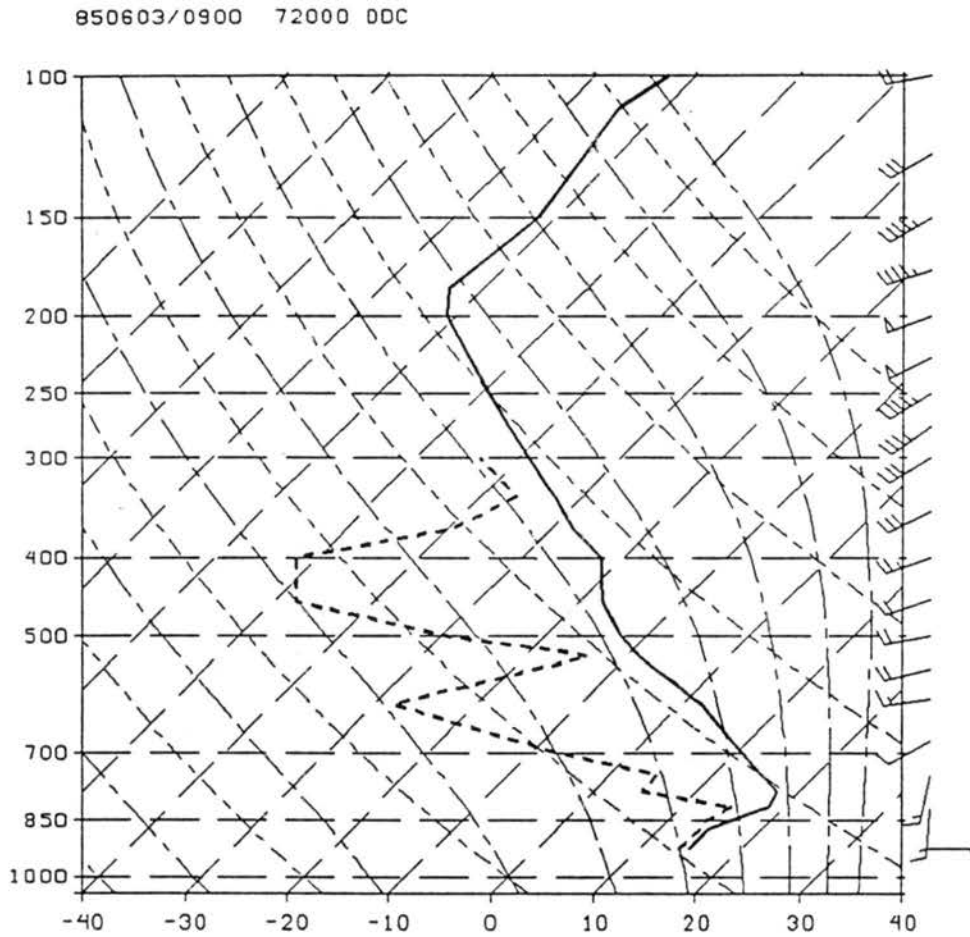


Figure 4.6: 0900 GMT 3 June 1985 Dodge City KS (DDC) vertical sounding of temperature, dewpoint, and actual winds.

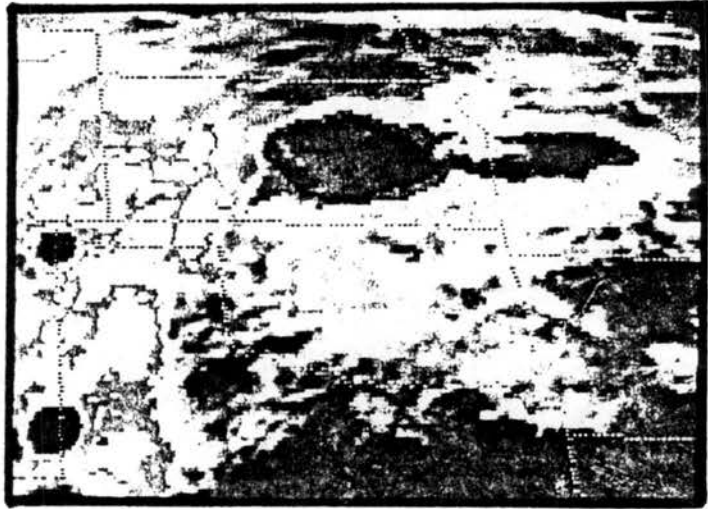


Fig. 4.7: Same as Fig. 4.5 except for 1600 GMT 3 June 1985.

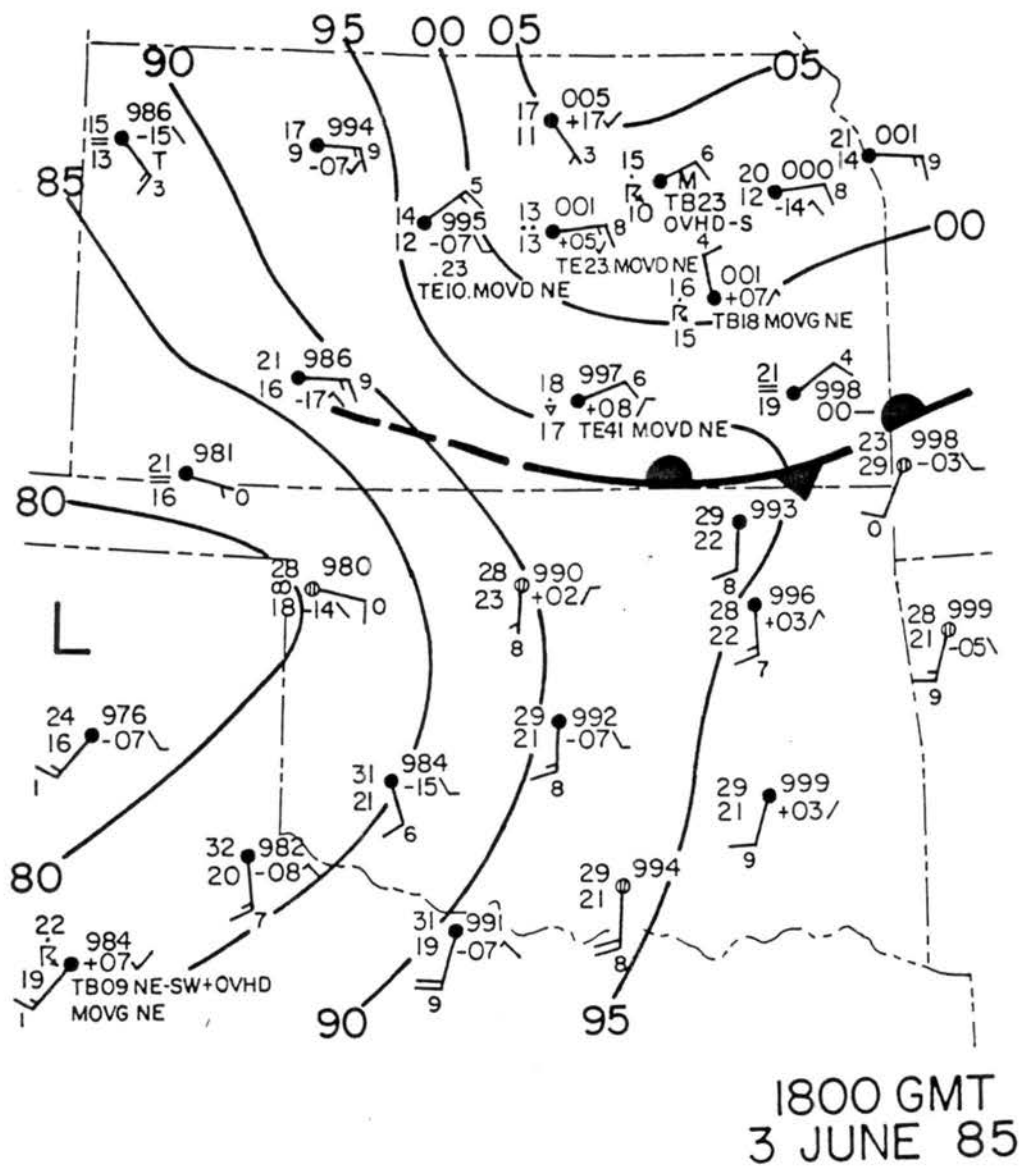


Figure 4.8: Same as Fig. 4.2 except for 1800 GMT 3 June 1985.

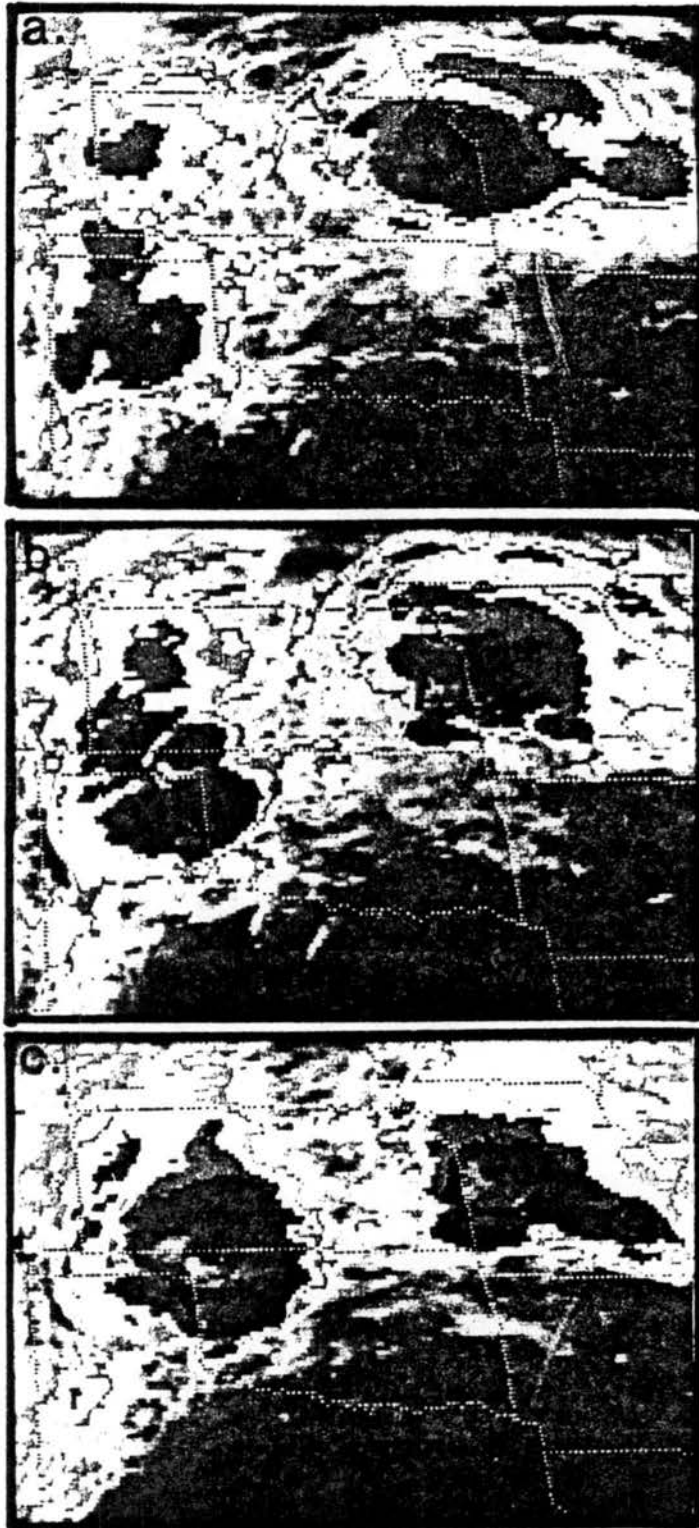


Fig. 4.9: Same as Fig. 4.5 except for: a) 1900 GMT 3 June 1985, b) 2000 GMT 3 June 1985, c) 2100 GMT 3 June 1985, d) 2200 GMT 3 June 1985, e) 2300 GMT 3 June 1985, f) 0000 GMT 4 June 1985, g) 0100 GMT 4 June 1985, h) 0200 GMT 4 June 1985, i) 0300 GMT 4 June 1985, j) 0400 GMT 4 June 1985.

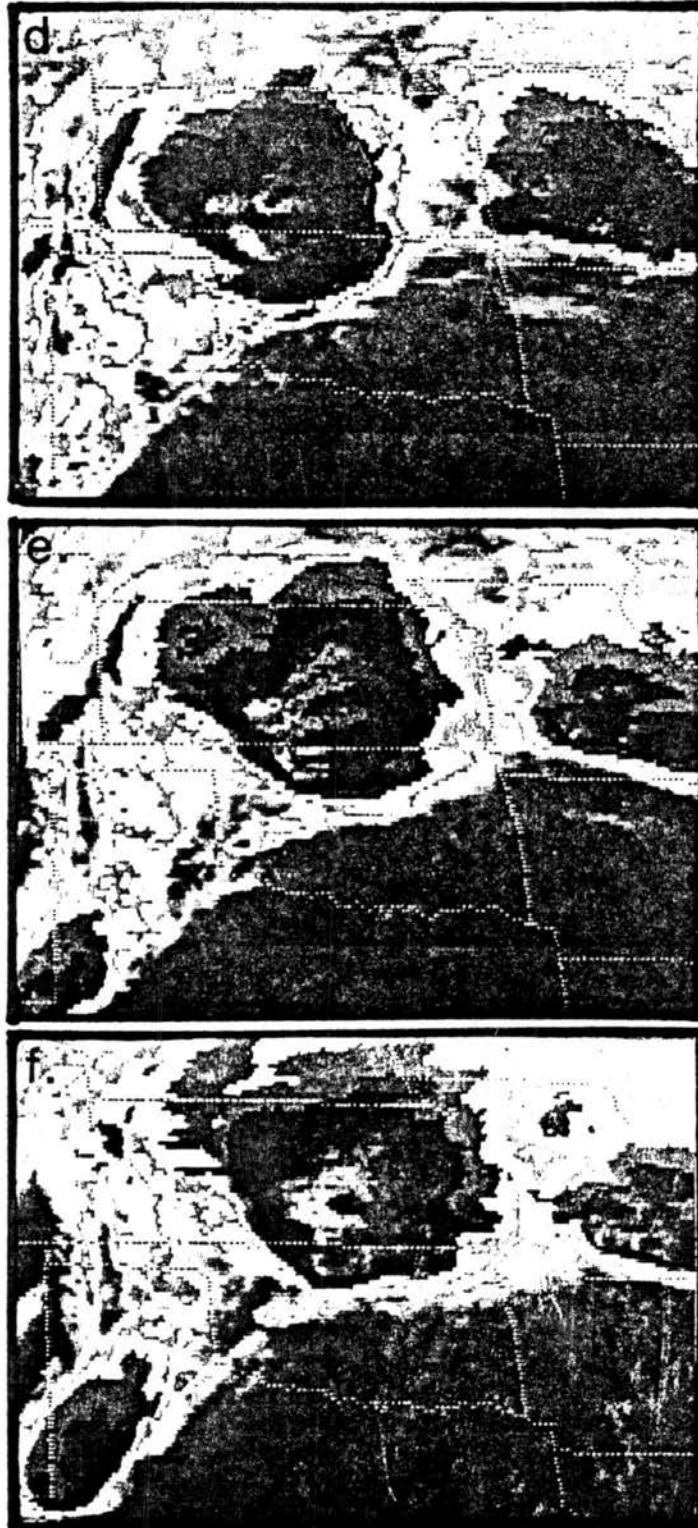


Fig. 4.9: Continued.



Fig. 4.9: Continued.

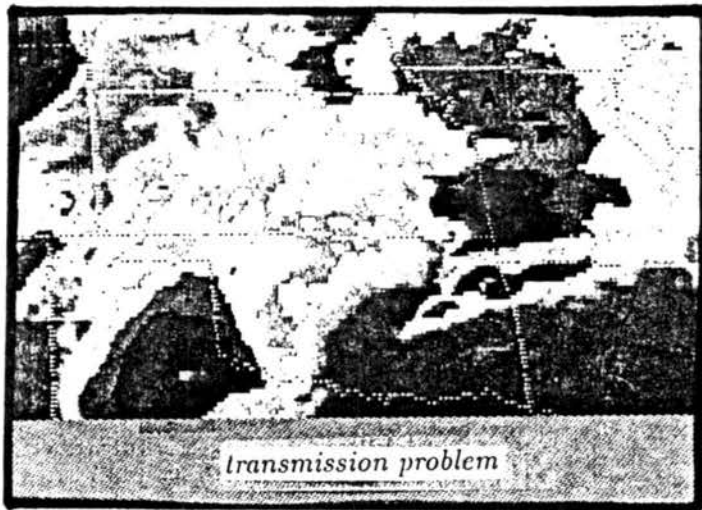
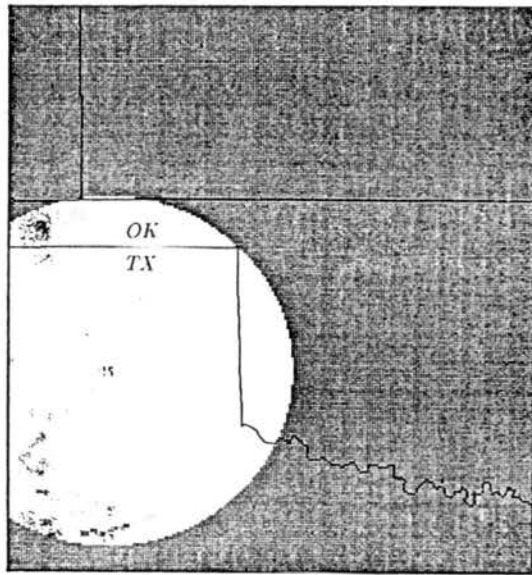


Fig. 4.9: Continued.

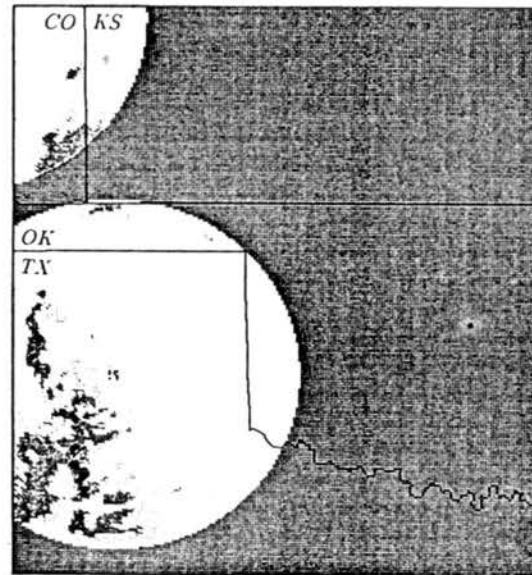
the Texas Panhandle. At 1752 GMT, the Lubbock TX (LBB) SAO had reported that a thunderstorm began within the last hour and that this storm was moving to the northeast. Also, at 1851 GMT, Amarillo TX (AMA) observed a similar report. Figures 4.9a-c show the area of convection was rapidly developing and moving to the northeast. The sequence of radar reflectivity patterns depicted in Figs. 4.10a-c shows the developing convection associated with MCS2 entering the PRE-STORM surface data domain, expanding in areal coverage, and strengthening. This represented the initial stage in the development of MCS2, a stage which was characterized by a "random" conglomeration of convective cells (Blanchard and Watson, 1987).

The coldest cloud tops were observed at 2200 GMT (temperatures $<-76^{\circ}\text{C}$; Fig. 4.9d), although the MCS had not reached maturity at this time. Also, the area of the cold cloud top with temperatures $<-54^{\circ}\text{C}$ had not expanded to its greatest extent yet. The largest areal extent of the cirrus cloud shield appeared to be around 0000 GMT 4 June (Fig. 4.9f). This is the approximate time when the MCS had reached its mature level. The cold cloud shield had assumed the size criteria for mesoscale convective complex (MCC) definition (Maddox, 1980). In fact, Augustine and Howard (1988) did classify this system as an MCC.

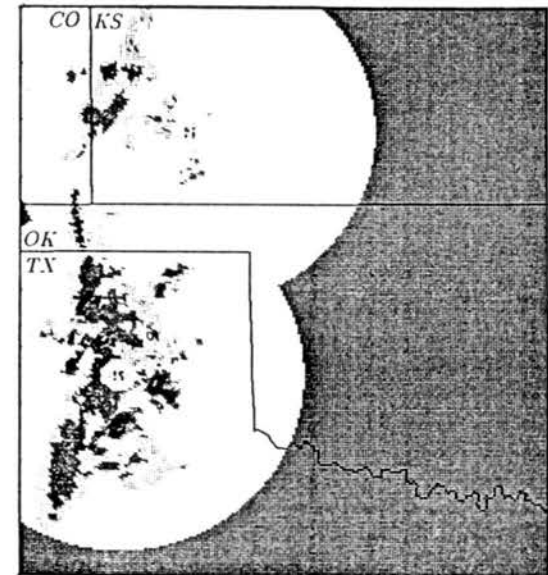
The radar sequence shown in Figs. 4.10a-l compares the surface precipitation development with the cloud features. Progressing through the radar overview, one can see that the system organizes from a "random" pattern of convective cells into a precipitation pattern resembling an occluded-type wave cyclone (Blanchard and Watson, 1986). This "occluded" pattern was associated with the mature phase of the MCS and is depicted in Figs. 4.10h,i. The northern part of the system was comprised mainly of stratiform rain with embedded WSW-ENE narrow bands of heavier precipitation. The southern part of the system was a north-south arc-shaped intense line of convection. This southern convective line led the list of severe weather reports (Storm Data, June 1985). An F1 tornado (Fujita, 1981) touched down around 0020 GMT in north-northeast Enid OK, and many reports of large hail were received, including golfball to baseball sized hail near Covington OK (the location of the tornado is represented by a "T" on Fig. 4.10h).



a) 1700 GMT 3 June 1985

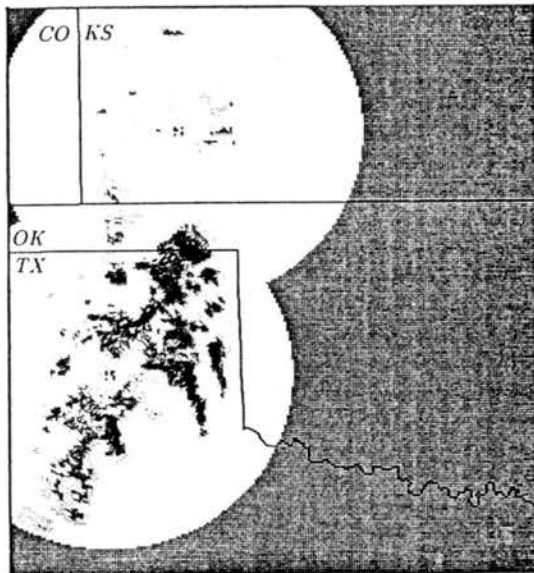


b) 1800 GMT 3 June 1985

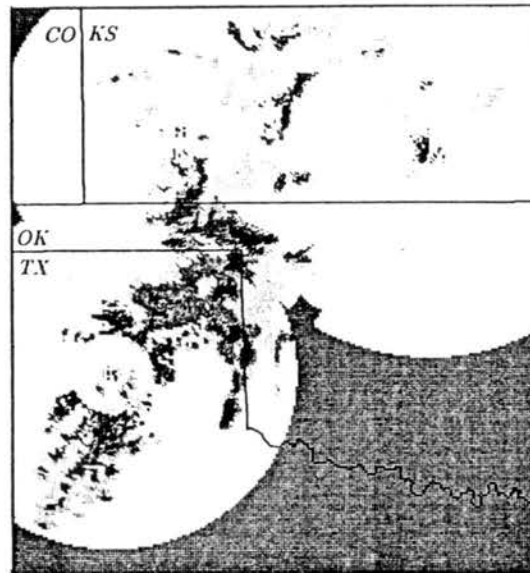


c) 1900 GMT 3 June 1985

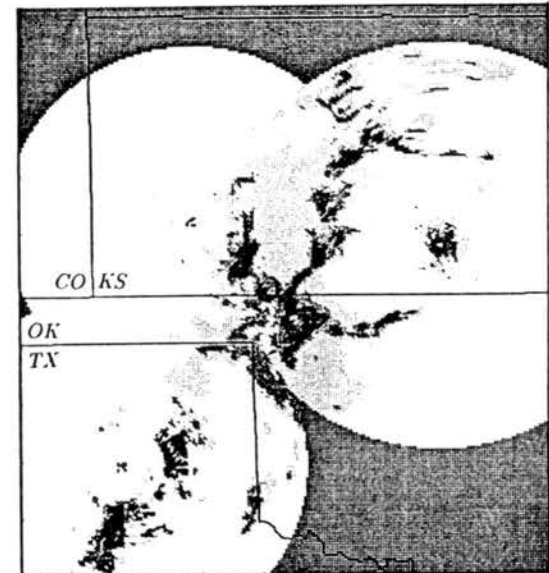
Fig. 4.10: Radar composites of RADAP-II digitized data. Reflectivity contours are 15, 25, 35, and 50 dBz. Figures include: a) 1700 GMT 3 June 1985 Amarillo TX; b) 1800 GMT 3 June 1985 Amarillo TX and Limon CO; c) 1900 GMT 3 June 1985 Amarillo TX, Limon CO, and Garden City KS; d) 2000 GMT 3 June 1985 Amarillo TX and Garden City KS; e) 2100 GMT 3 June 1985 Amarillo TX, Garden City KS, and Wichita KS; f) 2200 GMT 3 June 1985 Amarillo TX, Garden City KS, and Wichita KS; g) 2300 GMT 3 June 1985 Amarillo TX, Garden City KS, and Wichita KS; h) 0010 GMT 4 June 1985 Amarillo TX, Wichita KS, and Oklahoma City OK; i) 0110 GMT 4 June 1985 Amarillo TX, Wichita KS, and Oklahoma City OK; j) 0150 GMT 4 June 1985 Wichita KS and Oklahoma City OK; k) 0310 GMT 4 June 1985 Wichita KS and Oklahoma City OK; l) 0355 GMT 4 June 1985 Wichita KS and Oklahoma City OK.



d) 2000 GMT 3 June 1985

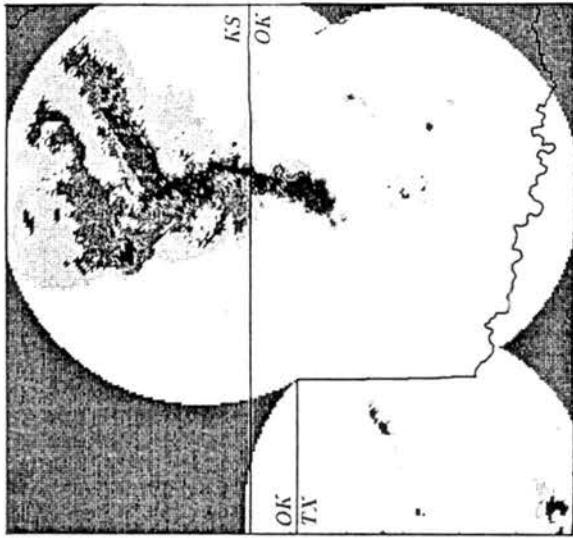


e) 2100 GMT 3 June 1985

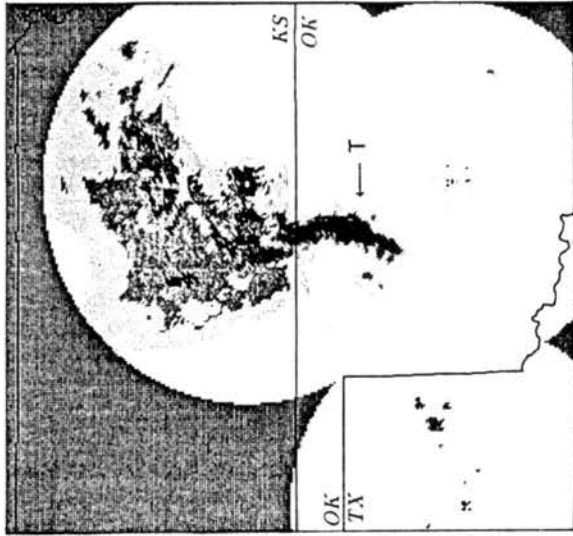


f) 2200 GMT 3 June 1985

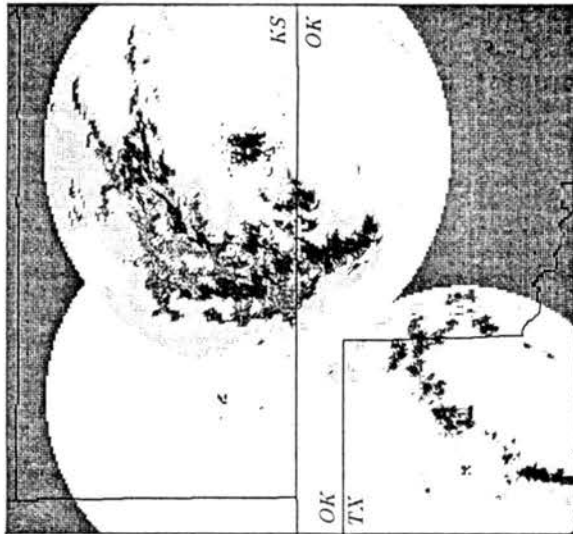
Fig. 4.10: Continued.



i) 0110 GMT 4 June 1985



h) 0010 GMT 4 June 1985

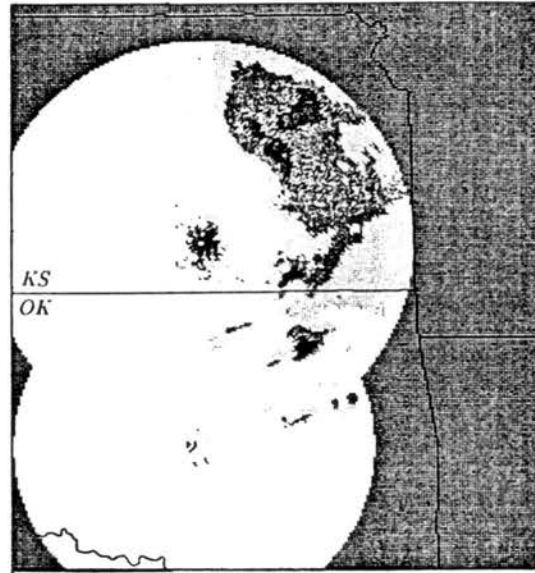


g) 2300 GMT 3 June 1985

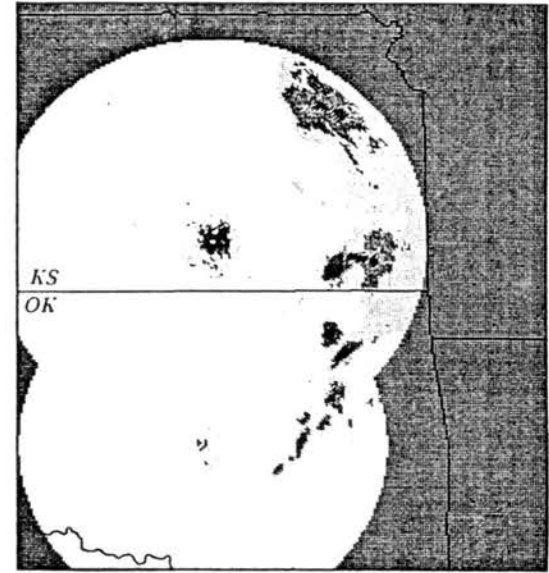
Fig. 4.10: Continued.



j) 0150 GMT 4 June 1985



k) 0310 GMT 4 June 1985



l) 0355 GMT 4 June 1985

Fig. 4.10: Continued.

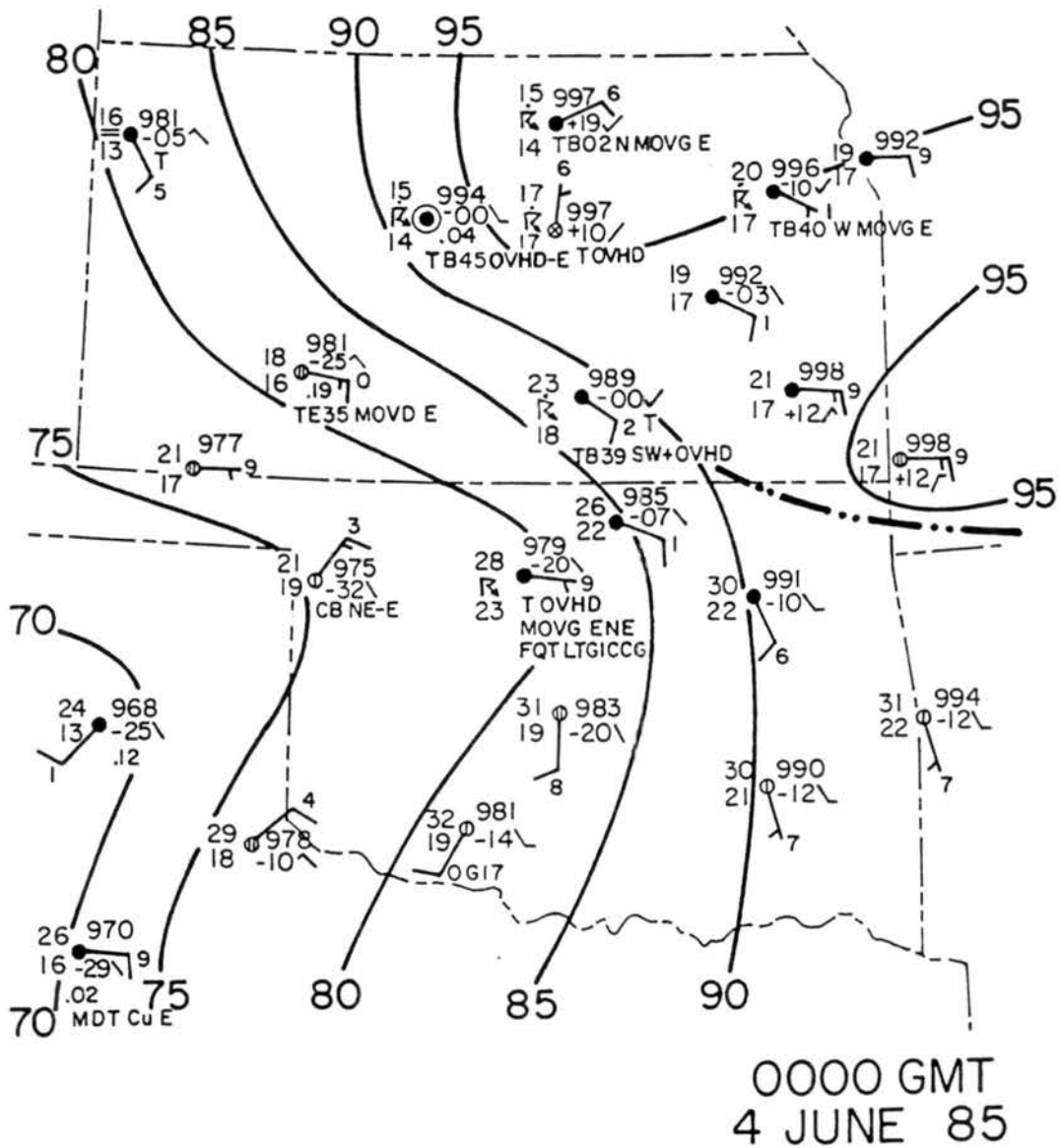


Figure 4.11: Same as Fig. 4.2 except for 0000 GMT 4 June 1985.

A surface analysis presented in Fig. 4.11 shows the situation at 0000 GMT. There is warm and moist surface inflow along the southeastern third of the analysis. Low-level outflow is in the west, to the rear of the MCS. Highest pressures are observed in the northcentral and northeast portion of the analysis. It will be shown in Chapter 5 that the sub-synoptic scale pressure features are much more complex than those shown in Fig. 4.11.

At 0000 GMT and 0100 GMT (Figs. 4.9f,g), it is somewhat apparent from the satellite pictures that the upper troposphere is characterized by a large amount of divergence associated with outflow at the top of the convection. As will be detailed in Section 5.2, the upper-level flow with MCS2 was basically along the line and divergent. Most of the upper-level flow is directed northeastward away from the strong convection in the southern segment of the MCS. This pattern is similar to that observed by Newton and Fankhauser (1964) and Fankhauser (1966). Some flow however is directed with a slight rearward component (to the north-northwest), but this is comparatively less than that directed northeastward (Smull and Jorgensen, 1987).

From 0100 through 0400 GMT, the cloud shield shows two maxima of coldest cloud tops (see "A" and "B" on Figs. 4.9g-j). Region "A" was over Central Kansas associated with the northern part of MCS2. Region "B" was associated with the intense convective line of the southern segment. By 0310 GMT, radar showed that the heavy convective cells within the southern segment of the MCS were separating from the northern area of stratiform rain (Fig. 4.10k). The convection was also weakening and the MCS had lost its "occluded" appearance. The last satellite picture in the sequence at 0400 GMT (Fig. 4.9j) shows a dissipating cloud mass. Cloud top temperatures were warming considerably. The coolest cloud tops were in southeast Kansas and northeast Oklahoma associated with the weakening southern convection (region "B"). The area of convection developing in the Texas Panhandle at this time (denoted by "C" on Fig. 4.9j) is the initial stage of MCS3 which was to move northeastward along a path similar to that followed by MCS2 (Fortune and McAnelly, 1986).

Chapter 5

THREE-DIMENSIONAL MESOSCALE STRUCTURE OF THE STORM AND ITS ENVIRONMENT: COMPARISON WITH LINEAR MESOSCALE CONVECTIVE SYSTEMS

The purpose of this chapter is to document the mesoscale surface and upper air life-cycle of the second MCS of 3-4 June 1985. Fortunately, the MCS matured near the center of the mesonet network. The observations presented in this chapter will be compared to observation of linear MCSs with trailing stratiform rain regions.

5.1 Surface observations

This section will document the detailed mesoscale surface features associated with MCS2. Some of the typical mesoscale pressure patterns associated with squall lines with trailing stratiform rain regions were identified in this case study, including a pre-squall trough, a mesohigh, and a wake low. Moreover, these features exhibited dramatic spatial and temporal intensity changes with this case. Also, some of the typical surface wind patterns found in relation to squall lines with trailing stratiform rain were discovered with this case.

The eighty-four automated observing stations deployed for the PRE-STORM project provided an excellent opportunity to record and observe the detailed spatial and temporal structure of MCSs traversing across the mesonet network. Data was collected in most instances at 5-minute intervals on a 50 kilometer grid providing excellent coverage and resolution to study the surface meteorological parameters associated with MCSs.

5.1.1 Pressure and wind analyses

The following analyses will present a series of maps which show contours of adjusted pressure (hereafter referred to as *pressure* in this section). Station plots of temperature, dewpoint, and winds are also provided on the analyses. These station plots were constructed using the meteorological plotting software available on Colorado State University's VAX 11/750 (GEMPAK¹; Vonder Haar *et al.*, 1987). Radar reflectivity composites at the time closest to the surface analyses are overlaid on these plots to compare the surface features to the precipitation patterns. Streamline analyses are also presented, with radar patterns overlaid on these analyses as well.

The sequence of surface analyses begins at 2000 GMT on 3 June 1985. MCS1 is still affecting the northeast corner of the mesonet network at this time and is retreating out of the PRE-STORM domain. Figure 5.1a shows the surface pressure pattern at this time. Highest pressures were observed in the northeast corner of the analysis domain in relation with MCS1. This mesohigh is associated with the precipitation-cooled air of MCS1. Light to moderate rain is being observed here with some embedded heavier areas of convection apparent on radar. Fig. 5.1b shows the wind pattern at this time, and a wind shift line is evident at the southwest portion of MCS1. The temperature difference across this boundary is roughly 11°C. It is believed that this wind shift is the warm front which was in Central Oklahoma at 1200 GMT (Fig. 4.2) and moved north to its location at 2000 GMT. Furthermore, it is felt that rearward low-level cool moist outflow from MCS1 has somewhat enhanced the temperature gradient and convergence across this wind shift line. Smull and Houze (1985) observed convergence along the south side of the wake of an Oklahoma squall line which enhanced future development. This boundary stretches into extreme northcentral Oklahoma and then curves northwestward where it becomes less defined.

Precipitation from the "random" (Blanchard and Watson, 1987) convective area in the Texas Panhandle associated with the developing MCS2 was just entering the western

¹GEneral Meteorological PAcKage.

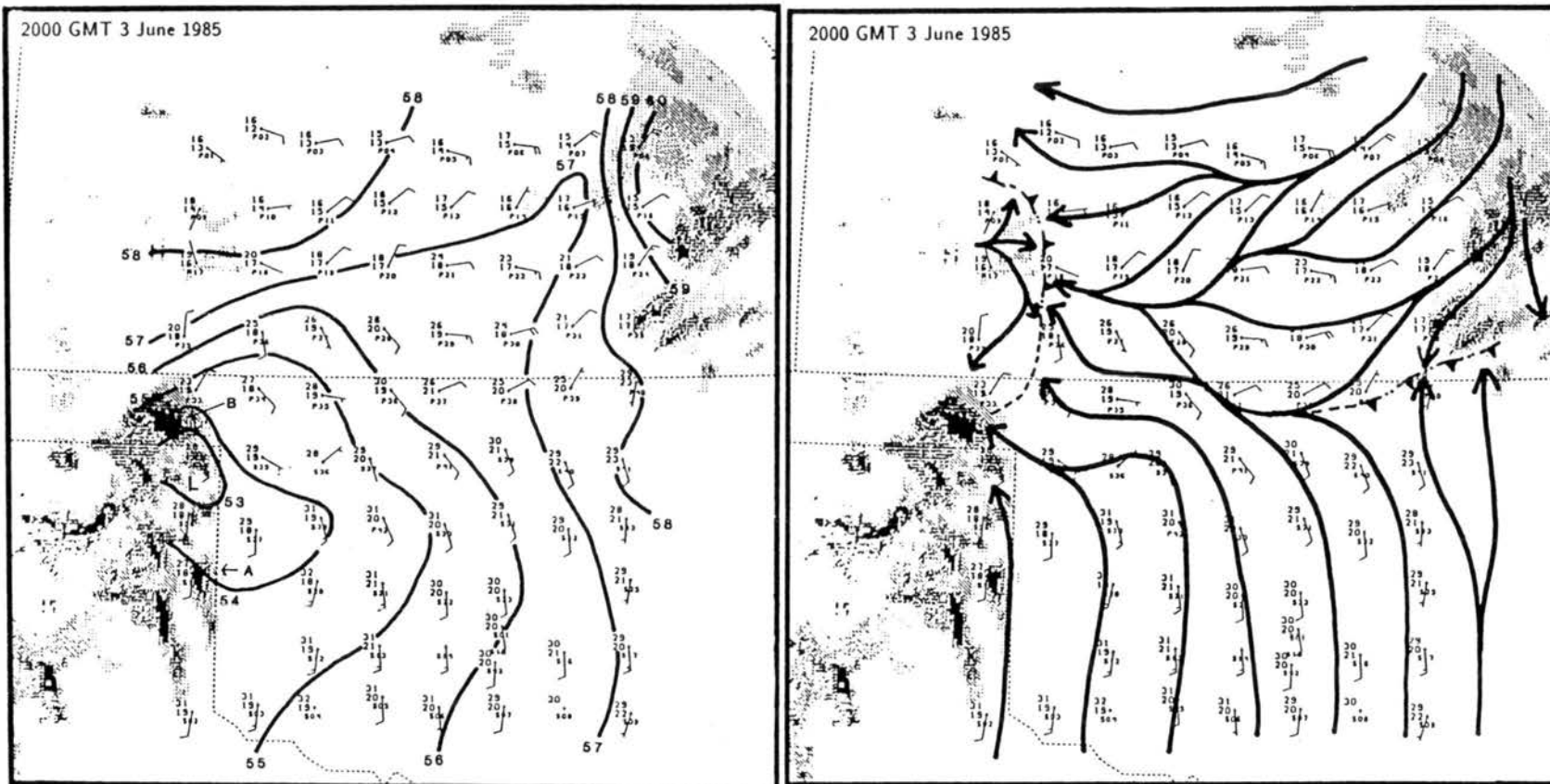


Figure 5.1: Surface analysis of: a) adjusted pressure in mb (e.g., 59 = 959 mb); and b) streamlines, at 2000 GMT 3 June 1985 for PAM and SAM. Station plots include temperature and dewpoint (in °C), and wind (one barb equals 5 m s^{-1}). Overlaid are radar reflectivity composites (from Fig. 4.10) with intervals of 15, 25, 35, and 50 dBz.

edge of the mesonetnetwork at 2000 GMT. A broad mesolow was in western Oklahoma, just ahead of the leading edge of convection associated with MCS2 (see Fig. 5.1a). A low pressure trough extended northeastward out of this mesolow through central Kansas and into the wake low of MCS1. This trough is in the same position of the trough analyzed at 1100 GMT (Fig. 4.3). Interestingly, the trough axis coincides with the approximate tracks of the three MCSs which traversed the mesonetnetwork during the 3-4 June 1985 period (Fig. 4.1). Two bands of intense convection aligned at about 340° are evident on the south side of the entire convective area. There has been no effect of the convection on the western edge of the SAM stations yet [the precipitation east of S18 (labelled "A" on Fig. 5.1a) apparently developed *in situ*]. Generally, winds were south to southeast in Oklahoma but east to northeast in most of Kansas (see Fig. 5.1b). One exception was where light showers were entering the western edge of the PAM mesonetnetwork. These showers were producing a weak arc-shaped outflow boundary in this area. An intense cell at the east end of the Oklahoma Panhandle (labelled "B" on Fig. 5.1a) may be the result of convergence along the southern end of this outflow boundary.

Continuing on to 2100 GMT, a mesohigh has appeared behind a band of heavier convection in the southwest portion of the mesonetnetwork (labelled "C" in Fig. 5.2a). This line of convection marks a wind shift boundary (Fig. 5.2b). Winds have shifted to the west behind the boundary, and temperatures have fallen. Precipitation in northwest portion of the analysis is increasing in intensity and areal coverage. Associated with this is an area of developing high pressure. The outflow boundary associated with this northern precipitation has disintegrated except along its south and southeast edges, where it continues to spread south. A pre-squall mesolow is now very well defined ahead of the convection (Fig. 5.2a). The lighter reflectivity areas here are indicative of a forward anvil since the Amarillo TX radar beam is well above the ground near these locations (rain had yet to be recorded at mesonetnetwork stations covered by these lighter reflectivities). Adiabatic warming aloft due to subsidence in the forward anvil could be causing a hydrostatic surface pressure reduction and strengthening the pre-squall low (Hoxit *et al.*, 1976). On the streamline analysis (Fig. 5.2b), four distinct wind flow areas are evident at 2100 GMT.

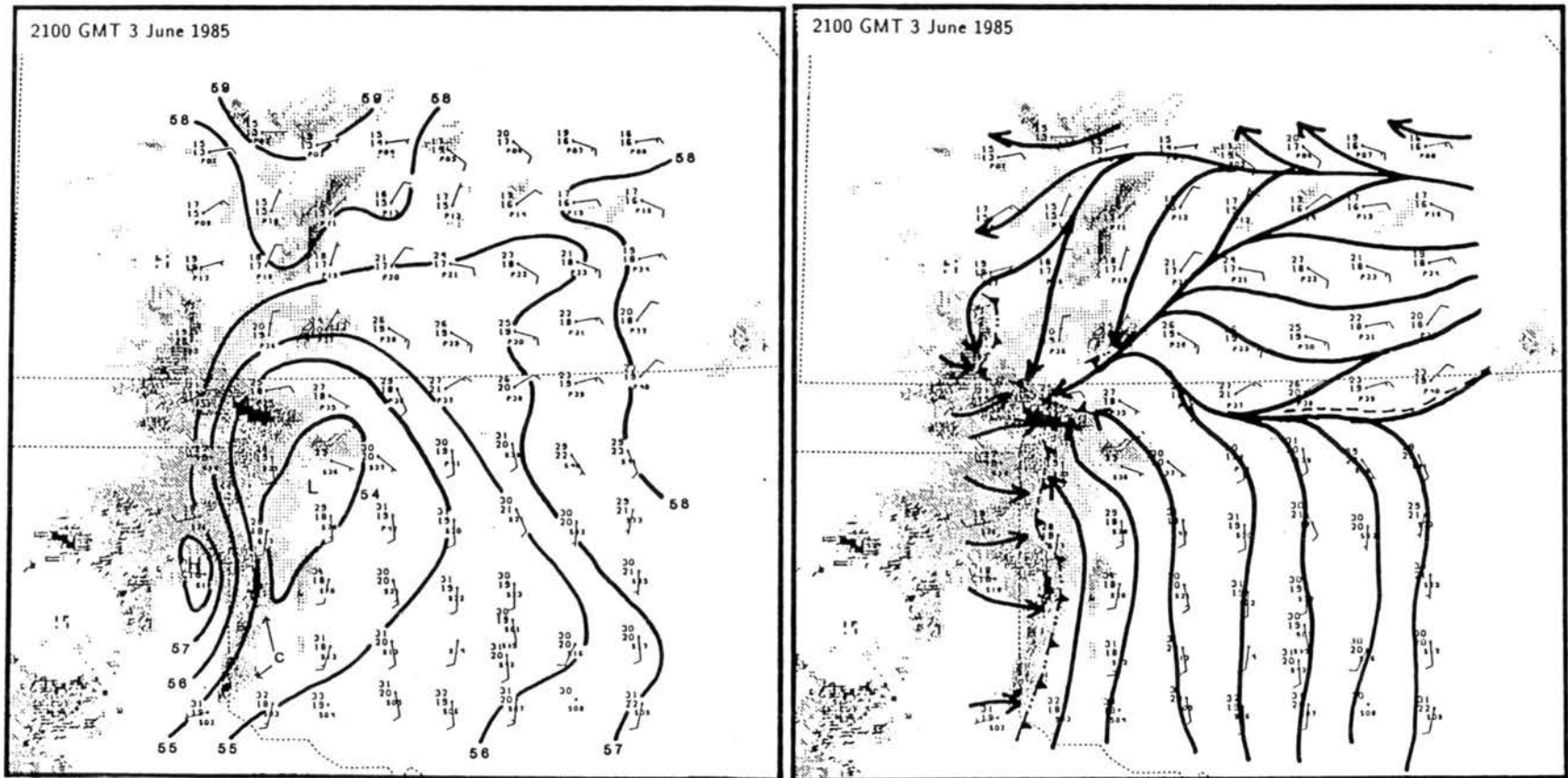


Fig. 5.2: Same as 5.1 except for 2100 GMT 3 June 1985.

First are the westerly winds behind the leading edge of the convection. Second are the warm moist southerly winds in Oklahoma ahead of the convection. Separated by the old warm frontal convergence boundary is the third area, the easterly outflow from MCS1 in the northeast section of the mesonetwork. And last are the north-northeast winds north and west of the persistent low pressure trough stretching out of the pre-squall low into Kansas (see Figs. 4.3, 5.1a).

By 2200 GMT, some dramatic developments are occurring across the surface mesonetwork (Fig. 5.3). The north-south band of convection in southwest Oklahoma ("C" on Fig. 5.3a) is breaking up, but the wind shift line associated with it still exists and continues to move east. As will be shown in section 5.2, a lower tropospheric inversion or "cap" was apparent in upper air soundings in southern Oklahoma. The strength of the "cap" may have prohibited convective development in this area. Also, lower tropospheric soundings were much drier in the south. Intense convection has evolved in an east-west line just south of the Kansas- Oklahoma border ("D" on Fig. 5.3a). This line, east of the main area of precipitation, developed along the convergence line/warm front. It is felt that the interaction of this new east-west convective line with the main convective area may have played a role in the redevelopment of an intense line of convection along the wind shift line in the southern portion of the MCS. As will be shown, this line of convection redeveloped in northcentral Oklahoma after 2300 GMT. This region had a more favorable vertical thermodynamic structure for intense convective development than that observed in southern Oklahoma (e.g., the "cap" was weaker).

The pre-squall mesolow and trough extending northeastward from it are moving east with the MCS at 2300 GMT (Fig. 5.3a). A mesohigh has appeared over the northern segment of the MCS in relation with an expanding stratiform rain area. Some embedded NE-SW bands of heavier convection are at the leading edge of this stratiform precipitation area in Kansas (labelled "E" on Fig. 5.3a). The wind flow under the mesohigh is strongly divergent with the rearward outflow from the system now discernible (Fig. 5.3b).

During the next few hours, MCS2 reaches its mature phase and assumes its "occluded" appearance (Blanchard and Watson, 1987). The typical surface pressure features found

in other studies of MCS, for instance squall lines with trailing stratiform rain regions, develop. At 2300 GMT, a broad mesohigh is centered over the stratiform rain area in the northern segment of the MCS (Fig. 5.4a). The mesohigh is located behind the leading edge of the rain instead of at its leading edge as observed by Johnson and Hamilton (1988) in a squall line case. In their case, the strongest radar reflectivities were at the leading edge whereas for MCS2, a maximum in reflectivity was observed closer to the center of the stratiform rain area. This suggests that the strongest cooling and subsequent greatest pressure rises are occurring where the heaviest rain is observed. A ridge of high pressure follows the developing heavier band of convection in the southern part of the MCS. The mesolow which was in western Oklahoma weakens while the pre-squall trough deepens slightly [a mesolow develops ahead of the MCS at 2330 GMT (figure not shown)]. A wake trough is now observed at the back edge of the stratiform rain in the northern segment of the MCS. Typically, the wake low forms a few hours succeeding the mesohigh [Fujita (1963), Johnson and Hamilton (1988)]. In this case, its existence is determined only after it entered the western edge of the mesonetwork.

The northern and southern parts of the MCS are developing contrasting pressure patterns at this time (Fig. 5.4a). The mesohigh and wake low are more pronounced in the northern part, while the pre-squall trough extends ahead of the entire system. This is interesting because the southern part of the system, begins to take on a more classic squall line shape, while the northern part is comprised of mainly stratiform rain with embedded heavier convection. It appears that the physical processes within the stratiform anvil are responsible for the intense pressure features. This will be discussed some more later.

The east-west convective line which was just south of the Oklahoma-Kansas border collapsed leaving a small pool of cold air about 50 to 100 km in diameter in its place (see "D" on Fig. 5.4a). The southern "squall line" (labelled "F") extended only about 100 km south of the border with a wind shift line continuing southwestward to the Oklahoma-Texas border at the Red River.

The surface wind patterns at 2300 GMT (Fig. 5.4b) on the northern part are very similar to what was found by Johnson and Hamilton (1988; see Fig. 2.1). East of the

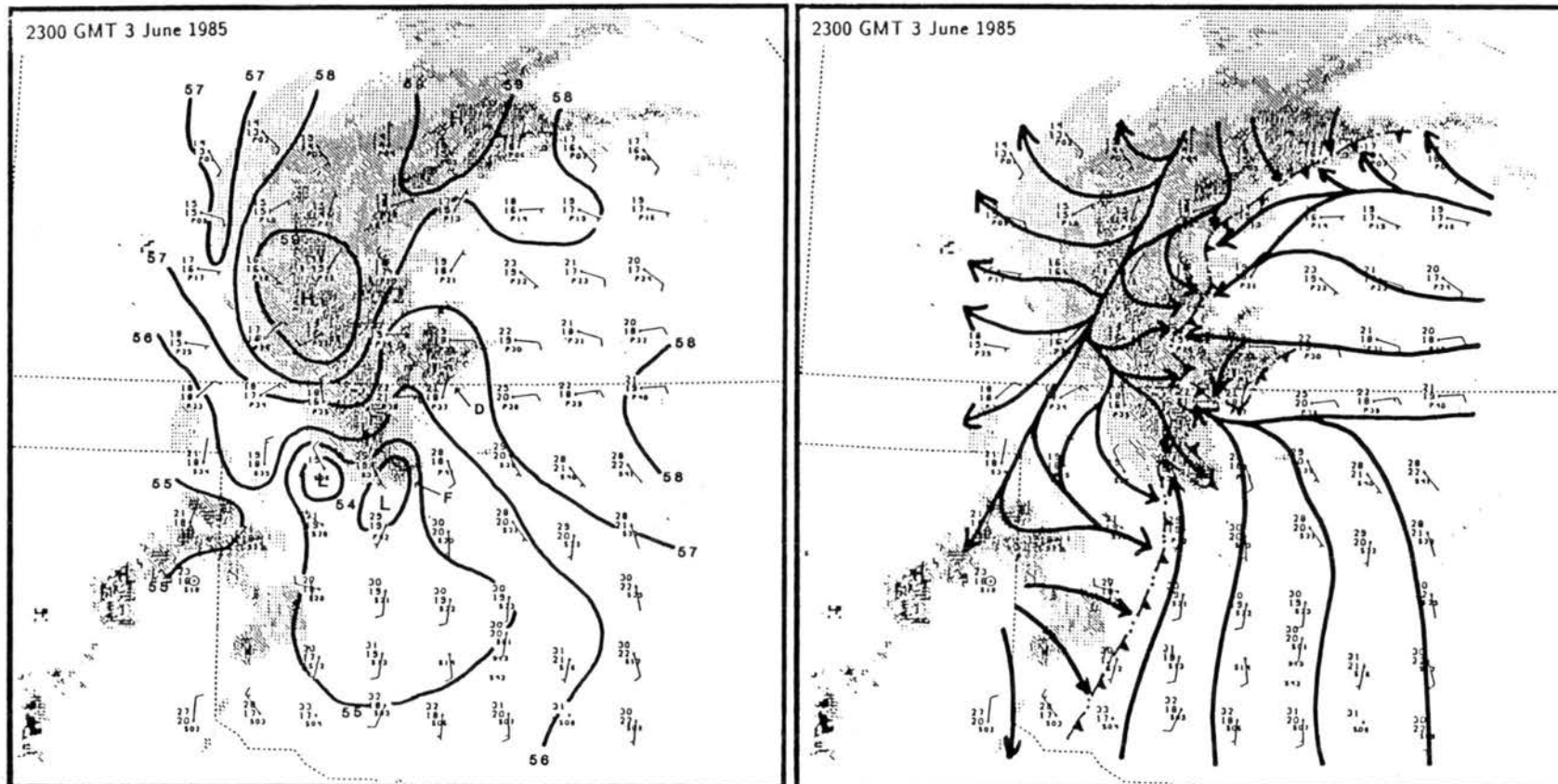


Fig. 5.4: Same as 5.1 except for 2300 GMT 3 June 1985.

convection, the wind is mainly easterly, inflowing into the system. However, behind the wind shift line at the leading edge of the precipitation, winds are strongly divergent. A divergence axis is situated on the back side of the mesohigh. Air is blowing to the east through the mesohigh and to the west through the wake low at nearly right angles to the isobars.

The system appears to peak in maturity at about 0020 GMT. As can be seen on Fig. 5.5, the system looks very similar to a miniature "occluded" wave cyclone. To the north is a large stratiform rain area with embedded bands of convection oriented about 240° . The southern part appears to be a narrow line (about 25-30 kilometers wide) of intense convection in a bow-like shape ("bow echo"; Fujita, 1981). One intense cell (denoted by a "T" in Fig. 5.5a) within this southern line produced an F1 tornado near Enid OK at this time. A leading area of stratiform rain seems to be developing a few tens of kilometers ahead of the windshift in Kansas. This indicates that a forward precipitating anvil is present in this area.

The pressure patterns at 0020 GMT (Fig. 5.5a) are very striking. The mesohigh is now over 961 mb and centered in the heart of the stratiform rain area. A high pressure ridge extends along the southern appendage. A wake trough with a mesolow centered near station P11 is "hugging" the rear edge of the the northern stratiform rain area. This was also observed by Johnson and Hamilton (1988; Fig. 2.1). Williams (1953, 1954) and Pedgley (1962) observed a cessation of precipitation at the time of the lowest pressure. An extreme pressure gradient is found along the back edge of the mesohigh and northern stratiform rain region, between it and the wake low. The pressure difference between the mesohigh and the wake low (whose centers are about 100 km apart) is close to 6 mb. Locally, the pressure gradient is nearly 1 mb per 10 km. Also, a "heat burst" (Johnson, 1983) occurred at station P19 at this time in the wake of the MCS (this is depicted as "HB" on Fig. 5.5a). Heat bursts are a manifestation of the downdraft in the trailing anvil. Appendix C discusses this heat burst in detail and gives insight into the physical mechanisms involved in heat burst production. The pre-squall trough is now evident only ahead of the southern part of the MCS.

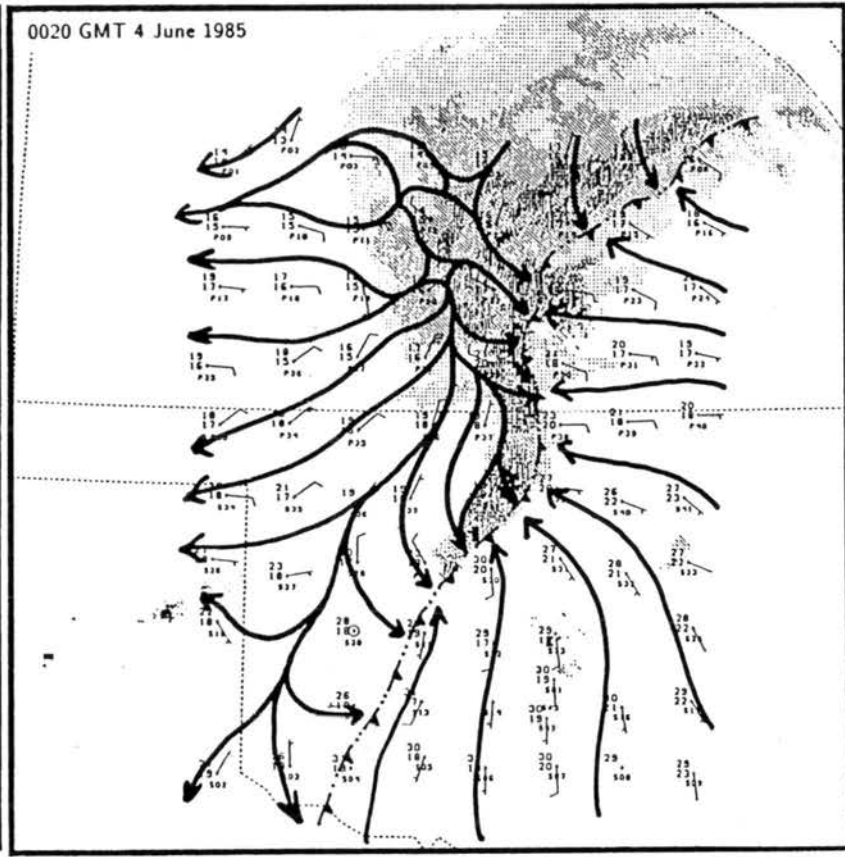
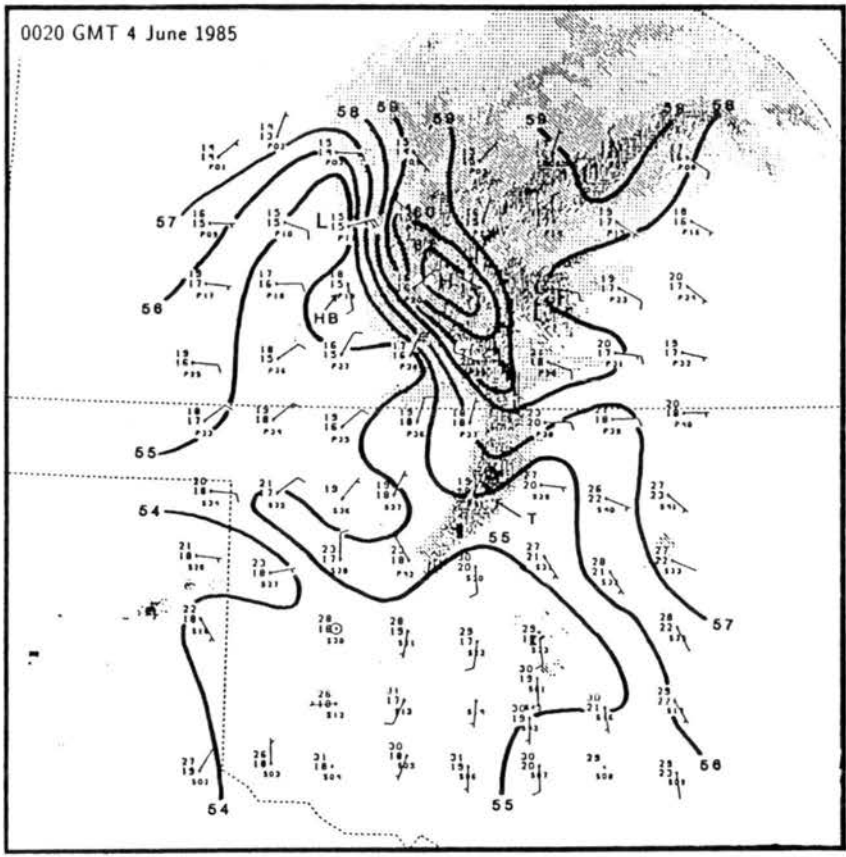


Fig. 5.5: Same as 5.1 except for 0020 GMT 4 June 1985.

Comparatively, the surface pressure features depicted on Fig. 5.5a are very different than those observed on Fig. 4.11, the NWS depiction. Although the analysis shown in Fig. 4.11 shows a gradual decrease in pressure from northeast to southwest, it completely misses the intense mesohigh observed within the stratiform rain region. This illustrates the advantage of high density surface observations in the study of mesoscale weather systems.

The surface wind pattern at 0020 GMT (Fig. 5.5b) reveals that easterlies are ahead of the MCS feeding the system with warm moist potentially unstable air. Convergence is at the leading edge of the rain along an unbroken wind shift line from the northeast corner of the mesonet network southwestward to the Oklahoma-Texas border along the Red River. Behind the wind shift is a divergent area associated with the outflow from the mesohigh. A large area of east to northeast outflow is evident behind the system (as was the case with MCS1), blowing through the wake low.

Through 0120 GMT, the MCS begins to enter its dissipating stage. The mesohigh appears to maintain the same intensity (≥ 961 mb), but the wake low has deepened to below 954 mb and was centered just to the rear of the stratiform rain at the northern edge of the mesonet network² (Fig. 5.6a). Fujita (1963), Williams (1963), and Johnson and Hamilton (1988) also observed that the peak in lowest pressure associated with the wake low coincided with the dissipating stage of an MCS. Recall that this wake low position at the rear edge of the rain was also found by Johnson and Hamilton (1988; Fig. 2.1) in a squall line with a trailing stratiform rain region. The pressure gradient between the mesohigh and the wake low increased further from the 0020 GMT analysis time. Locally, the gradient increased to an incredible 2 mb in 10 km! A 6 mb drop in pressure in about 30 minutes was recorded at station P12 between 0045 and 0015 GMT (Fig. 5.7). It is interesting to note that the wake low appears to be strongest just west of a maximum in the stratiform radar reflectivity. The southern convective appendage is beginning to weaken somewhat. A wake low is not observed immediately behind the southern segment, only a ridge of high pressure.

²The wake low may have been deeper north of the PAM mesonet network, but this is unknown given the data coverage.

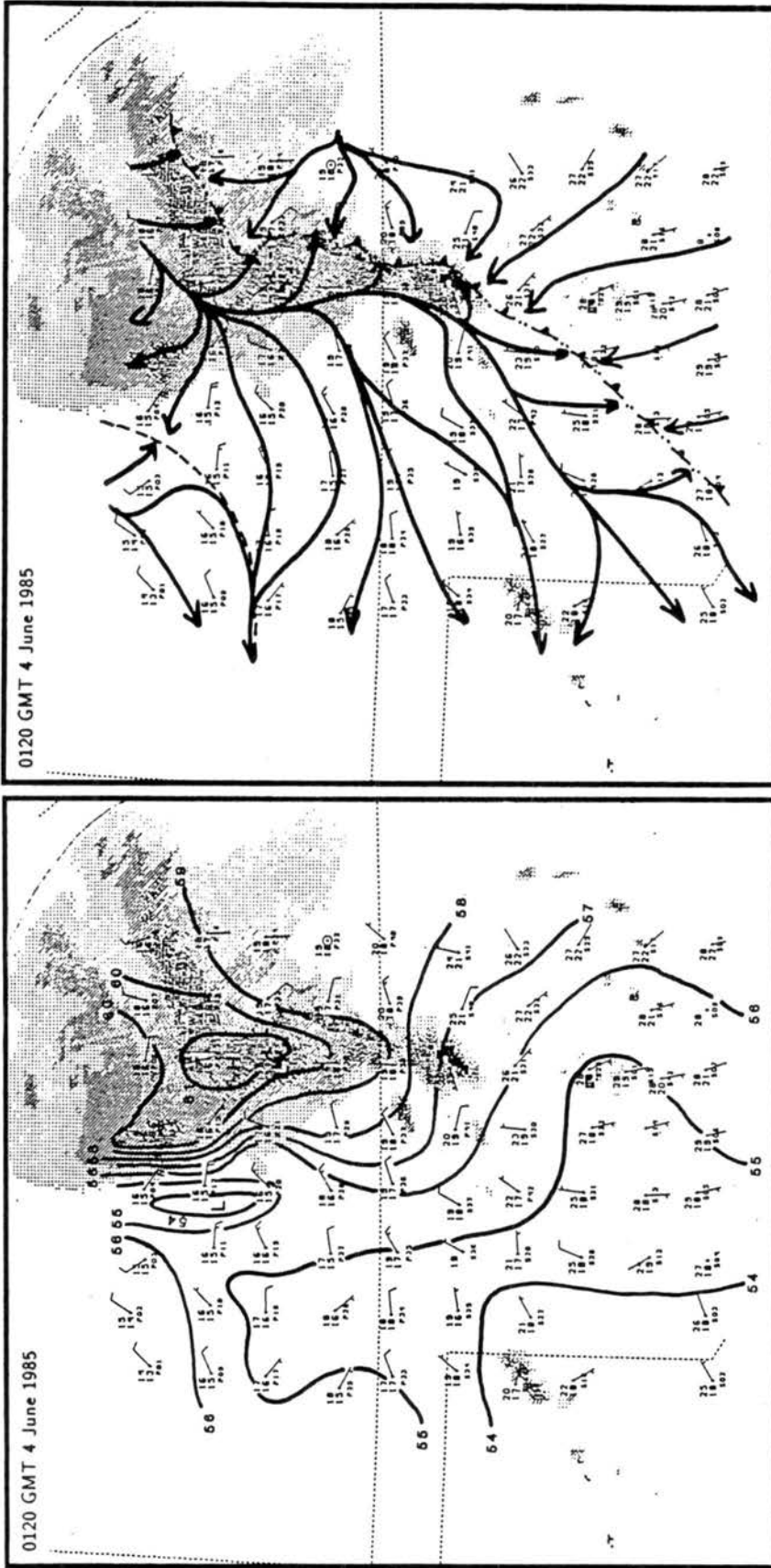


Fig. 5.6: Same as 5.1 except for 0120 GMT 4 June 1985.



Figure 5.7: Time series plot of adjusted pressure for station P12. Time is in GMT and increases to the left. Pressure is in mb.

A leading area of stratiform rain is developing ahead of the leading wind shift line in the northern segment of the MCS. It will be detailed in upcoming sections that a significant upper tropospheric forward storm-relative flow was present. This accounted for a predominantly forward leaning anvil coupled with the subsequent development of a forward stratiform rain region in the later stages of the MCS's history.

At 0120 GMT, winds blowing through the wake low are stronger now (up to 10 m s^{-1} sustained), and a convergence line is now observed to the rear of the wake low (Fig. 5.6b). In some case studies, a convergence line in an MCS wake has been documented to trigger new convection if the atmosphere is convectively stable in the region [Williams (1963), Koch and McCarthy (1982), Johnson and Hamilton (1988), Stumpf and Gallus (1989)].

At 0150 GMT, a deep wake low still is apparent at the rear edge of the northern stratiform rain region (Fig. 5.8a). The center of the wake low is not "hugging" the back edge of the stratiform precipitation anymore. However, the strong gradient on its east side still is. This suggests that there is still strong subsidence warming occurring aloft under the trailing anvil. The forward stratiform rain area is increasing in coverage, but the entire stratiform rain area as a whole is decreasing in intensity. A strong cell just south of the Kansas-Oklahoma border (see "G" on Fig. 5.8a) appears to be detaching from the northern section of the MCS. The most striking feature on the streamline analysis is the divergent outflow associated with the precipitation area of the MCS (Fig. 5.8b). A diffluence axis runs through the middle of the stratiform rain area in the north, lining up with the rear edge of the convective line in the south. Convergence still exists along the leading edge of the convective southern line, but extends northward into the forward stratiform rain area, just ahead of the heavier rain. The southernmost portion of this convergence line is starting to decompose. Convergence still resides in the area immediately to the rear of the wake low.

By 0300 GMT, the MCS2 is all but gone from the mesonet network. Pressure associated with the mesohigh was the greatest just before this time (at 0230 GMT, pressure reached $\sim 964 \text{ mb}$ at station P16). The wake low still has about the same central pressure, but

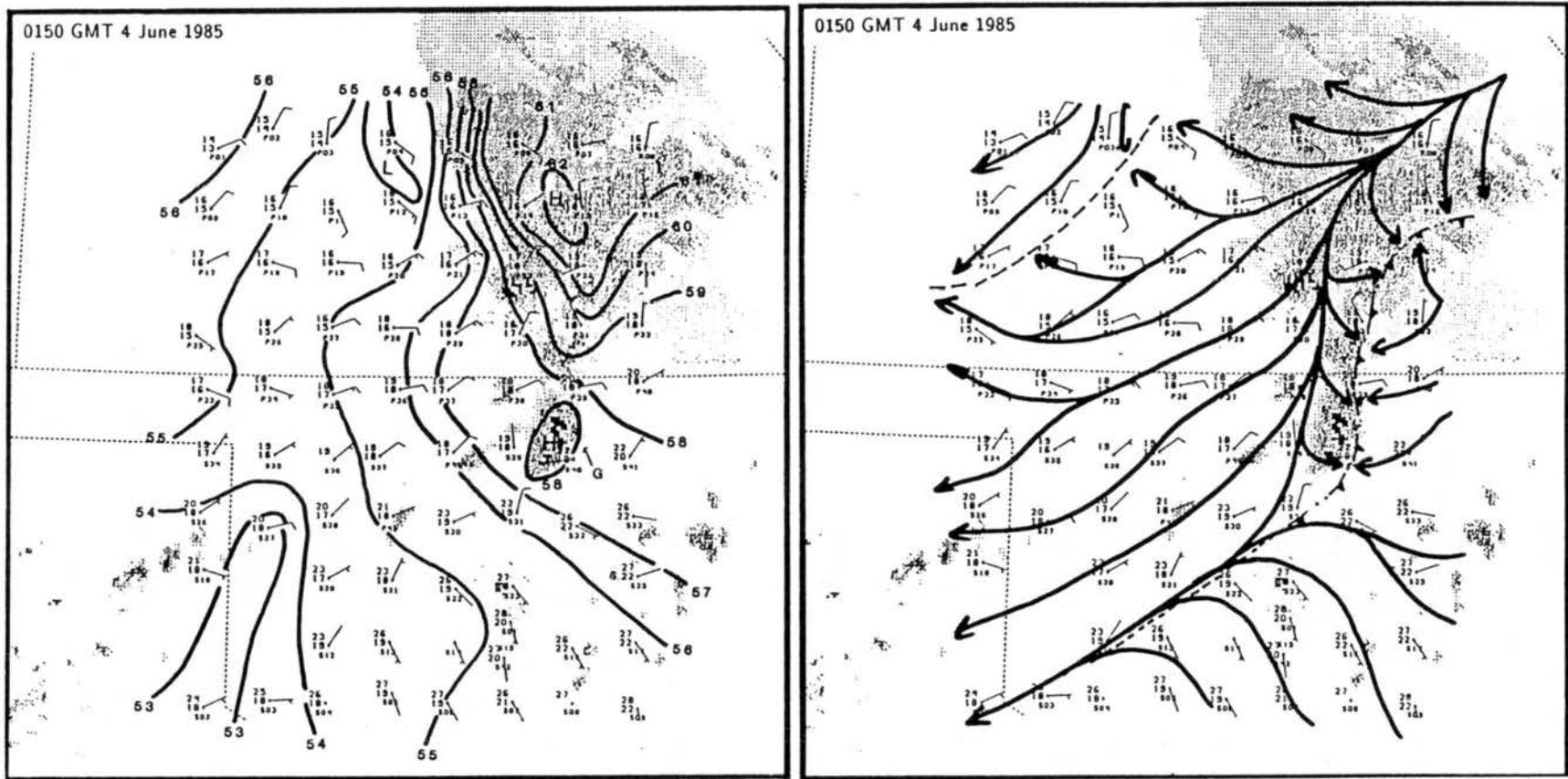


Fig. 5.8: Same as 5.1 except for 0150 GMT 4 June 1985.

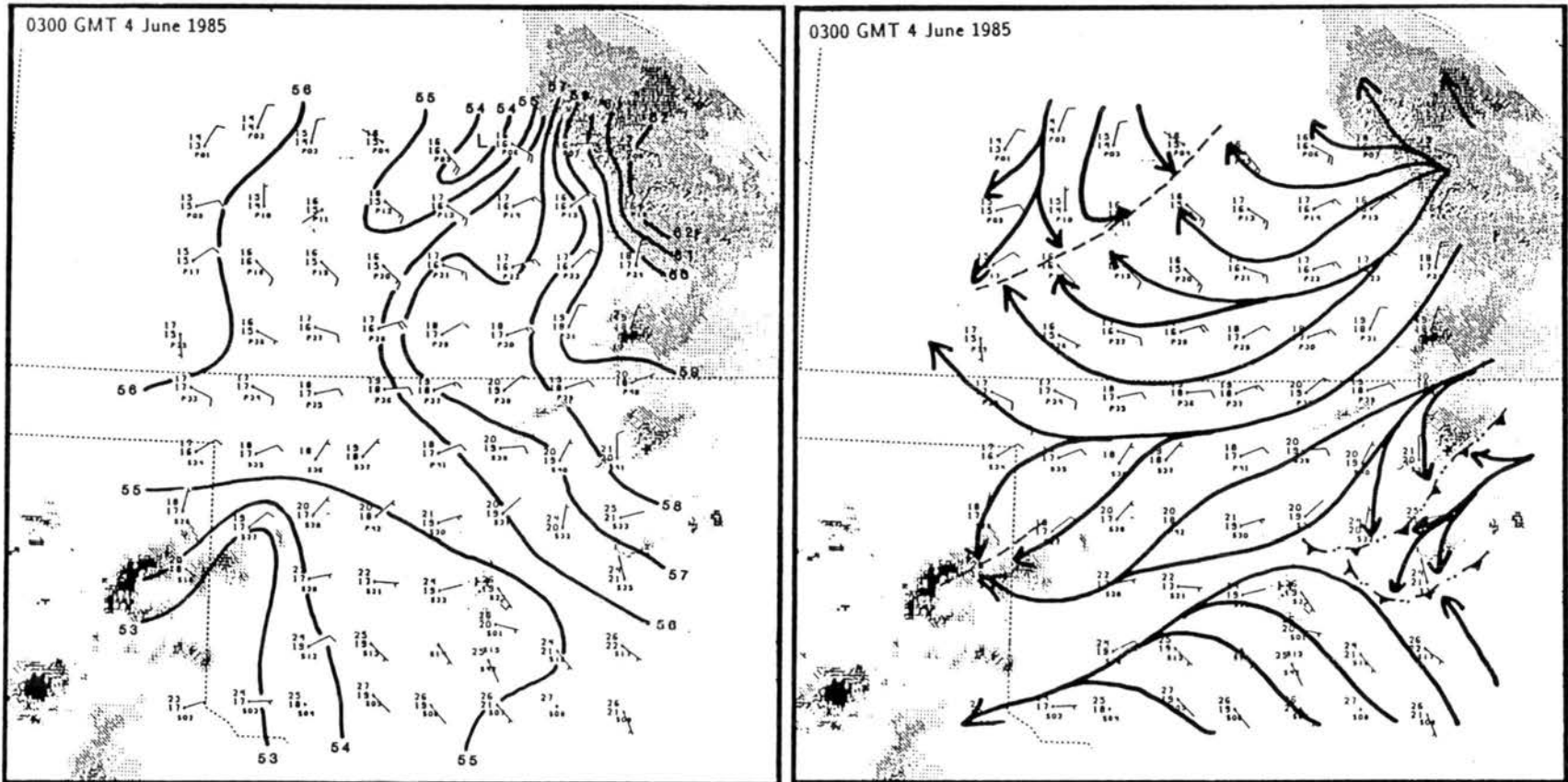


Fig. 5.9: Same as 5.1 except for 0300 GMT 4 June 1985.

appears to be lagging the rear edge of the stratiform rain (Fig. 5.9a). Winds are sustained at 10 m s^{-1} blowing through the wake low to convergence to its rear (Fig. 5.9b). The southern convective line broke apart, and several convergence boundaries associated with some dying convective cells are apparent in eastern Oklahoma. Convection developing in the Texas Panhandle is the initial stage of MCS3 [Fig. 4.9i; Fortune and McAnelly (1986) have studied this system].

This surface mesonet network overview showed the complex structure of the MCS, its ever changing features, and its similarities to linear MCSs with trailing stratiform rain regions. Important findings included the discovery of an intense gradient between the mesohigh and the wake low. Also, the absence of a significant wake low and mesohigh in the southern part of the MCS appears to have some important implications. As the paper continues, upper air observations will highlight the reasons why we believe the most intense surface pressure features were only observed in the north.

5.1.2 Time series of surface pressure

Time series plots of adjusted pressure for most of the mesonet network stations have been reduced in size and are arranged together in Fig. 5.10. The format of the plots are the same as Fig. 5.7 (station P12). Horizontal lines represent pressure with a spacing of 1 mb. Vertical lines represent time, with the spacing one hour. Time increases to the *left* on each plot. The advantage of having time increase to the left is to simulate a “cross-section” from west to east (left to right) of pressure through the MCS as recorded at each station. For example, wake lows will appear on the plot to the west (left). The pressure scale goes from 952 mb to 964 mb. The time scale goes from 1900 GMT 3 June to 0700 GMT 4 June for the PAMs and to 0300 GMT for the SAMs.

Viewing Fig. 5.10, one can see how the “shape” of the pressure perturbation varied across the domain. A mesohigh was recorded at stations in a wide path or “swath” from the westcentral edge of the mesonet network northeastward to the northeast portion of the mesonet network. The highest pressures were recorded later in time in a direction towards the northeast on the figure. Figure 5.11 displays isochrones of the axis of the mesohigh (or the highest pressure recorded at each station affected by the MCS) as it crossed the

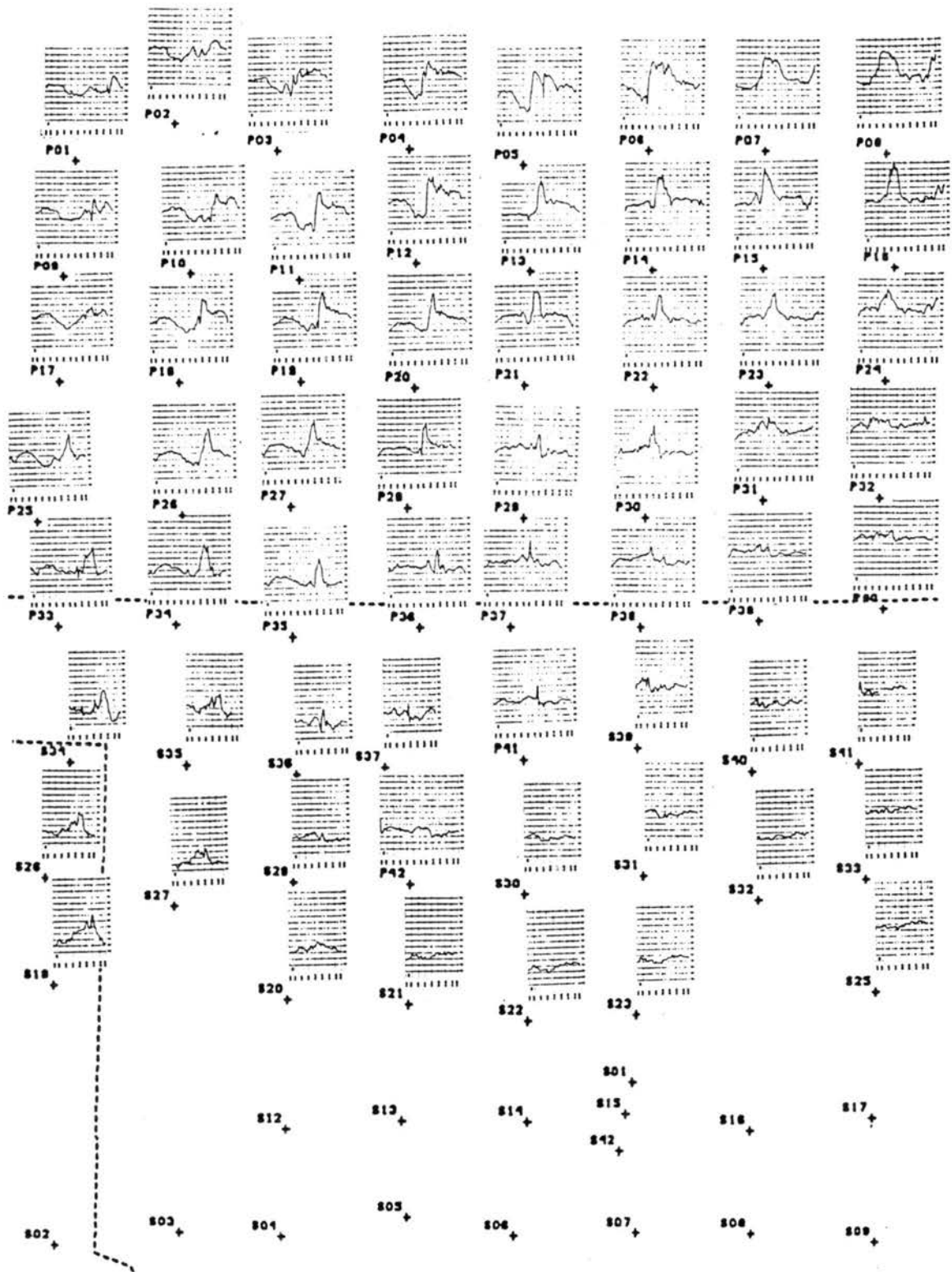


Figure 5.10: Time series plots of adjusted pressure for each mesonet station (base figure is Fig. 5.7). Time scale on PAM stations is 1900 GMT 3 June 1985 to 0700 GMT 4 June 1985. For SAM stations, it is 1900 GMT 3 June 1985 to 0300 GMT 4 June 1985.

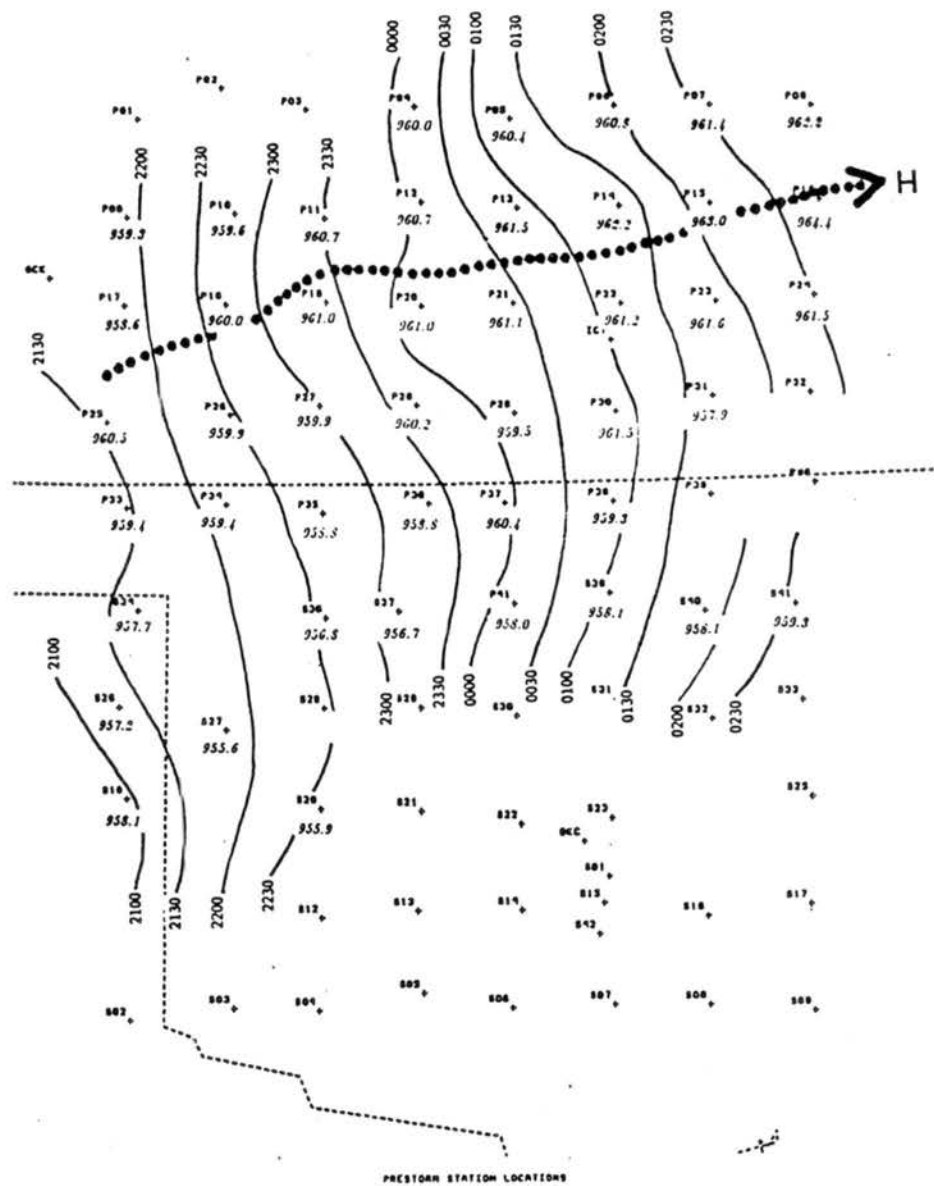


Figure 5.11: Isochrones of the mesohigh axis. Times are GMT. Peak adjusted pressure is plotted at each station. Track of mesohigh centroid is given as a dotted line.

mesonet network. Peak pressure values at each station are plotted. Also included on this figure is the approximate track of the mesohigh centroid. The mesohigh contained its lowest maximum centroid pressures during the MCS's formative stage. During the mature phase, the mesohigh maintained approximately a constant maximum pressure. During its dissipating stage, the mesohigh strengthened, however, the maximum pressure may have been recorded east of the mesonet network. The isochrones split at the Oklahoma-Kansas border near the latter stages of the MCS. This was observed in the radar overview in Chapter 4 as the convection in Oklahoma detached from the northern stratiform rain area.

The structure of the mesohigh also varied across the mesonet network. Along the southern part of the MCS, the mesohigh shows up as a sharp "spike" in pressure, lasting a short duration (examples include traces at P37, S37, P41, etc.). To the north however, the mesohigh trace is broader and greater in amplitude, lasting a few hours at some stations (examples include traces at P07, P08, P14, etc.). Precipitation affected the southern stations for a much shorter duration. This suggests that cold downdrafts were minimal in the southern segment of the MCS. Precipitation loading (a non-hydrostatic effect) could have contributed to a 1 to 2 mb rise (Nicholls *et al.*, 1988) in the southern segment. In the north, the large stratiform rain area is generating a large cold dome, and the hydrostatic effects of the cooling here are probably adding to the strength of the mesohigh [Byers and Braham (1949), Fujita (1955), Fritsch and Chappell (1980)].

The pre-squall trough can be seen on the pressure curves at a number of stations (examples include S34, S35, P29, P30, etc.; Fig. 5.10). More impressive are the pressure traces associated with the wake low. In the north-central PAM network, the wake low is nearly 3.5 mb deeper than the pressure recorded after its passage. The wake low is broader (longer lived) but shallower in the westcentral mesonet network area. A much larger drop in pressure (up to 6 mb in 30 minutes) was observed between the mesohigh and the wake low, for example, at stations P04, P12, P05, and P06. The gradient at the forward edge of the mesohigh in the northeast portion of the mesonet network was not as steep as the rear edge. A large amount of subsidence warming to the rear of the stratiform rain area

in the northern part of the MCS must be accounting for the extreme drop in pressure into the wake low. This will be studied in greater detail in the next chapter.

Figures 5.12 and 5.13 show isochrones and centroid tracks of the pre-squall trough and the wake low respectively. The pre-squall trough was best defined on the pressure traces during the initial stage of the MCS (Fig. 5.10). Between 2300 and 0000 GMT, a pre-squall mesolow formed ahead of the MCS in Kansas, and the trough associated with it became much broader (Figs. 5.4a, 5.5a). A pre-squall trough was not observed after 0000 GMT, although one may have existed east of the mesonet network in conjunction with the forward anvil. Isochrones of the wake low (Fig. 5.13) are somewhat hard to follow except along the northern edge of the mesonet network where the lowest pressures were recorded (3.45 mb at station P04). It appears that the wake low moved more slowly than the mesohigh throughout most of their lifetimes within the mesonet network.

5.1.3 Rainfall characteristics

Total rainfall measured at the PAM and SAM stations during the passage of MCS2 is shown in Fig. 5.14. To the north and northeast is a maximum which was associated with the northern stratiform rain area. A band of heavier stratiform rainfall (although not as heavy as the maximum rainfall recorded in the extreme northeast) is found along a path from P11 to P05. Interestingly, this is the approximate track of the wake low. Referring back to Fig. 5.6a, the center of the wake low was positioned just behind a local stratiform rain maximum, an interesting feature to be discussed later.

Comparatively, in the southern part of MCS2, the rain was more intense, but shorter-lived. Just south of the Oklahoma-Kansas border is a swath of heavier precipitation which was associated with heavy convection embedded within the southern segment. Note that rainfall amounts in eastern Oklahoma decreased suddenly. This is because the convection associated with the southern line weakened rapidly as it moved into this area. Some convective cells still remained in the latter stages of the MCS as the rain moved east out of the mesonet network, but these cells apparently travelled between stations.

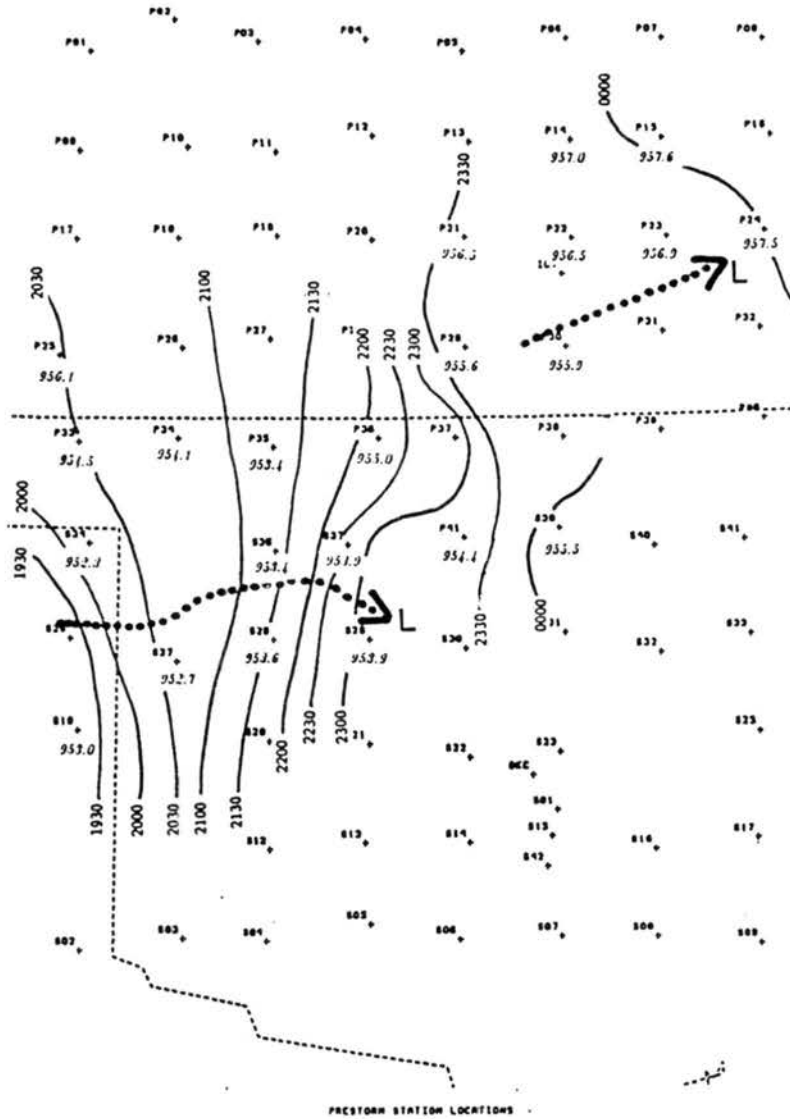


Figure 5.12: Same as 5.11 except for pre-squall mesolow.

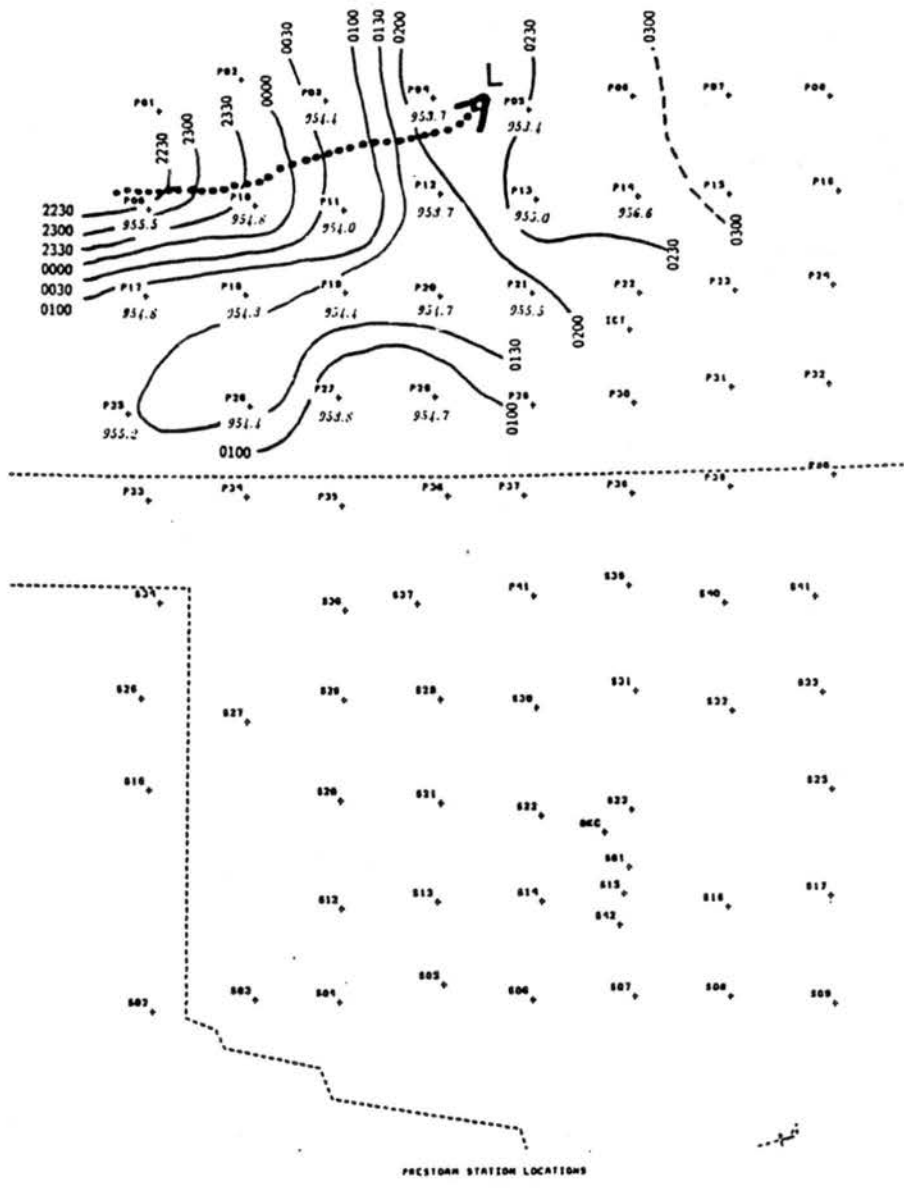


Figure 5.13: Same as 5.11 except for wake low.

Digitized radar data from the NWS WSR-57 radars were broken down into areal coverage of certain reflectivity ranges³. Stratiform rain rates were denoted as 15-35 dBz and convective rain rates were denoted as >35 dBz. Shown in Table 5.1 are the percentages

Table 5.1: SUMMARY OF RADAR REFLECTIVITY COVERAGE AS PERCENTAGE OF TOTAL RAIN (>15 dBz).

Time	15-35 dBz	>35 dBz
1900	90.9	9.0
2000	70.0	30.0
2100	79.0	21.0
2200	81.7	18.2
2300	80.9	19.1
0010	83.6	16.3
0110	85.5	14.5
0150	86.3	13.7
0309	87.1	12.9

of stratiform rain and convective rain to the total measurable rain (total measurable rain was given as any radar reflectivity exceeding 15 dBz). At 1900 GMT, the largest percentage of stratiform rain was observed with the developing precipitation. Soon after, the precipitation intensified rapidly and the peak in convective precipitation occurred. This stage was characterized by “random” convective cells over the Texas and Oklahoma Panhandles (note the precipitation maximum on Fig. 5.2 at P25). As time progressed, as the

³Ground clutter was not removed from the digitized data, so some biases toward convective rain may exist.

stratiform anvil developed and spread into a larger area, more stratiform rain developed. The proportion of stratiform to convective rainfall increased through the mature phase and into the dissipating stage, a feature also documented by Leary and Houze (1979) and Johnson and Hamilton (1988)

Figure 5.15a,b compare two precipitation time series plots for stations in the southern and northern parts of the MCS. At P41, a southern station, the rainfall rates were very high ($\sim 120\text{mm/hr}$) but the rain fell in a short duration. To the north, station P07 shows a gentler slope in the rainfall trace ($\sim 25\text{mm/hr}$) associated with the stratiform rain area. The beginning of the trace starts off with a steeper slope, indicative of some leading convection. The latter half of the rainfall at P07 was of an even lesser rate ($\sim 5\text{mm/hr}$), indicating the dissipation stage of the MCS, and lighter stratiform rain. Station P21 (Fig. 5.15c) shows a rainfall trace which is similar to a midlatitude squall line with a trailing stratiform rain region (Hamilton and Johnson, 1987). Higher rates associated with the leading convection are followed by lesser rates of the stratiform rain. However, a "transition zone" (Smull and Houze, 1987a) was not observed with the MCS.

5.2 Horizontal upper air analyses

Upper air data collected during PRE-STORM operational periods provided the detailed three-dimensional information of MCSs passing through the area. Ninety-minute upper air operations began during the 3 - 4 June 1985 period at 1930 GMT and continued through the next day. Most of the supplemental sounding sites provided data throughout this period [one exception, Hominy OK (HOY) was not operating throughout this period]. For some soundings, data terminated at certain vertical levels due to instrument failure or other causes.

An overview of the upper air features is presented here to detail the three-dimensional structure of MCS2. Shown will be horizontal analyses at certain constant-pressure levels of storm-relative wind, geopotential height, temperature, dewpoint, and relative humidity at various times.

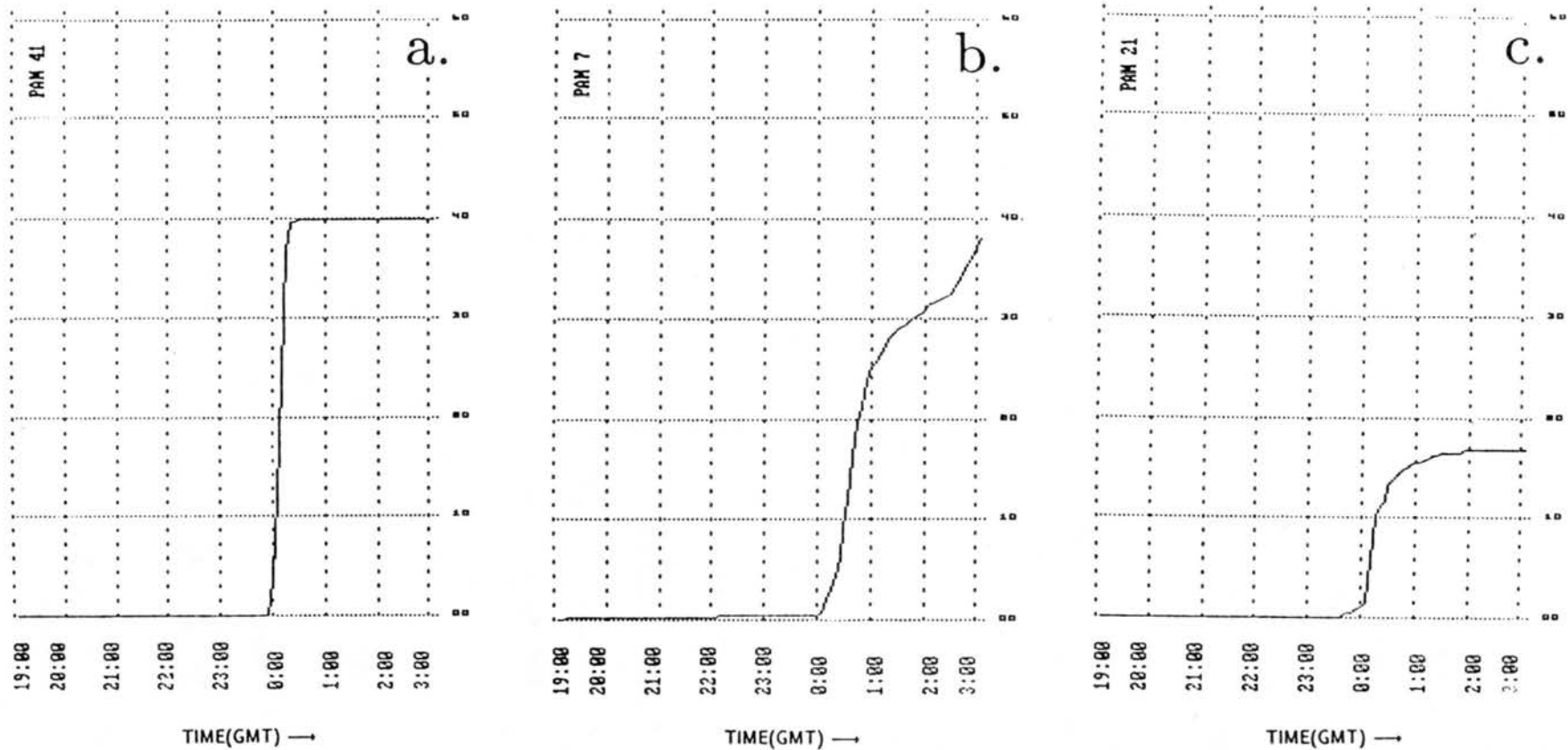


Figure 5.15: Same as 5.7 except for rainfall in mm: a) station P41; b) station P07; c) station P21. Time increases to the right and is GMT.

Storm relative winds are those winds with the mean motion of the storm subtracted out. To determine the mean motion of the storm, isochrone analyses of various meteorological features were conducted. One of the primary focuses of this research is to investigate the structure of the main surface pressure features, namely the mesohigh and the wake low. Therefore, meteorological parameters accompanying the northern stratiform rain area during the mature phase of the MCS were used to determine the system motion. Isochrones of the mesohigh axis, rear edge of the stratiform rain echo, and the axis of the maximum stratiform rain rate (as observed by PAM rainfall traces) are shown in Fig. 5.16. The direction of each set of isochrones didn't vary by more than 10° . The speed of the rear edge of the stratiform rain lagged the other parameters but only after the storm reached maturity. The velocity vectors of all three parameters were subjectively averaged and the storm motion was found to be 18 m s^{-1} from a direction of 240° ($u=15.6 \text{ m s}^{-1}$, $v=9 \text{ m s}^{-1}$). By comparison, Augustine and Howard (1988) used a motion vector of 21 m s^{-1} from 225° for MCS2, and Smull (1988, personal communication) used a storm vector of 15 m s^{-1} from 240° in a Doppler study of the MCS2 case (Smull and Jorgensen, 1987). In the latter study, the speed of individual convective cells embedded within the precipitation area determined the mean system motion. The movement of the centroid of the upper level cloud shield had been suggested for determining a mean system motion as well. This method was not used because winds aloft may have influenced the movement and shape of the upper-level cloud shield (anvil) much differently than the movement of the storm as viewed at the surface (the anvil associated with MCS2 appeared to expand in a forward direction in relation to the surface features).

Overlaid on the following analyses are contours of radar reflectivity at 15 dBz and 35 dBz respectively as well as the approximate edge of the cold cloud shield as inferred by infrared satellite. Wind data from the three profilers have been included on the analyses. Dual-Doppler derived winds constructed using data from the NCAR CP-3 and CP-4 C-band radars at about 0107 GMT were composited on the 0000 GMT and 0130 GMT supplemental sounding maps.

The first set of maps presents the upper air data at 2100 GMT on 3 June 1985. Since the storm was at the western edge of the mesonet, the lack of data in this region at

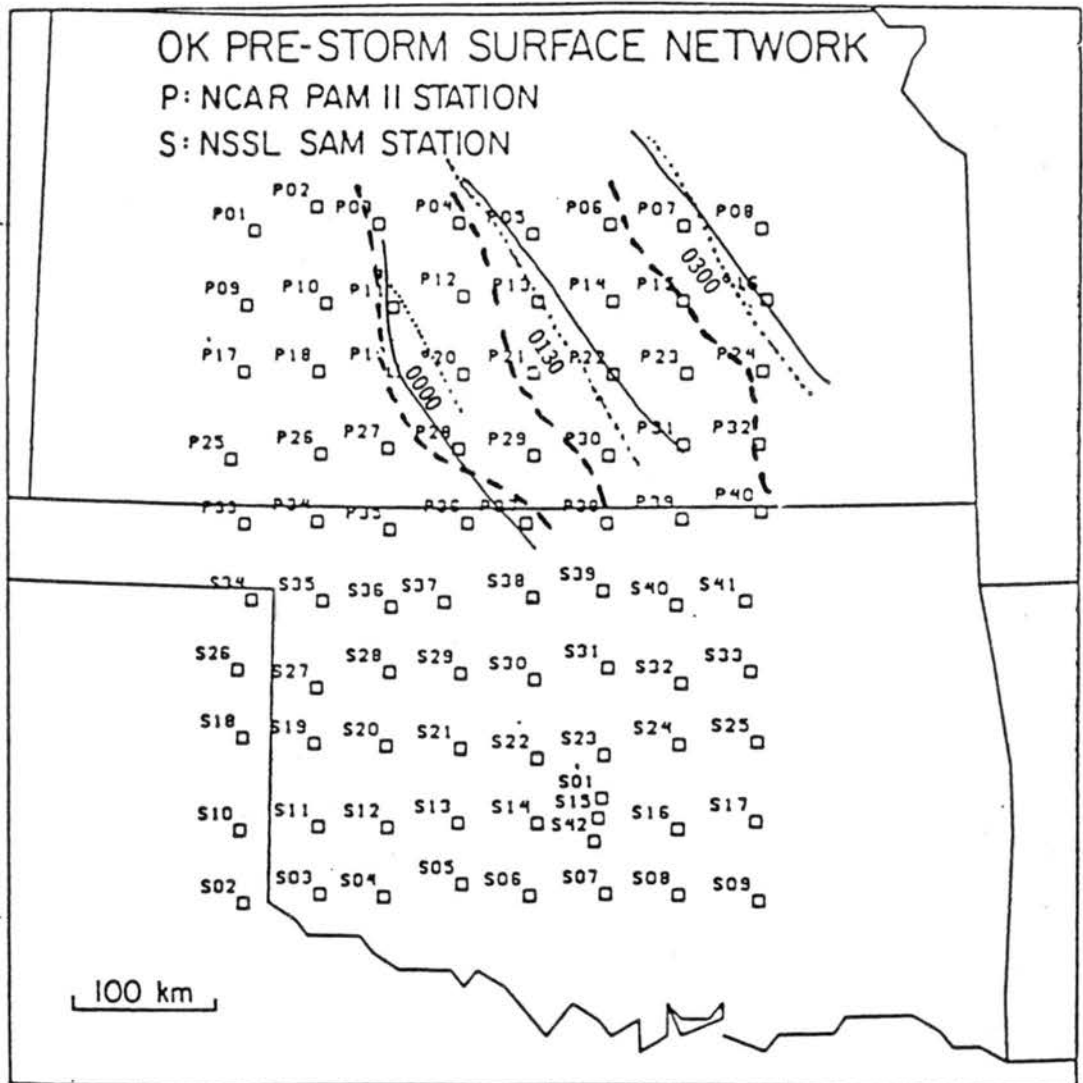


Figure 5.16: Isochrones of axis of mesohigh (solid line), rear edge of stratiform rain (dashed line), and axis of maximum stratiform rain rate (dotted line). Times are GMT.

this time makes interpretation of the analyses rather difficult. Nevertheless, it is presented here to provide a picture of the storm structure during its developmental stage. At 700 mb (Fig. 5.17) the relative air flow has a strong easterly component. Flow in Oklahoma is southeast into the MCS. Flow in the eastern half of Kansas is northeast and is most likely low-level outflow behind from MCS1. The wind field at 700 mb depicts front-to-rear (FTR) inflow into the system. A jet of maximum winds lies from Enid OK (END) to Woodward OK (WWR). A low level inversion at END at 750 mb (figure not shown) was present, and the inflow into the MCS may have been in part a low-level inflow jet [Uccellini and Johnson (1979), Schaefer *et al.* (1985)]. The southeast wind at LBL depicts low-level FTR outflow behind the system.

At 500 mb (Fig. 5.18), rear inflow (Smull and Houze, 1987b) is apparent at LBL. Convergence exists somewhere within the MCS at this level (between LBL and PTT), but its exact location is difficult to detect given the spatial resolution of the sounding data. The west wind at LBL is being sampled within a rear inflow jet which was evident on the LBL profiler time series of relative wind (Augustine and Howard, 1988; Fig. 5.19). The rear inflow is apparent on this time series behind the leading edge of the convection. The axis of the inflow runs around 6 km and maintains this level until it descends slightly at the back edge of the MCS. A 12 m s^{-1} northeast wind at FRI at this time suggests RTF inflow into MCS1 was occurring as well.

Analysis of the storm-relative winds at 300 mb (Fig. 5.20) depicts a general southwesterly flow. These winds are consistent with the observation of a forward leaning anvil ahead of the surface precipitation, as was also found in other cases [Newton and Fankhauser (1964), Newton (1966)]. To be shown in succeeding paragraphs, the upper-tropospheric flow during the mature phase of the storm is similar, but the mid-tropospheric flow is a bit more complex.

Figure 5.21 portrays a map of vertical thermodynamic profiles from the surface to 300 mb at the supplemental sounding sites at 2100 GMT. What can be seen in this figure is the varying thermodynamic structure of the low- to mid-troposphere throughout the PRE-STORM domain. At the southern sounding locations, a low-level inversion or

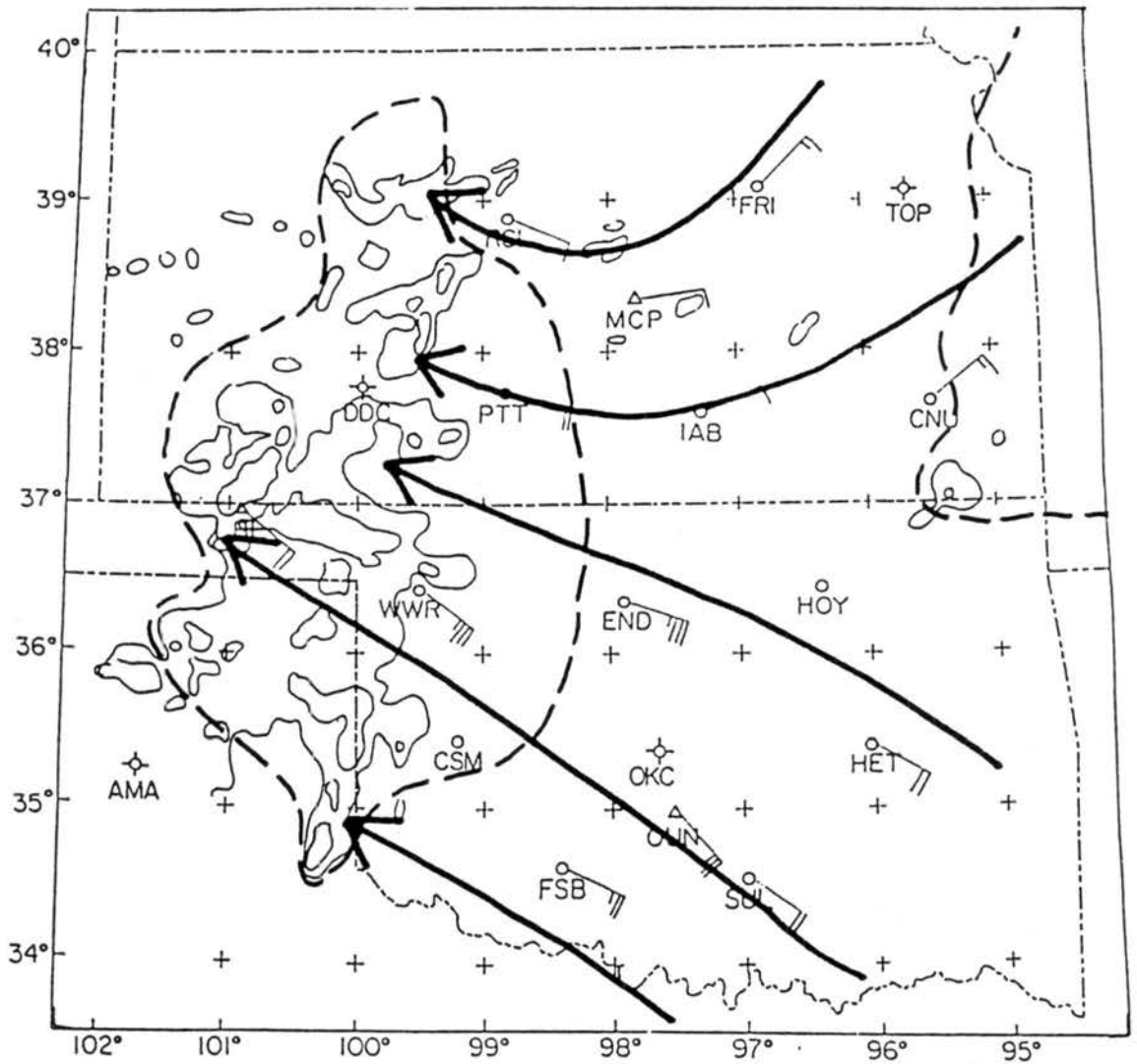


Figure 5.17: Mesoanalysis of storm-relative winds for 700 mb at 2100 GMT 3 June 1985. One wind barb equals 5 m s^{-1} . Overlaid are radar reflectivity contours of 15 and 35 dBz. Dashed contour represents edge of -54°C cloud shield from IR satellite.

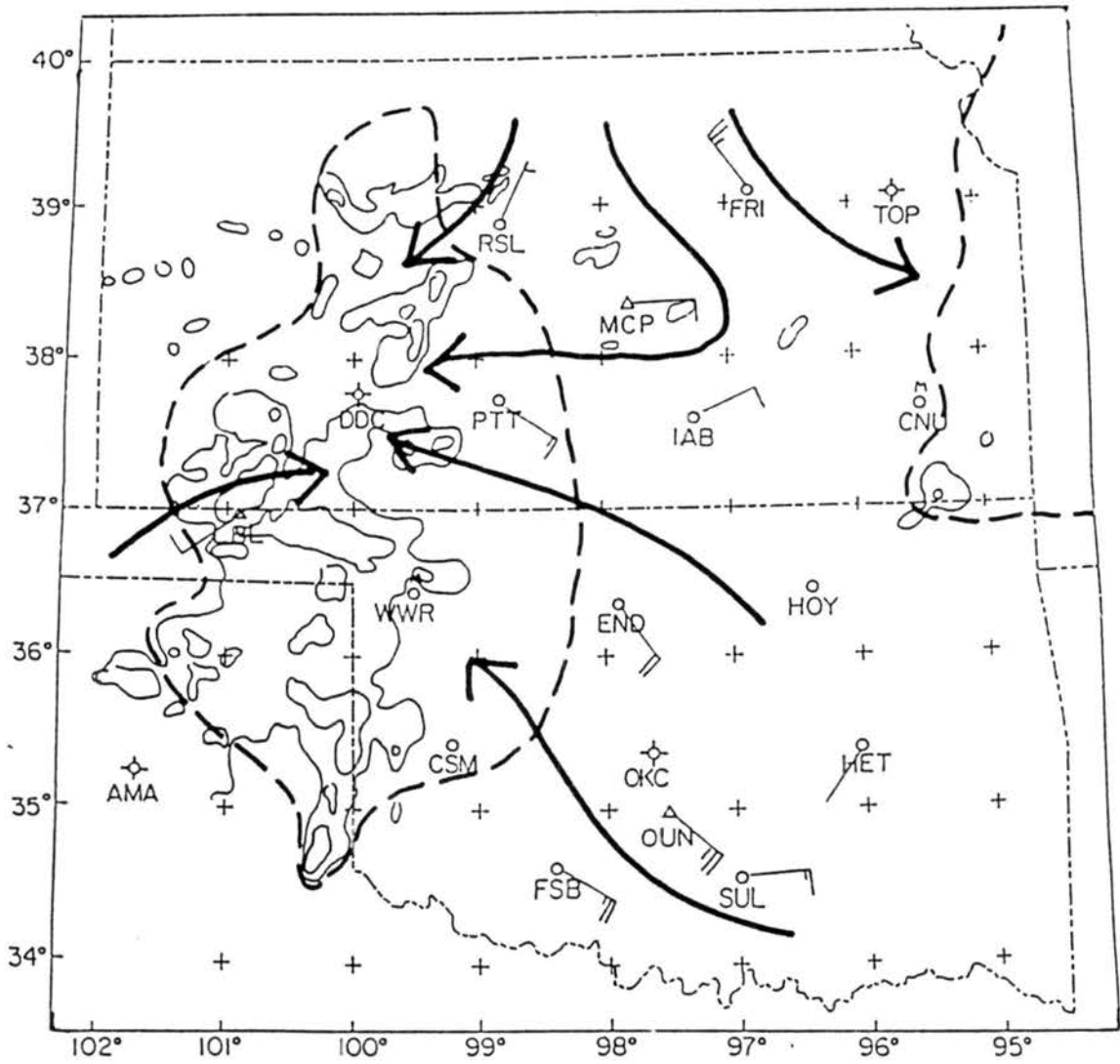


Figure 5.18: Same as 5.17 except for 500 mb at 2100 GMT 3 June 1985.

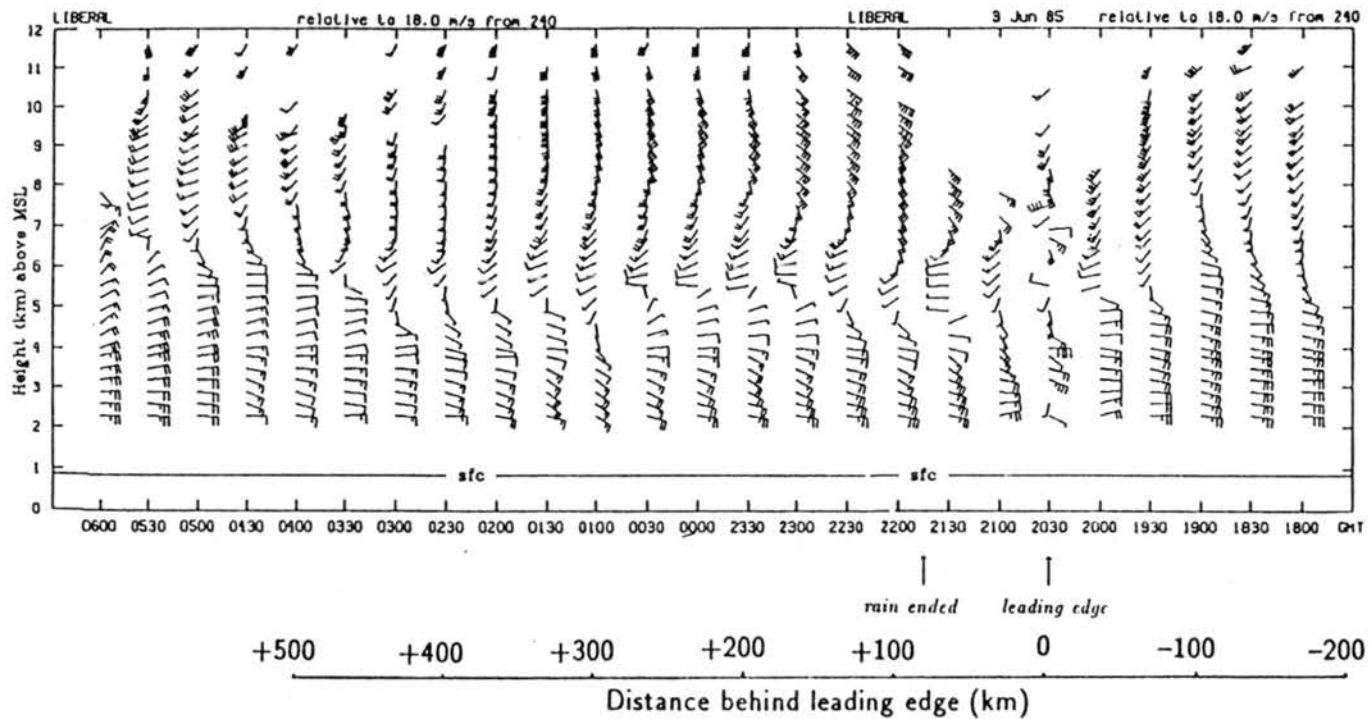


Figure 5.19: Liberal KS profiler time series. Plotted are storm relative winds. Time interval is 30 minutes. Time increases to the left and is GMT. Time to space conversion was used to determine storm relative distance in km.

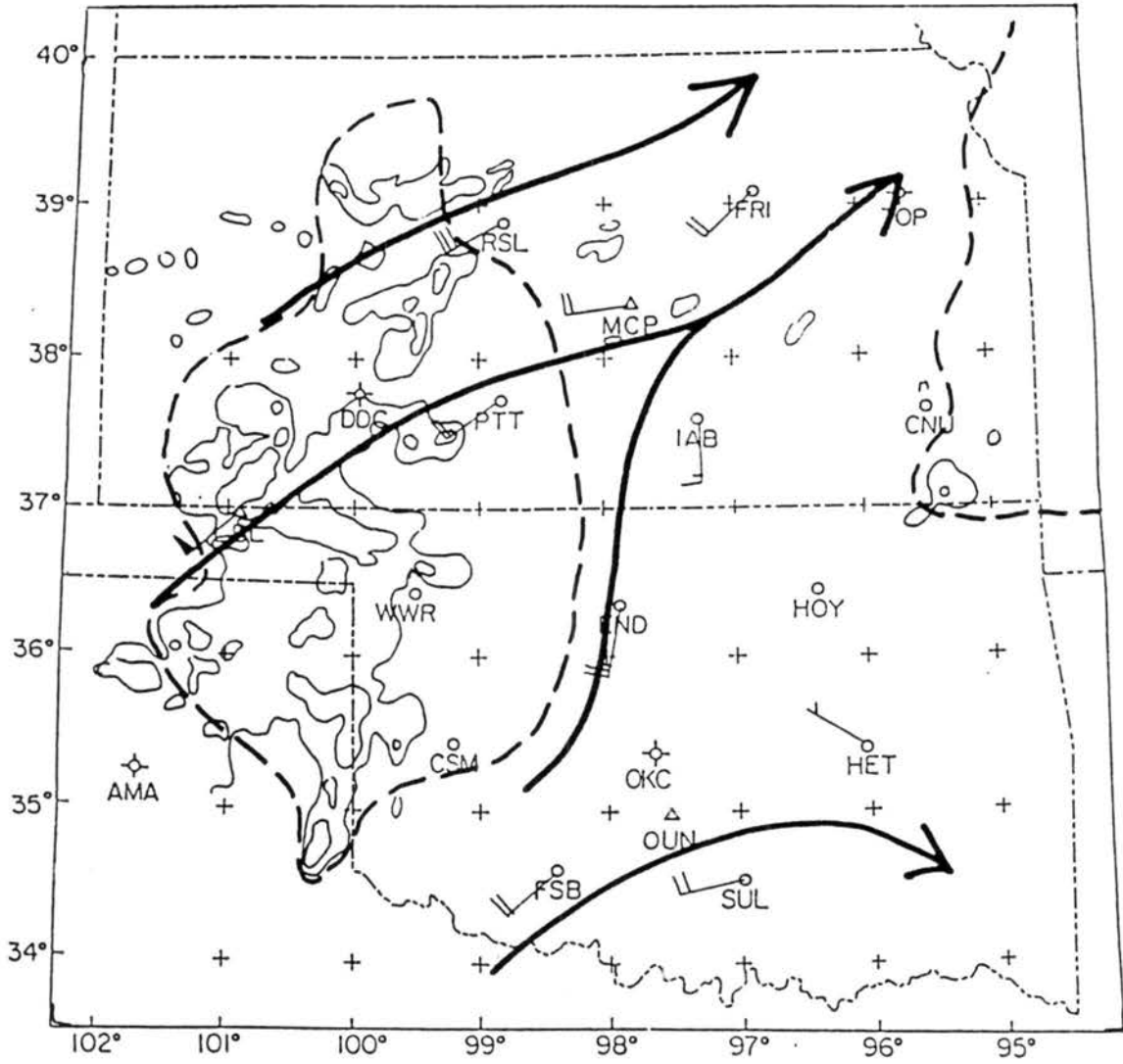


Figure 5.20: Same as 5.17 except for 300 mb at 2100 GMT 3 June 1985.

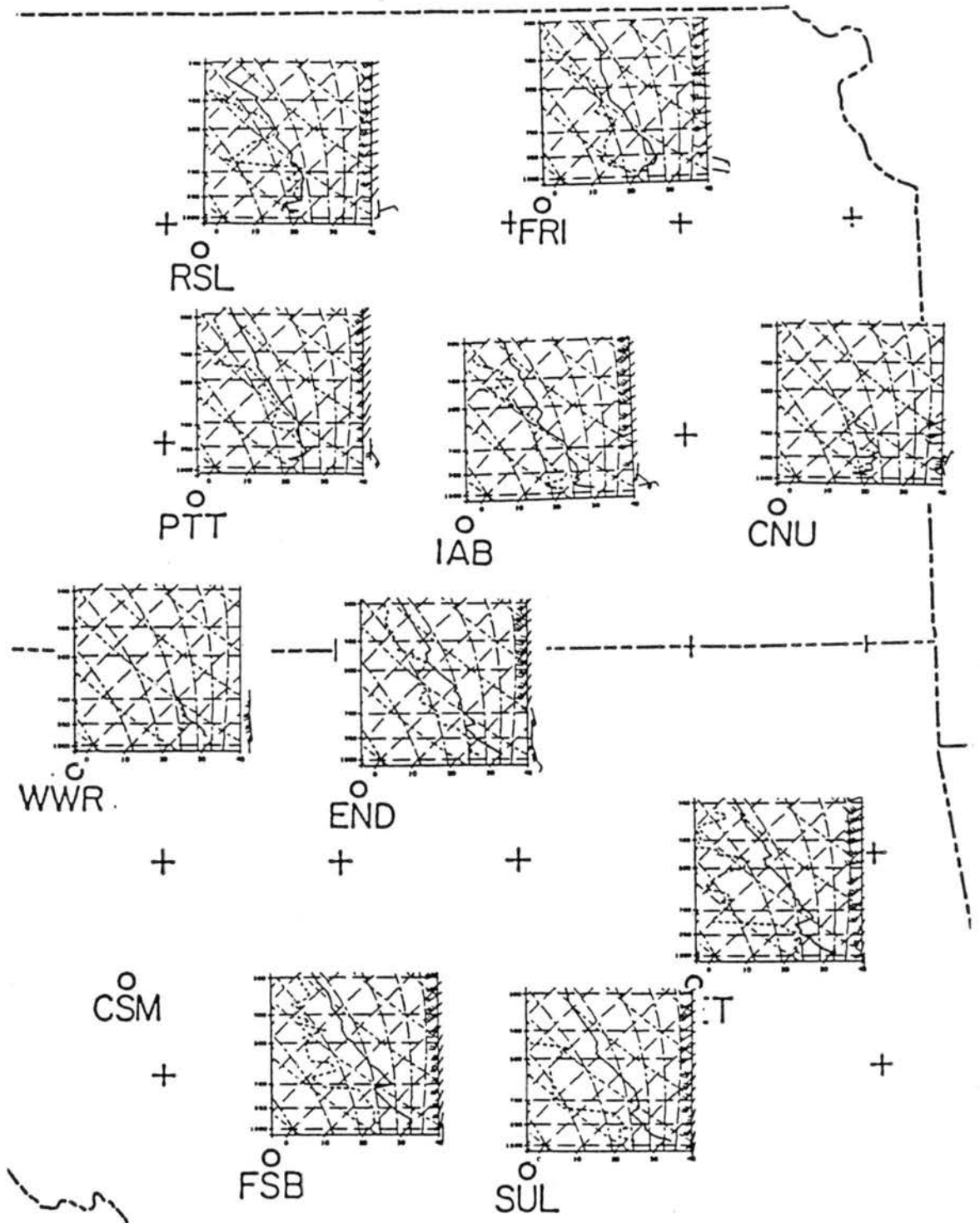


Figure 5.21: Thermodynamic profiles at 2100 GMT. Skew-T diagrams include temperature, dewpoint, and actual winds up to 300 mb. Base figure is Fig. 4.6.

“cap” is pronounced near 750 mb. To the north, these “caps” are nonexistent. Perhaps this explains why convection did not develop in southern Oklahoma. Also, the lower troposphere was drier in the non-convective areas. Note the “onion” shaped sounding (Zipser, 1977) at FRI, a sounding taken in the wake of MCS1. “Onion”-shaped soundings were also observed in the wake of MCS2, and will be discussed in the next chapter.

The MCS reached its mature stage within the next three hours. The sounding data set was most complete at 0000 GMT 4 June. Also, wind data from the CP-3/CP-4 Doppler radar pair were utilized in construction of the analyses. Profiler data from the McPherson KS site is slightly contaminated at this time due to overhead convection. The 700 mb analysis at 0000 GMT shows again that mainly FTR flow exists at most stations (Fig. 5.22a). The FTR flow found to the rear of the MCS is low-level moist outflow, and will be detailed with Doppler data later. An area of weak RTF flow is evident at WWR. Relative winds along the northern part of the system are mainly northeast roughly aligned along the embedded heavier bands of convection in the stratiform rain region.

Figure 5.22b shows the 700 mb geopotential height field, actual winds, temperatures, and dewpoints at 0000 GMT. The lowest heights are situated within the region of the precipitation area, and higher heights are found just to the rear of the system. Warm dry air is located to the rear of the system and cool moist air is found within the precipitation area. This warmer air shows the effects of the subsidence beneath the trailing anvil. The cool moist air within the precipitation depicts the upper part of the surface mesohigh dome.

Going up to 500 mb, a complex wind pattern becomes evident (Fig. 5.23a). The salient feature found here is the convergence line along the rear edge of the stratiform rain region in the northern segment (this is verified by Doppler data to be shown later). By comparison, Augustine and Howard (1988) analyzed a cyclonic circulation at the southwest quadrant of the MCS (see their Fig. 10b) using a slightly different storm motion vector than in this paper. The flow on the east side of the convergence line is characterized by a FTR current. To the rear of the system, an area of RTF inflow is found. This rear inflow is most likely depicting a rear inflow jet (Smull and Houze, 1987b) associated with mesoscale circulations within the trailing anvil.

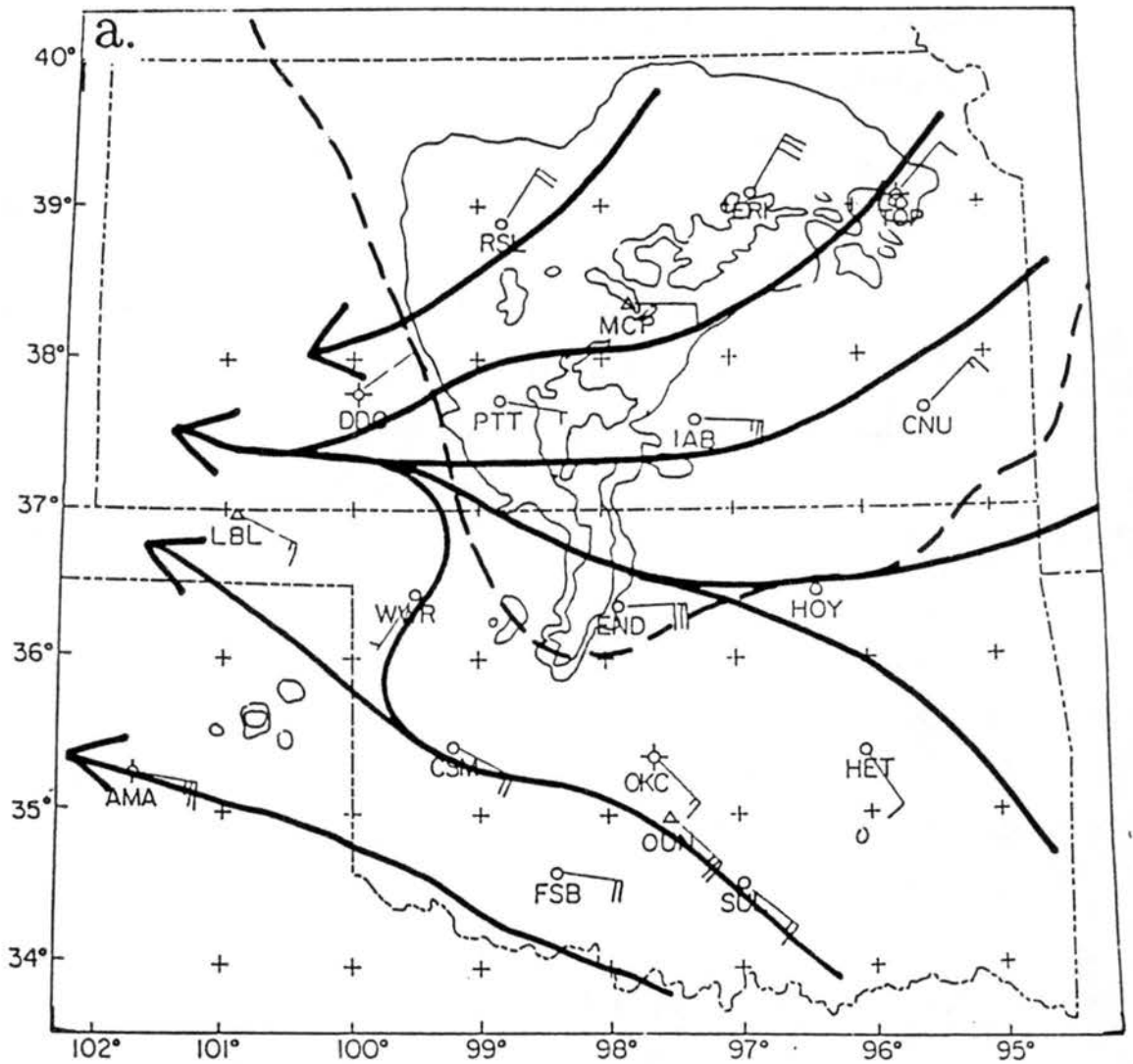


Figure 5.22: a) Same as 5.17 except for 700 mb at 0000 GMT 4 June 1985; b) Meso-analysis of geopotential height, temperature, and actual winds for 700 mb at 0000 GMT 4 June 1985. Solid contours depict geopotential height in Dm. Dashed contours depict temperature in $^{\circ}\text{C}$. One wind barb equals 5 m s^{-1} . Temperature and dewpoint are plotted.

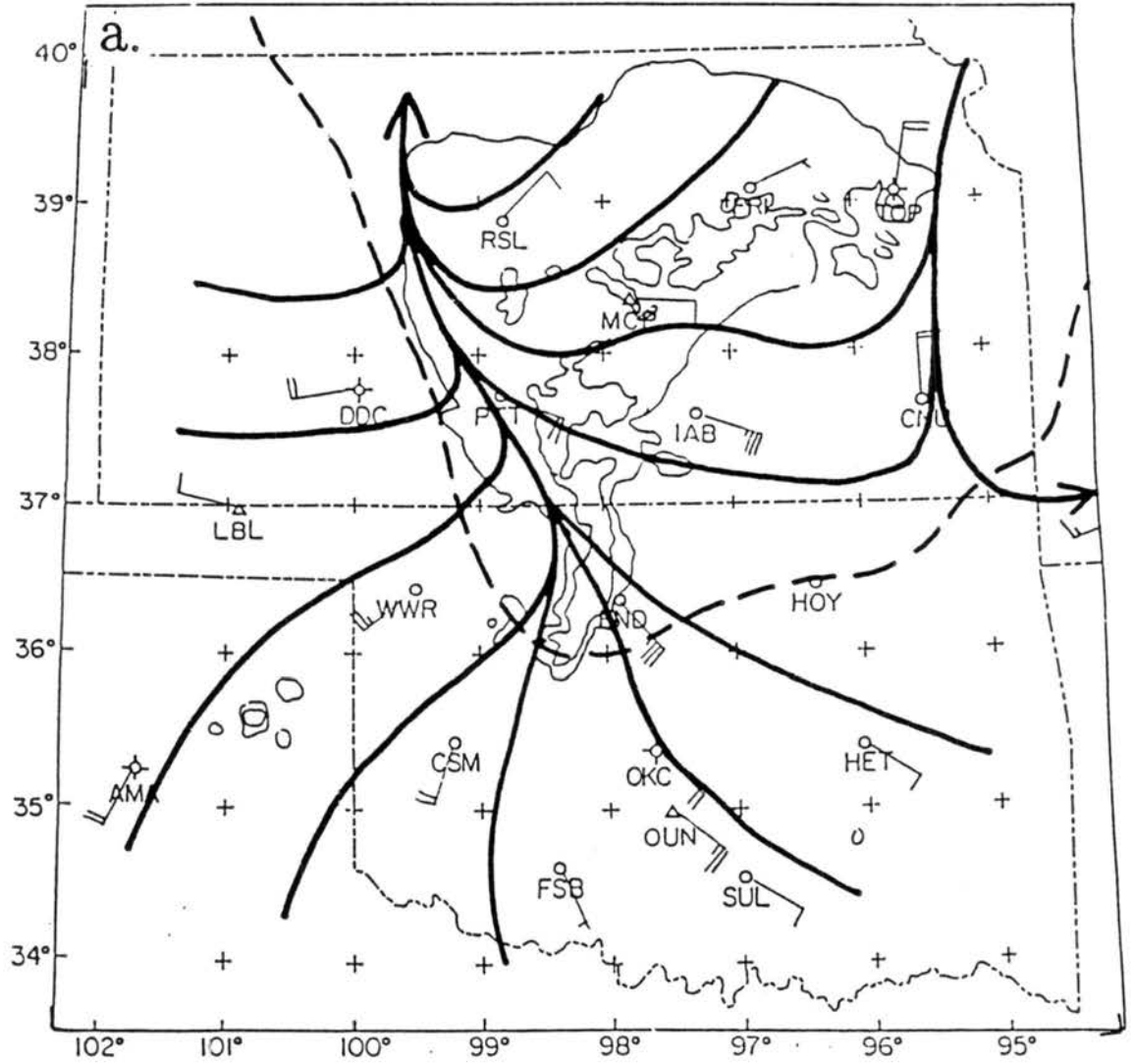


Figure 5.23: Same as 5.22 except for 500 mb at 0000 GMT 4 June 1985.

The character of the flow between the northern segment which was comprised of stratiform rain differs from the southern segment which was characterized as a short convective line. In the northern segment, the flow has a much more pronounced easterly component. Confluence is obvious in the data along a band of heavier stratiform rain stretching from just east of PTT northeastward to FRI. The relative flow is convergent and along the line in the southern segment of the MCS. The convergence curves north-northwestward along the line of convection and then along the back edge of the stratiform rain. This mid-tropospheric analysis here shows that the transport of convective debris is basically parallel or slightly rearward to the convective line.

The geopotential height field at 500 mb shows a trough situated over the stratiform rain area, and higher heights in the wake (Fig. 5.23b). A trough found at this location may be similar to the midlevel mesolow found by Brown (1979), Smull and Houze (1987b), Rutledge *et al.* (1988), and Johnson and Gallus (1988). Fankhauser (1974) observed a trough at 575 mb just ahead of a squall line he studied. He also found a ridge in the wake of the squall line at this level. The coolest air can be found within the stratiform rain area in the northern part of the system (Fig. 5.23b). Slightly warmer and drier air is found in the wake region.

At 300 mb (Fig. 5.24), a highly divergent storm relative flow is observed. A slight hint of an anticyclonic outflow is seen over the northern segment of the MCS. Environmental air originating from the southwest is being deflected around the MCS (Augustine and Howard, 1988). The majority of the air exiting the updrafts is being fed into a leading anvil at this level. This upper-tropospheric flow is partially responsible for the hydrometeor transport into the stratiform region in eastern Kansas⁴.

By 0130 GMT, the MCS is continuing to travel northeast. At 700 mb (Fig. 5.25a), FTR inflow is evident ahead of the system. Convergent outflow is emanating from the rear of the system at RSL and PTT. Unfortunately, since the MCS is beginning to exit the

⁴The embedded weaker convection within the northern stratiform rain area may have enhanced the "pool" of hydrometeors.

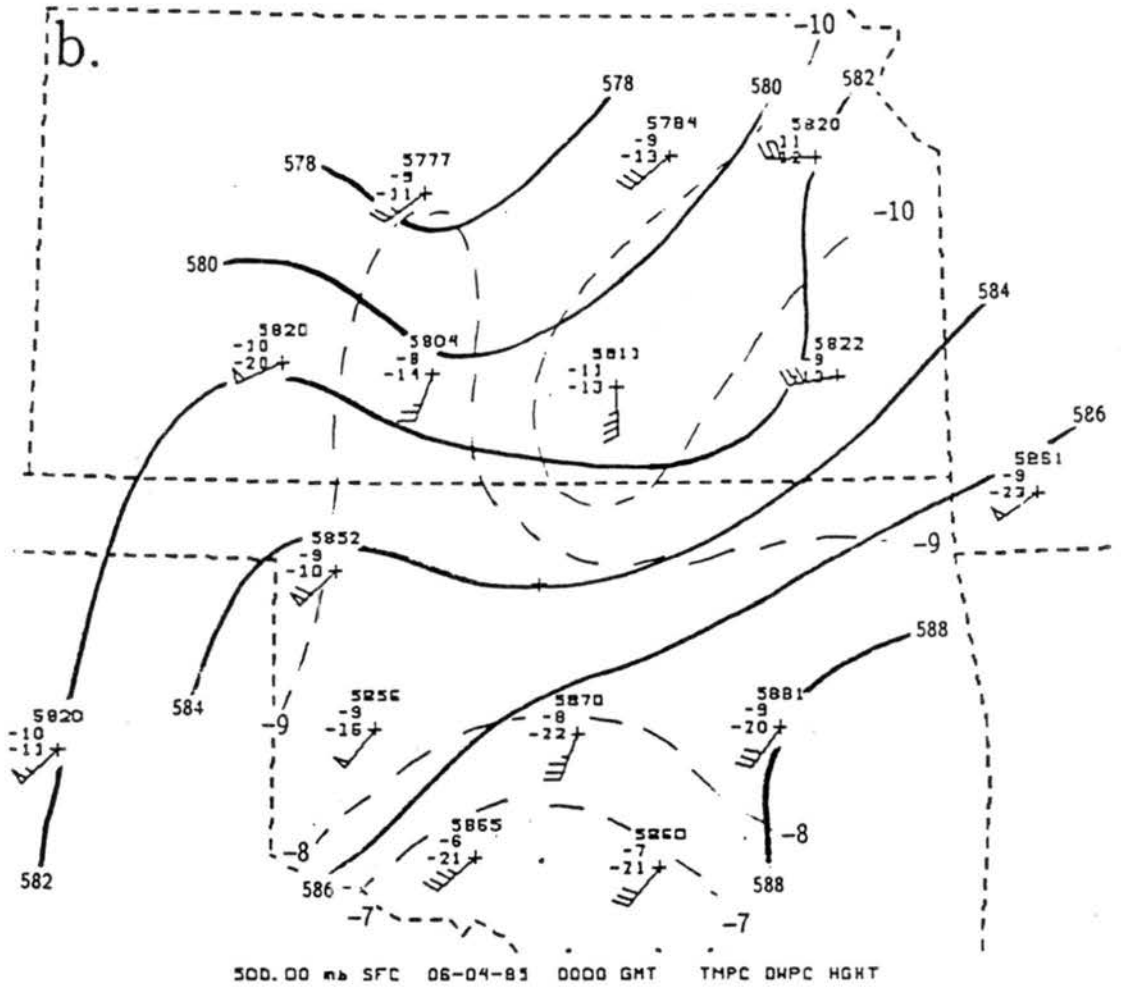


Figure 5.23: Continued.

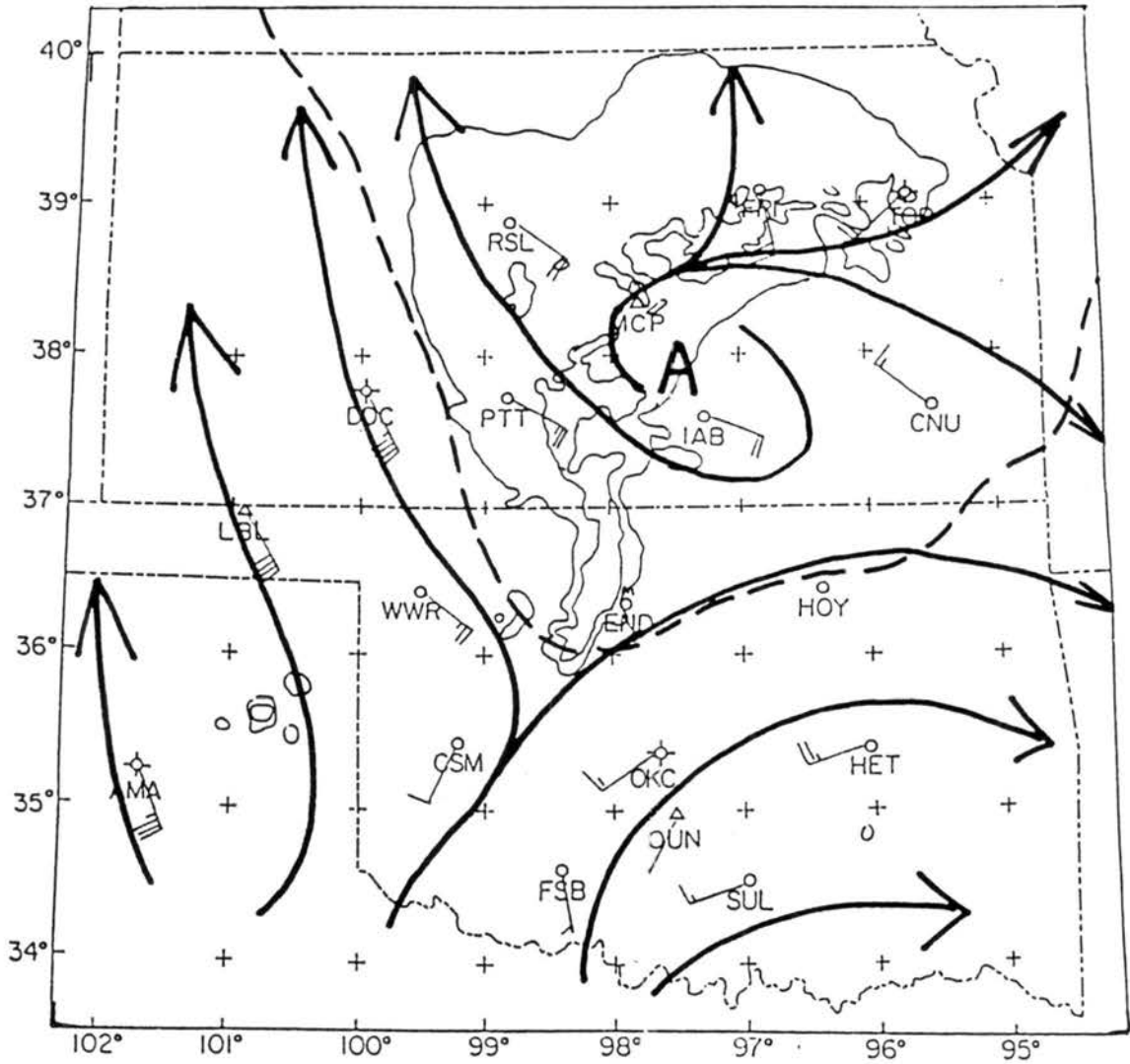


Figure 5.24: Same as 5.17 except for 300 mb at 0000 GMT 4 June 1985.

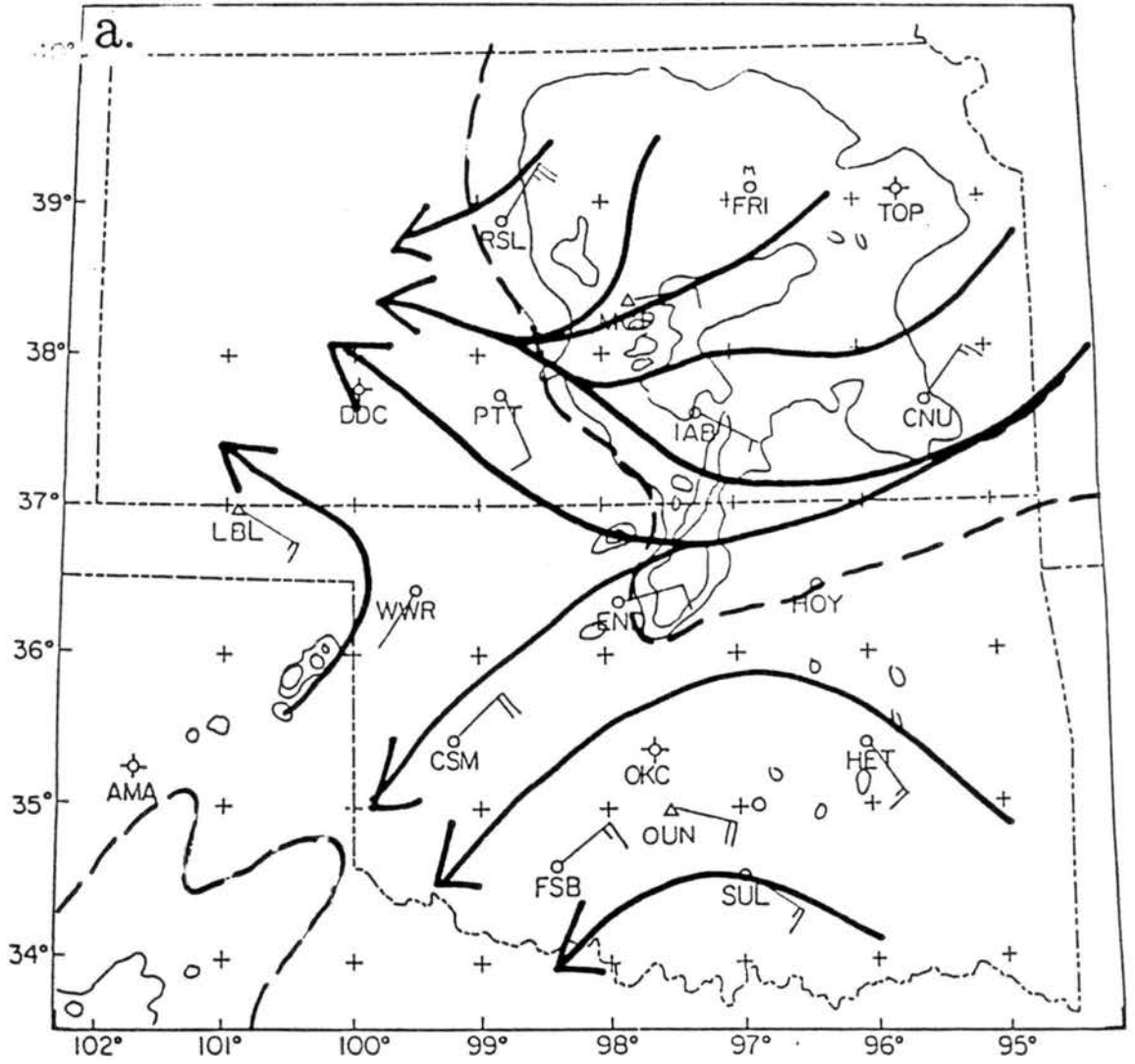


Figure 5.25: a) Same as 5.17 except for 700 mb at 0130 GMT 4 June 1985; b) Relative humidity in % for 700 mb at 0130 GMT 4 June 1985.

mesonet network and FRI did not launch a 0130 GMT sounding, upper air data is somewhat sparse within the forward stratiform rain region at this time. Figure 5.25b shows dry air located behind the stratiform anvil near RSL and PTT, but little data is sampled within the main region of stratiform rain to compare to this area. The dry intrusion of air with the rear inflow will be better illustrated later on time-height cross-sections.

At 500 mb (Fig. 5.26), convergence is still evident at the rear edge of the precipitation area in the form of a cyclonically curved trough of RTF inflow. The resolution of the sounding data doesn't permit a complete picture of the circulations present within the stratiform rain area to be constructed. In the next chapter, Doppler data will be presented to study in greater detail these circulations during the mature phase of the MCS.

Finally at 0300 GMT, the relative airflow analysis at 700 mb (Fig. 5.27) shows FTR outflow evident at all stations behind the MCS. This is similar to the wind pattern observed behind MCS1 at 2100 GMT (Fig. 5.17). The 500 mb analysis (Fig. 5.28) shows the rear inflow behind the MCS. The strongest rear inflow is observed at stations just within the rear of the stratiform rain echo. Srivastava *et al.* (1986) observed a continuing mesoscale updraft/downdraft circulation within a decaying stratiform anvil. Smull and Houze (1987b) felt that the rear inflow aids in the mesoscale updraft/downdraft circulation in the anvil region. The presence of the rear inflow during the dissipating stage of the MCS lends support to Smull and Houze's argument.

In summary, these upper air observations show that the relative flow structure of the MCS was very complex. During the MCS mature phase, the upper level flow pattern spread the stratiform anvil predominantly northward and northeastward away from the strongest convective towers in the southern "squall line". The mid-tropospheric flow was directed to the northwest in the northern segment of the MCS, leading to a relatively short trailing anvil there. In the southern portion, the relative flow was basically along the line, and a trailing anvil was not observed. Convergence was observed at the rear edge of the stratiform rain region and rear inflow was observed to its west. In the upper-troposphere, most of the flow was to the northeast, but some anticyclonically divergent flow was observed.

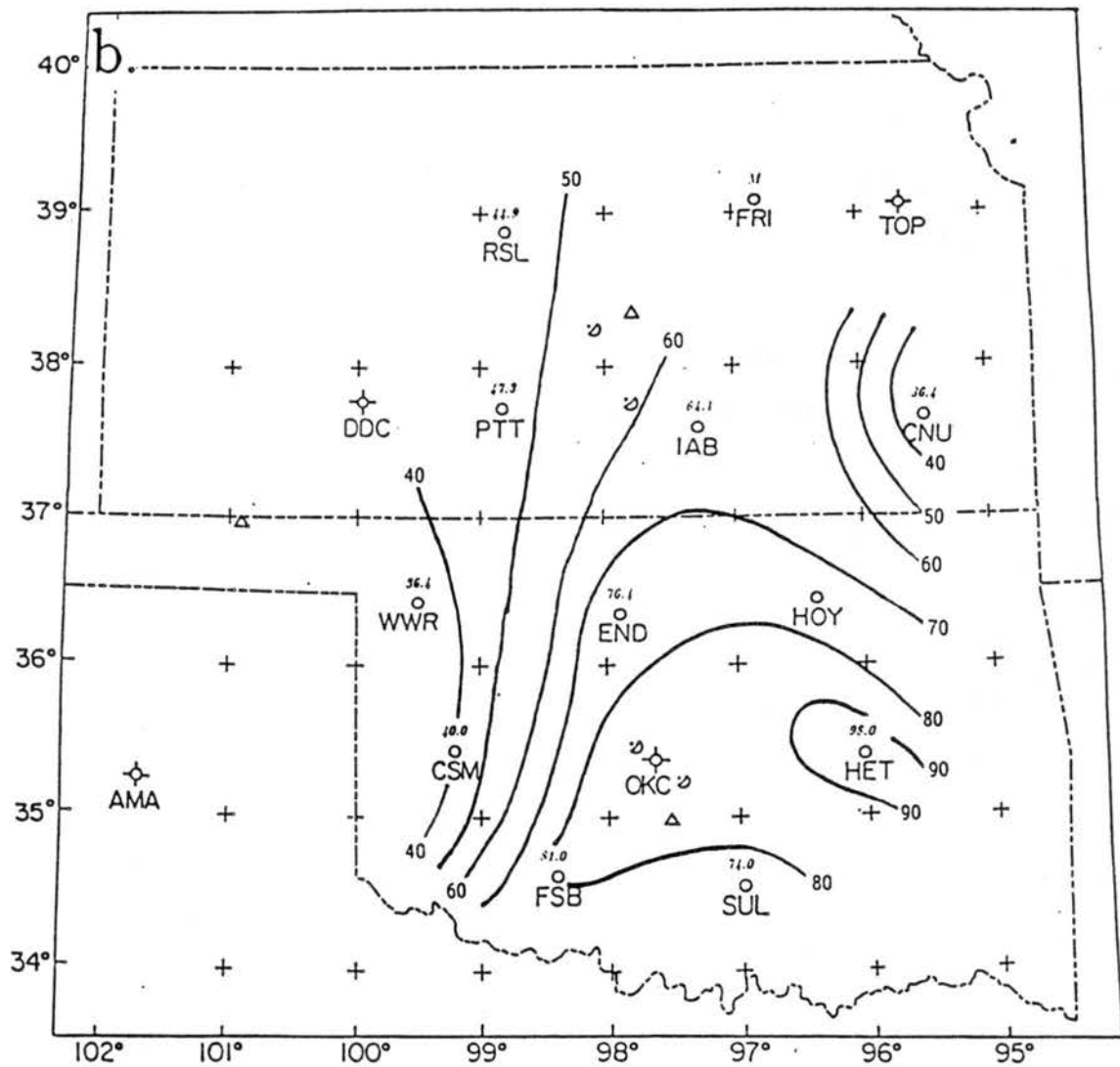


Figure 5.25: Continued.

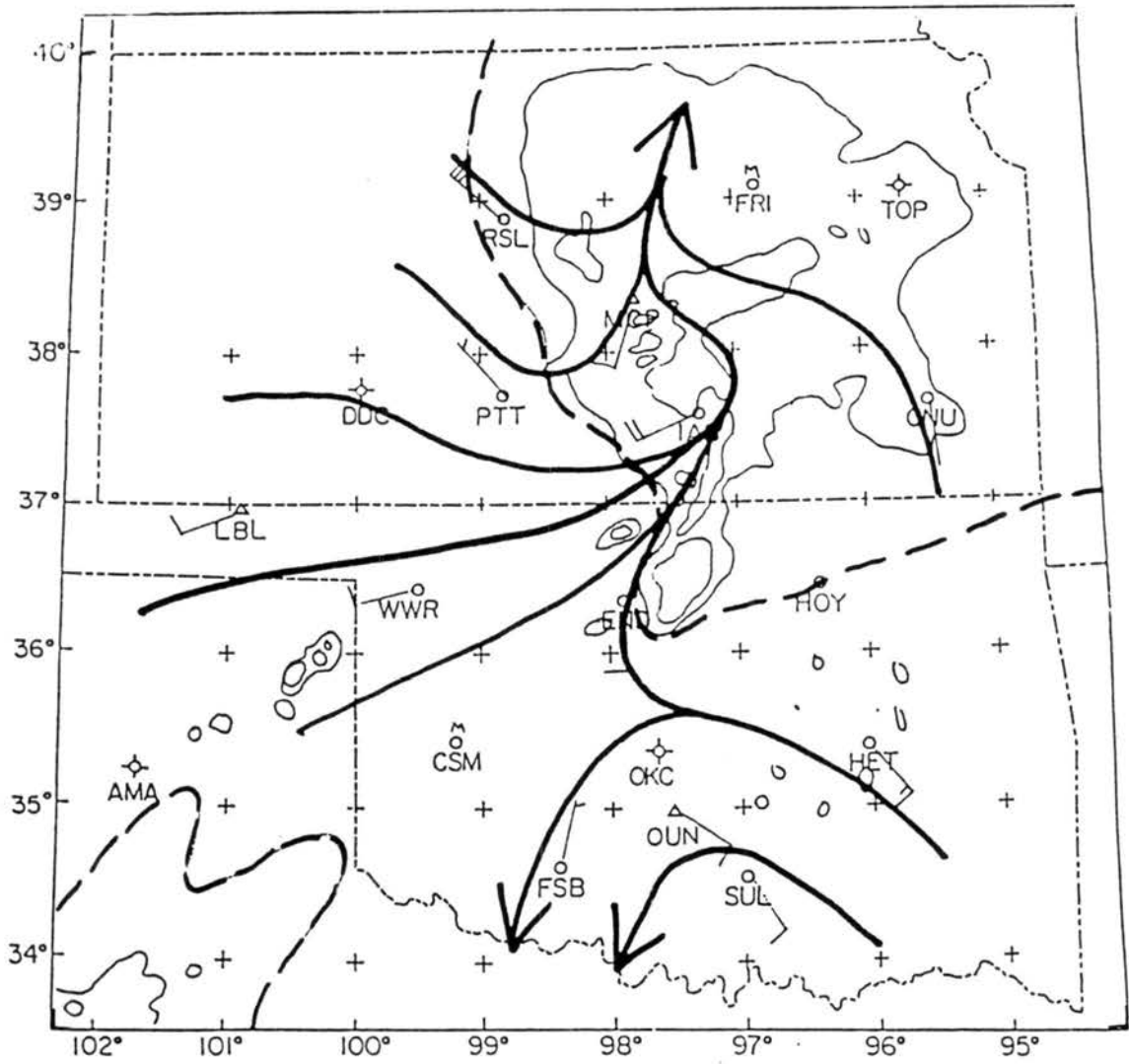


Figure 5.26: Same as 5.17 except for 500 mb at 0130 GMT 4 June 1985.

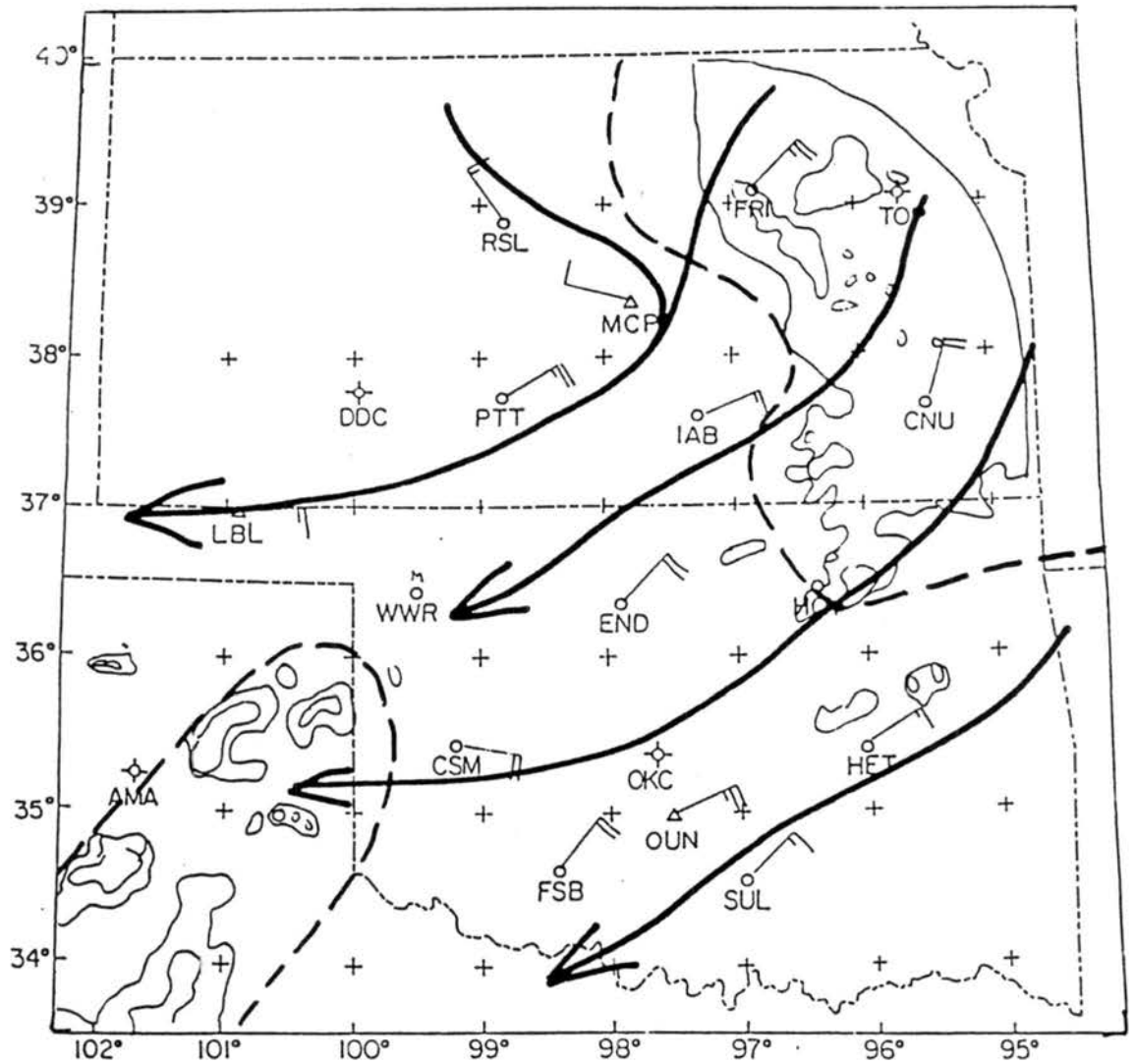


Figure 5.27: Same as 5.17 except for 700 mb at 0300 GMT 4 June 1985.

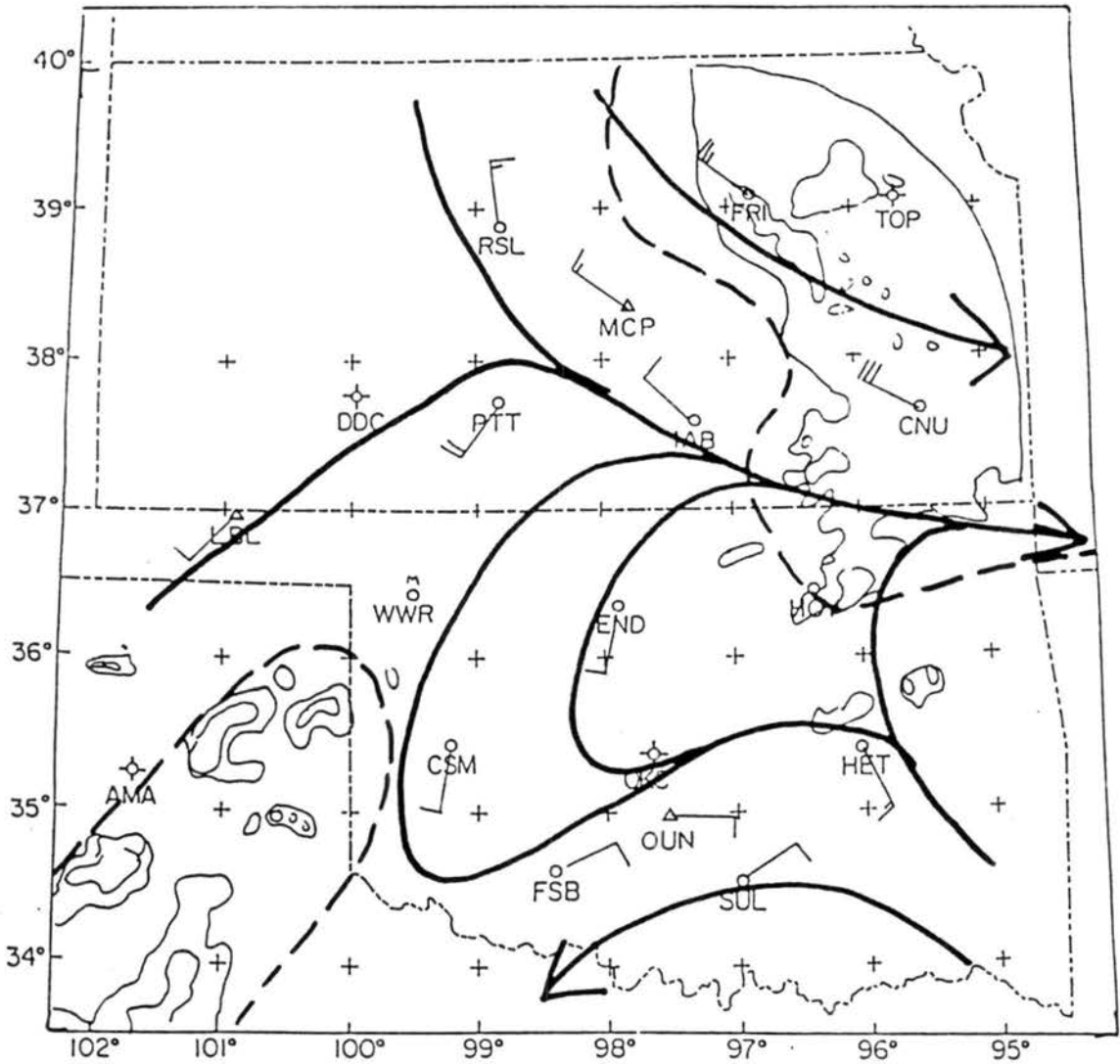


Figure 5.28: Same as 5.17 except for 500 mb at 0300 GMT 4 June 1985.

The observations shown in this chapter can be compared with Johnson and Hamilton's (1988) schematic presented in Fig. 2.1. In their case, most of the mid- to upper-tropospheric flow was directed rearward with very little of it directed ahead of the system. A wake low was also observed in their case behind the trailing stratiform rain region. The next chapter will attempt to detail the storm features responsible for the development of the wake low and mesohigh in the northern section (and their lack of development in the south).

Chapter 6

STORM CIRCULATION CHARACTERISTICS LEADING TO OBSERVED PRESSURE FEATURES

The analyses presented in Chapter 5 illustrate the remarkable surface features associated with the passage of the second MCS of the 3-4 June 1985 series. Shown was the progression of a strong mesohigh across the PAM network coupled with a wake low which tracked behind the mesohigh at the rear edge of the stratiform rain. These two surface pressure features tracked along with the MCS in a fashion that had been repeatedly observed with the passage of linear MCSs (squall lines), notably those with trailing stratiform regions of rainfall (Johnson and Hamilton, 1988, etc.). The 3-4 June MCS2 however, illustrates a case that did not have the typical visual (precipitation and cloud) features of a linear MCS with a trailing stratiform rain region, but did demonstrate the surface pressure features commonly observed with the linear genre of MCS. Surface observations of MCS2 revealed that these surface pressure features may not be confined to just linear MCSs but a variety of MCS with stratiform rain areas. Since the most pronounced surface pressure perturbations were observed in the northern stratiform rain region of MCS2, the question arises: *Are the mesoscale circulations associated with the stratiform anvil accompanying some MCSs the primary contributor to the development of a surface wake low?* This chapter details more of the mesoscale upper air features associated with the 3-4 June 1985 MCS2. Attention is given to the mature phase of the MCS when the wake low was at its strongest.

6.1 Vertical flow structure along the plane of motion

In an attempt to understand the physical processes for the development of the mesohigh and the wake low and their associated strong gradient, time-height cross-sections have

been prepared for several upper-air sounding stations in the vicinity of the mesohigh/wake low pair. These cross-sections consisted of PRE-STORM supplemental 90-minute data beginning at the time of first operational balloon launch (normally 1930 or 2100 GMT 3 June) to about 0430 GMT 4 June. These cross sections depict the passage of the MCS through the mesonet. In the following figures, time increases towards the left (resembling a profiler cross-section). This portrays an x-z cross-section of the MCS with a view from the south (west is on the left, east on the right). For the locations of all the cross sections, consult Fig. 3.4.

Caution was used when interpreting upper air information displayed in this manner. These cross-sections do not actually represent a true cross-section through the MCS at a given time but a sequence of events recorded at one station. Actual x-z cross sections were not used due to the lack of data at any given time across the MCS (i.e., most cross sections would only have three stations). Also, since the MCS was highly three-dimensional and not very steady-state, composite sounding cross-sections were not used in this study.

Cross-sections of various parameters were produced. These included storm- relative winds, potential temperature, equivalent potential temperature, relative humidity, and geopotential height perturbations. Storm relative wind analyses included plots of total relative wind and contours of the relative wind component in the plane of the section. Relative humidities were adjusted for frozen liquid where air temperatures were below 0°C (c.f. Prupacher and Klett, 1978, Fig. 4-8). Geopotential height perturbations were calculated by finding the difference of the observed height to the mean height throughout the cross-section period for each 10 mb increment.

The first cross-section using the soundings at Russell KS (RSL) samples the mesohigh and the wake low better than any other sounding station. Fig. 6.1a shows a cross-section representing storm-relative winds. What can be seen are several distinct regions of air flow. Strong low-level easterlies are apparent ahead of and to the rear of the storm's leading edge (depicted by the right arrow on Fig. 6.1a). This flow is strongest below 850 mb. At 1920 and 2030 GMT, strong southwesterly flow is found above 300 mb. This coincides with the observation of a forward leaning anvil in the northern segment of the

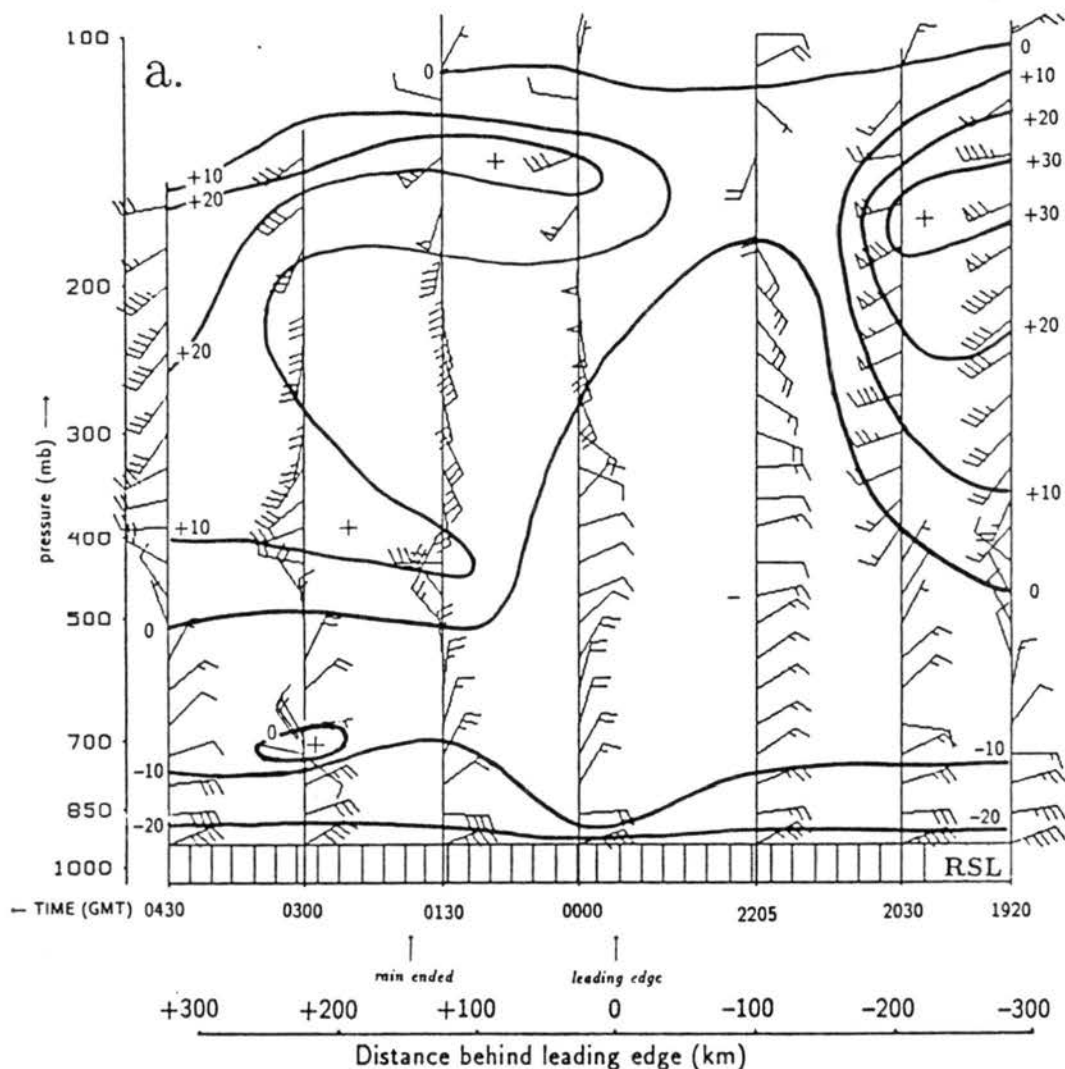


Figure 6.1: Time-height vertical cross section at Russell KS (RSL). Arrows indicate significant weather events. Time increases to the left and is GMT. Time to space conversion was used to determine storm relative distance: a) Wind barbs represent storm-relative horizontal winds (each full barb = 5 m s^{-1}). Relative motion along the plane of the cross section is contoured (“+” indicates a rear-to-front relative maximum, “-” represents a front-to-rear relative maximum); b) relative humidity (adjusted for frozen liquid where air temperatures were below freezing). Shaded regions represent relative humidities greater than 80%.

MCS at these times. The FTR (front-to-rear) flow ahead of the system becomes as deep as 200 mb at 2205 GMT. Low-level FTR outflow is retreating from behind the system.

To the rear of the system, three areas of RTF (rear-to-front) inflow are evident. The first, and the most prominent of the three, is at 150 mb. This first tier is the ambient flow responsible for blowing the anvil ahead of the MCS. The second and third RTF tiers are rear inflow jets (Smull and Houze, 1987b) under the trailing anvil. One rear inflow jet is at about 400 mb at 0430 GMT and descends slightly to 500-450 mb at 0130 GMT. The second jet, a weaker inflow area, is evident only at 0300 GMT at 700 mb. The strongest jet observed, about 12 m s^{-1} , would be defined by Smull and Houze (1987b) as a "Strong Rear Inflow". This stronger jet was found to be above the 0°C level. Interestingly, Rutledge *et al.* (1988) also found in the 10-11 June squall line that a stronger wake low was observed where the rear inflow was above the 0°C level (as opposed to being at or below the freezing level). This might account for the strong wake low found with MCS2 in the area of the RSL sounding site. The second jet observed at RSL could be defined as a "Stagnation Zone" (Smull and Houze, 1987b). Both of these inflow jets correspond to bands of very low relative humidities (Fig. 6.1b). This double banded structure of dry air is also evident on the 0000 GMT sounding for Dodge City KS (figure not shown).

Apparent from the RSL cross-section is the absence of any strong relative FTR flow penetrating rearward through the leading convection and into the stratiform anvil. Instead what is observed at RSL is a very weak FTR component at 0130 and 0300 GMT in a 400-200 mb level. Ahead of the system appears to be strong mid-level FTR inflow, but this flow does not penetrate through and to the rear of the system.

Based on observations using the Garden City KS (GCK) digitized radar data and IR satellite pictures, a non-precipitating anvil extends about 50-100 km west of the surface stratiform rain. Comparing with Johnson and Hamilton (1988), this distance is somewhat less (their anvil extended ~ 150 km rearward from the back edge of the surface stratiform rain). In their squall line case, the line-normal FTR flow penetrated much deeper rearward from the leading convective line.

The rear inflow found at RSL is similar to a feature observed by Johnson and Hamilton (1988) and Smull and Houze (1987b). One dramatic difference is noted however. The rear

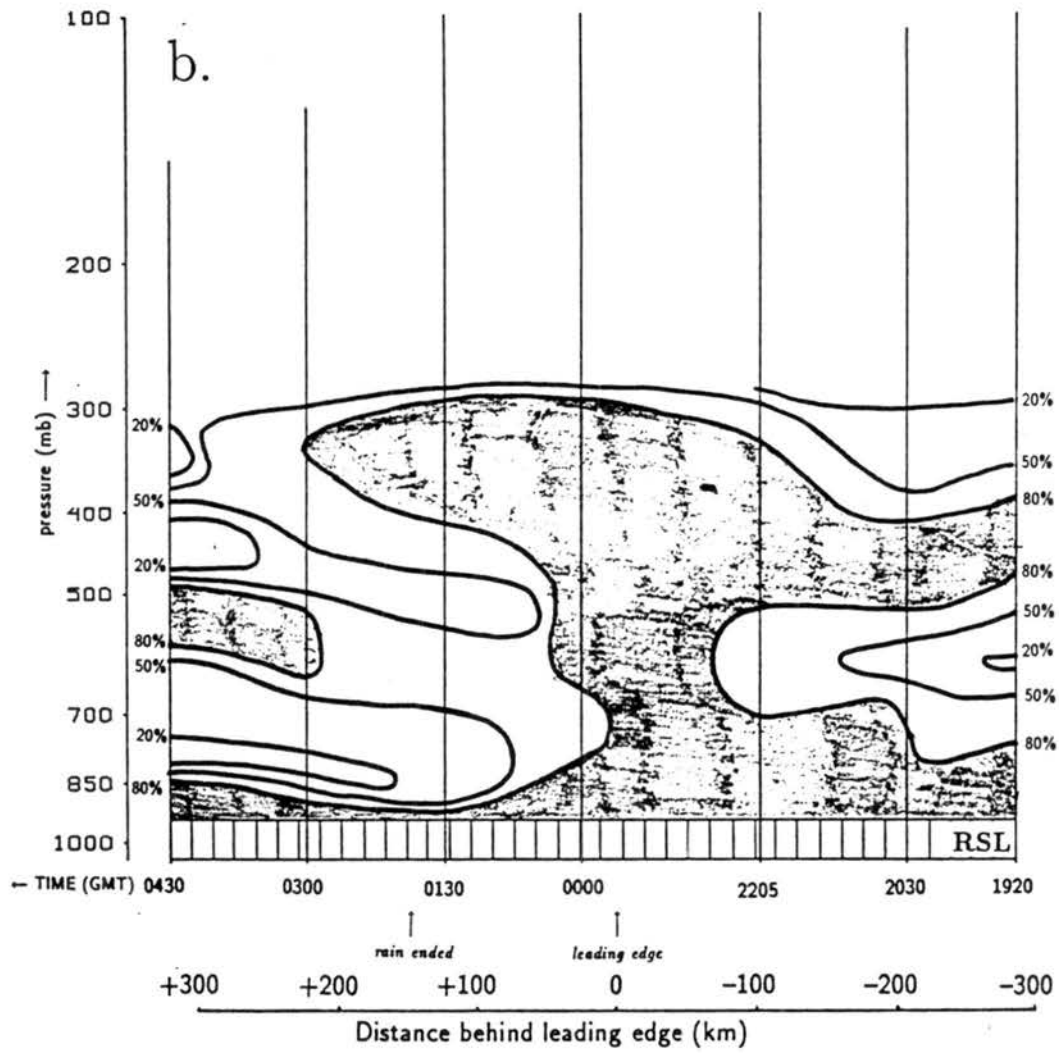


Figure 6.1: Continued.

inflow jet they studied appeared to descend from about 6-9 km AGL about 125 km behind the wake low down to the ground, through the convective line, and into the leading gust front. In the case of the RSL cross-section, the inflow jet descends only about 100 mb toward the leading edge of the rain, as sampled by the soundings. However, what happens to this inflow jet between 0000 and 0130 GMT is not clear given the data density in this cross section. Johnson and Hamilton (1988) and Rutledge *et al.* (1988) have shown that the rear inflow in the 10-11 June squall line penetrated to the surface and merged with the gust front outflow at the leading edge of the system. A strong gust front was not observed in the RSL area (stations P03, P04) which suggests that the rear inflow jet probably did not dip all the way to the surface in this vicinity. It may have descended at least partially to the ground, but this cannot be determined with this sounding data. To be shown in the next section of this chapter are detailed descriptions of the rear inflow jet as depicted with Doppler radar. The Doppler sections will show that the rear inflow did not penetrate far into the stratiform rain area, at least during the mature phase of the MCS.

Similar features are noted with the cross-section at Wichita KS (IAB; Fig. 6.2a). A band or "jet" of moderate rear inflow ($\sim 10 \text{ m s}^{-1}$) is found at 400 mb at 0430 GMT and descends slightly toward the leading edge of the system. This rear inflow extends down to 700 mb at 0130 GMT. The rear inflow here may be descending to the surface towards the leading edge of the MCS. A strong gust front was observed at station P23 near IAB. At IAB, dry air also accompanies the rear inflow (Fig. 6.2b), although it is not as dry as the rear inflow observed at RSL (the minimum relative humidity is $>40\%$ at IAB while at RSL it is $<20\%$). Strong low-level FTR flow is also apparent at IAB and FTR relative outflow exceeds 25 m s^{-1} to the rear of the system. At IAB, the relative flow behind the leading edge and above the rear inflow shows no FTR component. There is a moderate mid-level inflow ahead of the system, and southwesterly outflow is apparent ahead of the system above the 250 mb level. This cross section clearly shows the preference for forward storm relative flow in the upper-troposphere directed into the leading anvil as depicted in Section 5.2.

The cross section at Pratt KS (PTT; Fig. 6.3a) shows a slightly different structure than that observed at RSL and IAB. This cross section also samples the wake trough and

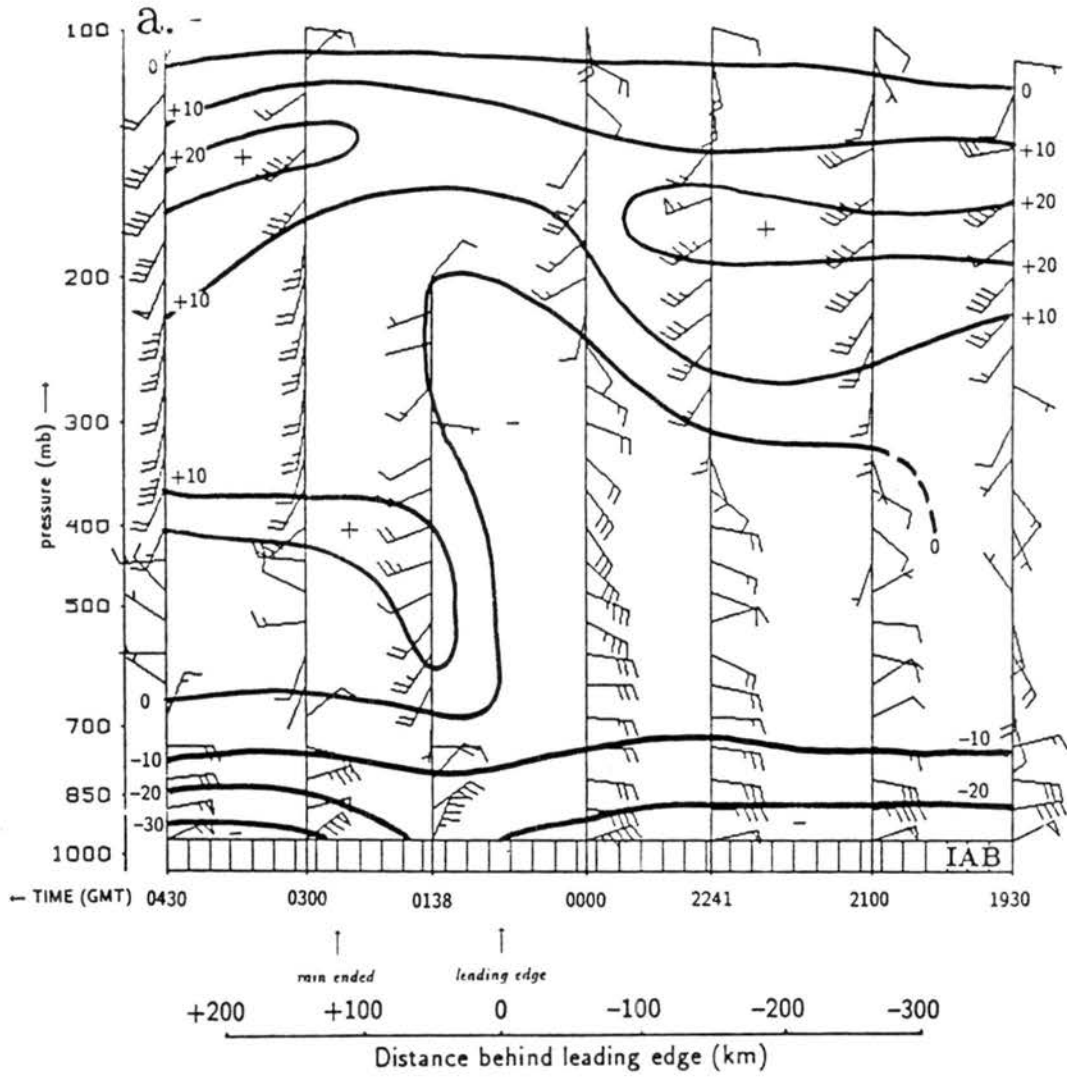


Figure 6.2: Same as 6.1 except for Wichita KS (IAB).

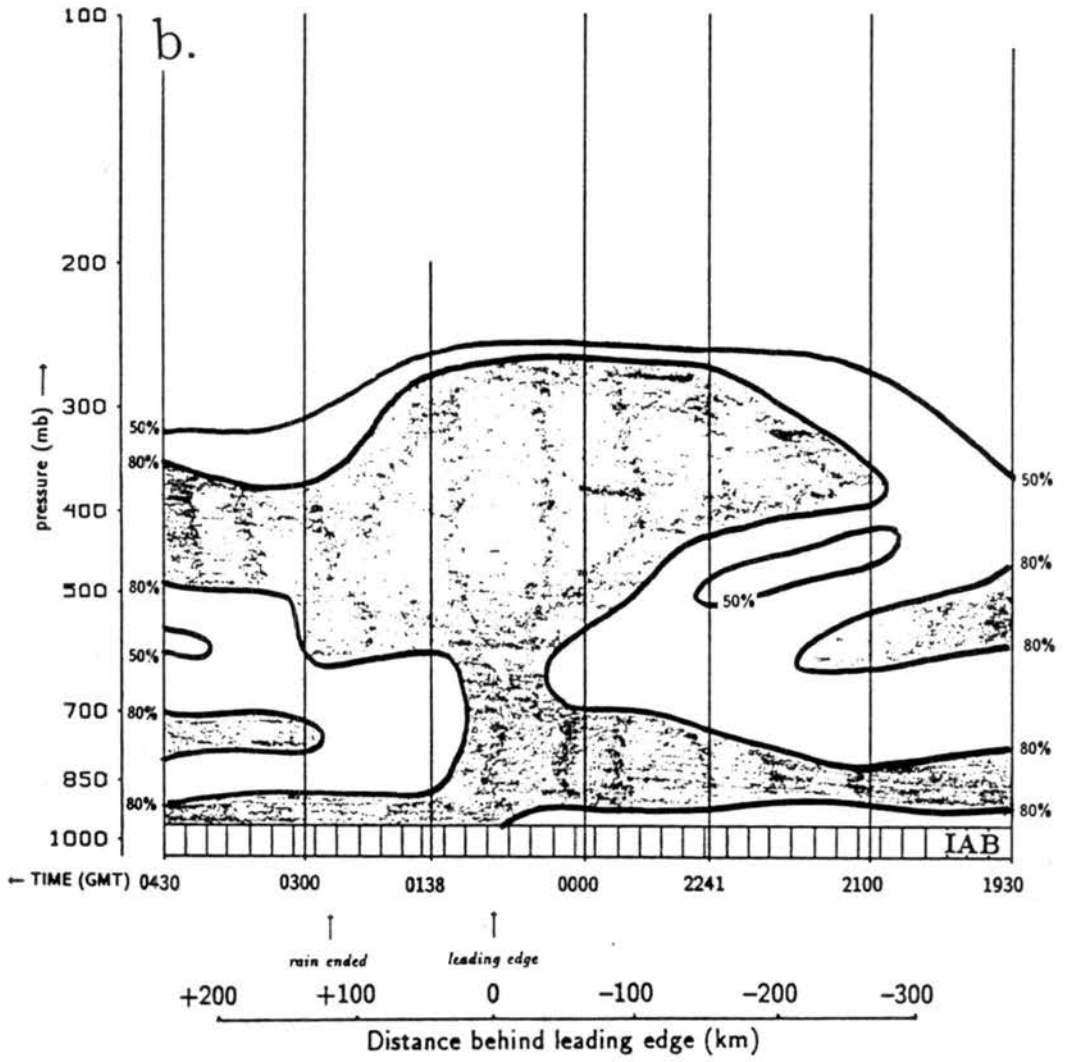


Figure 6.2: Continued.

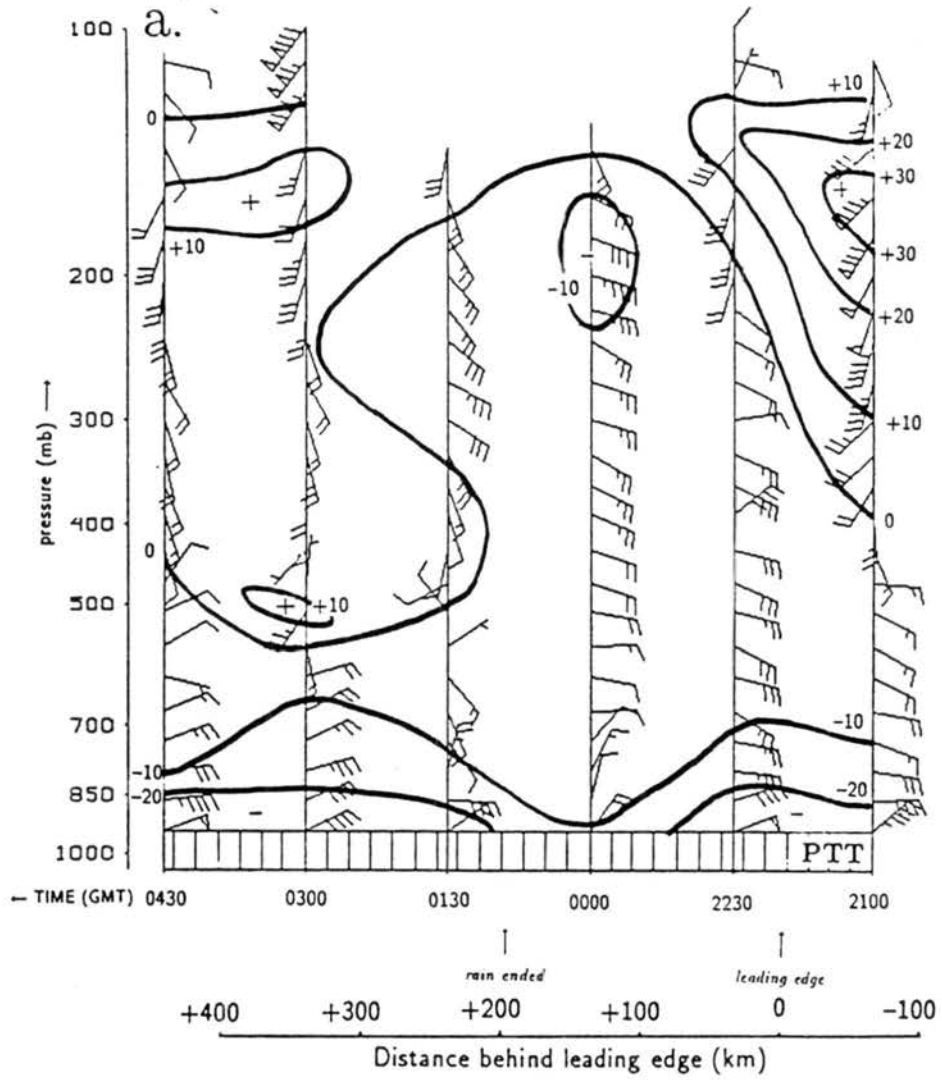


Figure 6.3: Same as 6.1 except for Pratt KS (PTT).

the stratiform anvil region but is south of the wake low center. A "Weak Rear Inflow" (Smull and Houze, 1987b) near 500 mb is observed at PTT accompanied by a band of lower relative humidities (Fig. 6.3b) slightly descending toward the system's leading edge. A second area of low relative humidities is observed behind the system's leading edge between 700 mb and 900 mb. Fig. 6.4 shows the thermodynamic profile at 0130 GMT for PTT. Note the strong drying in the lower layers and a moist surface layer. This is similar to the "onion" sounding (Zipser, 1977). At PTT, a strong relative flow extends through the leading line at mid-levels rearward compared to RSL (Fig. 6.3a), however, this flow is directed northwesterly instead of west-southwesterly which would be normal to the leading edge of the system.

The cross section at Fort Riley KS (FRI; figures not shown) is not complete enough to give a full detailed analysis of the upper levels in that location. There is evidence in the sparse data of a weak rear inflow at 600 mb at 0139 GMT. Also, strong RTF outflow is evident above 300 mb ahead of the system in conjunction with the leading anvil.

The following two cross sections represent the airmass associated with the southern segment of the MCS, namely the intense convective line. At Enid OK (END; Fig. 6.5), RTF outflow exists above 300 mb ahead of the system. To the rear of the system however, above 600 mb, the flow is basically south-southwest, which was along the motion of the MCS. The absence of a strong FTR flow at END correlates well with the absence of a trailing anvil here. A well defined rear inflow jet was not present at END. The lack of a well defined rear inflow jet at END suggests that pressure perturbations induced by the trailing anvil region are associated with the development of the rear inflow jet. Furthermore, the lack of a strong surface wake low to the rear of the southern segment of MCS2 suggests that the rear inflow jet is responsible for the production of the surface wake low, as proposed by Johnson and Hamilton (1988). The time height cross section at Woodward OK (WWR; figure not shown) is also devoid of a strong rear inflow jet.

Profiler wind data provided additional detail of the storm structure. These data offered slightly better temporal resolution (30-minute intervals) than the supplemental

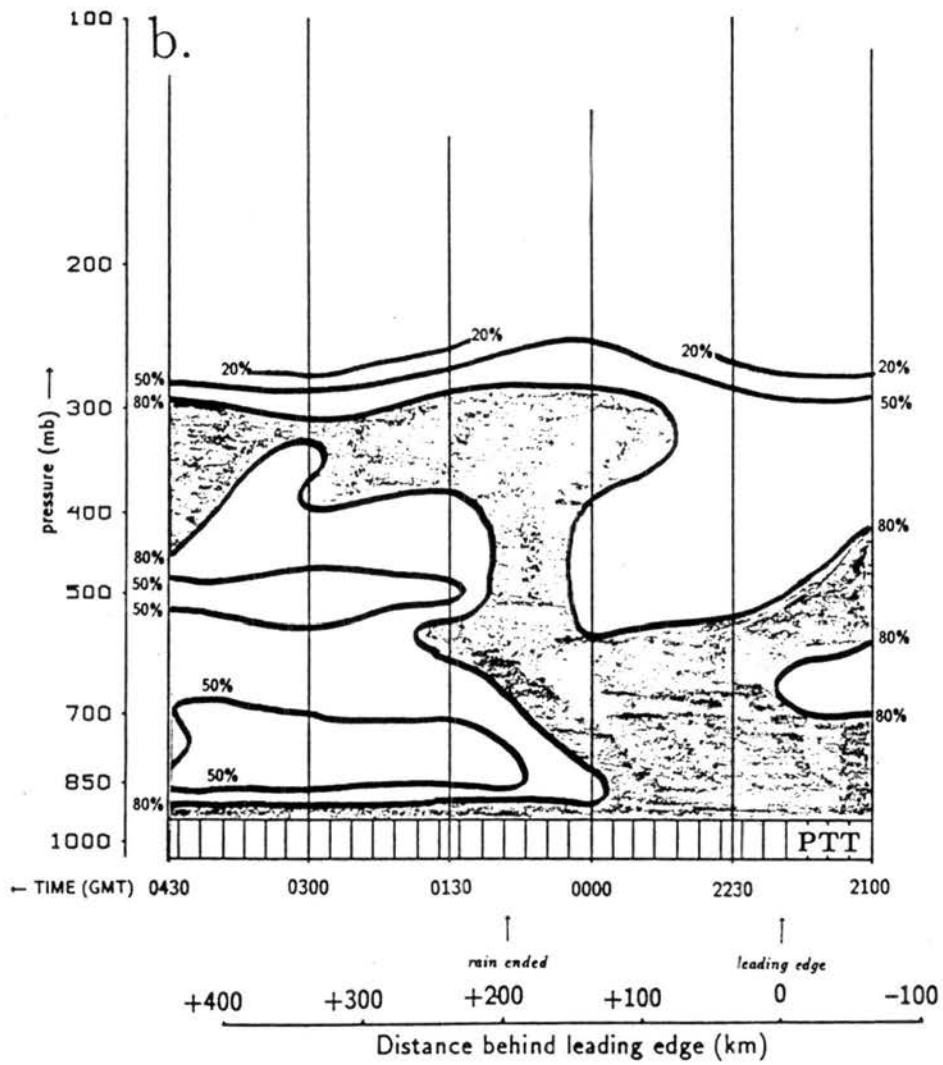


Figure 6.3: Continued.

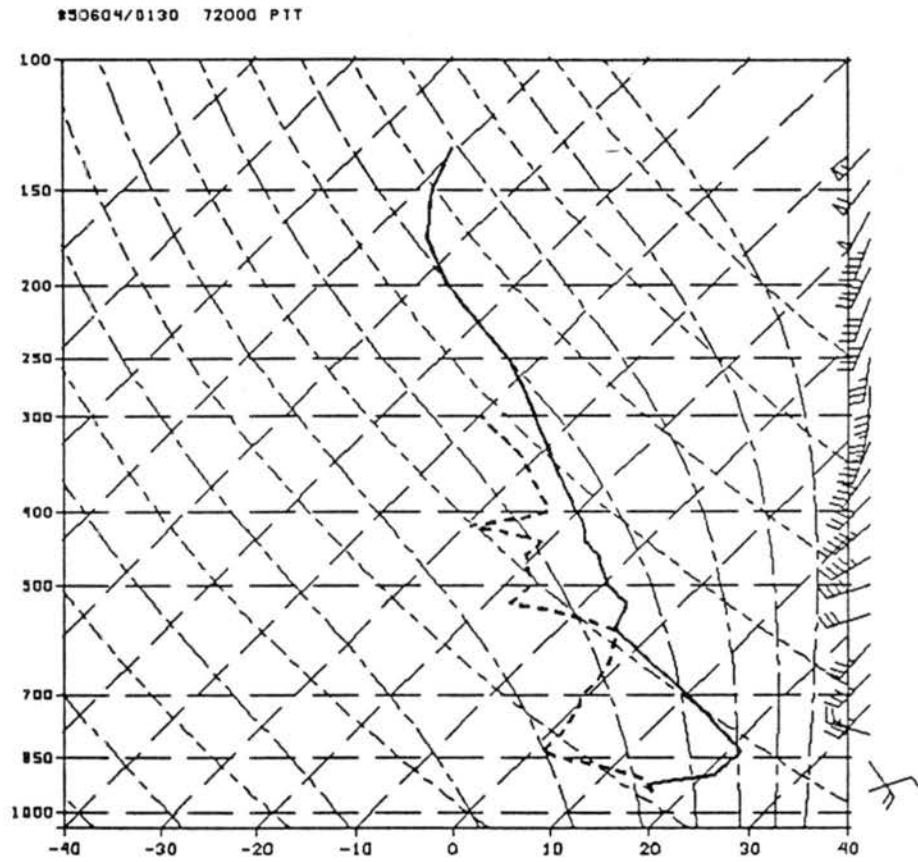


Figure 6.4: Thermodynamic profile at 0130 GMT 4 June 1985 for Pratt KS (PTT).

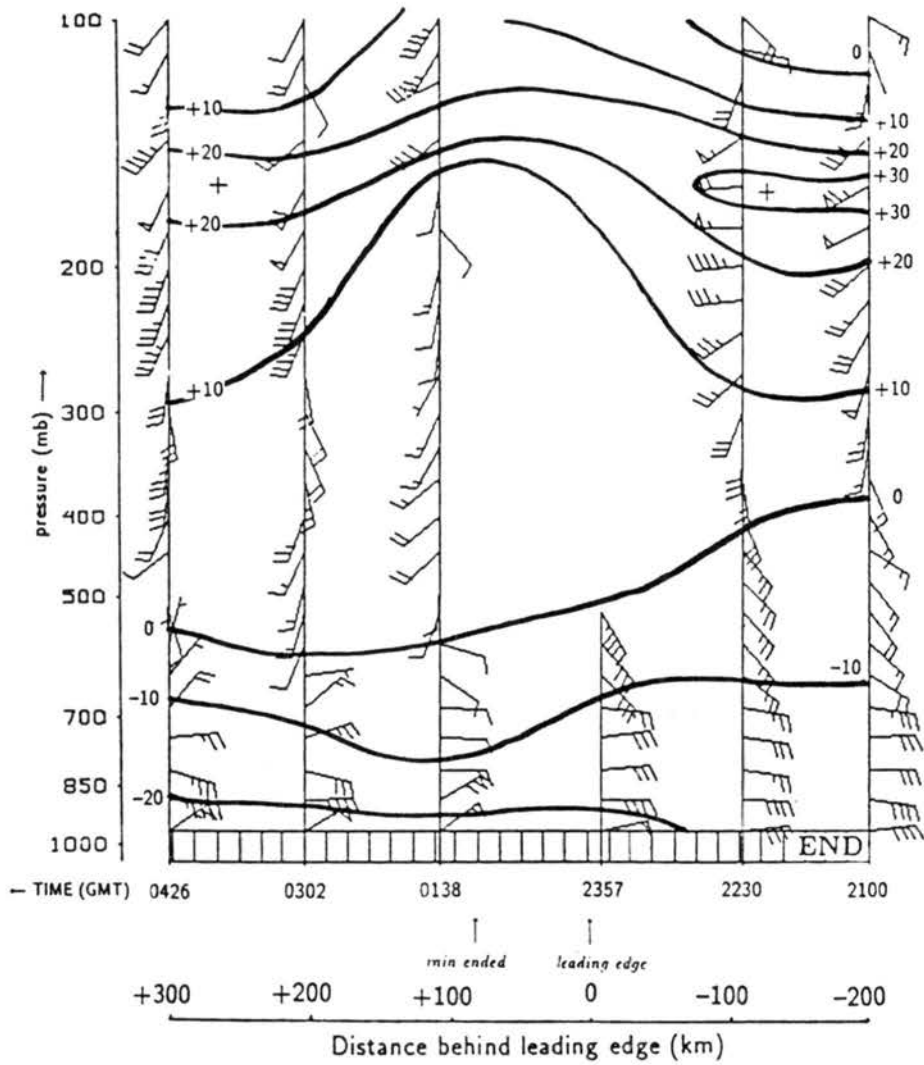


Figure 6.5: Same as 6.1a except for Enid OK (END).

sounding data. As was seen earlier at Liberal KS (Fig. 5.19), weak rear inflow was apparent behind the MCS. Low-level FTR flow was evident ahead of and behind the system. Aloft was strong RTF outflow ahead of the system and FTR outflow above the rear inflow. This time series represented the MCS during its initial stage.

The MCS crossed the McPherson KS profiler site during its mature phase (Fig. 6.6). Strong RTF flow is evident throughout a deeper layer than observed at RSL. A clearly defined axis of stronger rear inflow is not observed at midlevels. The very strong RTF flow found above 6 km could be indicative of the ambient wind flow observed blowing most of the anvil forward in this region of the MCS. Just behind the rear edge of the rain is strong rear inflow at 3 km and above (observed at 0200 GMT) which has descended slightly from higher levels. Most apparent from this time series is the lack of a strong mid- and upper-tropospheric FTR flow behind the back edge of the rain, as was observed by Johnson and Hamilton (1988) in a squall line case (see Fig. 2.2). Using the storm relative distance scale in Fig. 6.6, mid to upper level FTR flow could only have penetrated no more than 50 km behind the back edge of the surface rain. This observation shows further evidence of the short trailing anvil.

A cross section of potential temperature at RSL is shown in Fig. 6.7a. There is a region of warming at 200 mb ahead of the system's leading edge at 2205 GMT (denoted by "A" on Fig. 6.7a). This could be associated with subsidence beneath the forward leading anvil. Subsidence in these regions has been argued to be the primary factor in the development of a pre-squall low (Hoxit *et al.*, 1976). At lower levels, a cold dome is observed in a column through 700 mb at 0000 GMT ("B" on Fig. 6.7a). This low-level feature is also observed at PTT (figure not shown). To the rear of the system is a strong low-level inversion associated with the top of the surface layer containing moist cool FTR outflow. Above this is a warm unstable region through 400 mb associated with the subsidence warming beneath the trailing anvil. Similarly, the potential temperature cross section and END (Fig. 6.7b) shows a cool stable low level behind the system. However, a cold dome is not observed at END. This is because a broad mesohigh was never present in the southern region of the MCS. No significant warming is evident in the mid-levels behind the system (as no trailing anvil or rear inflow were observed at this station).

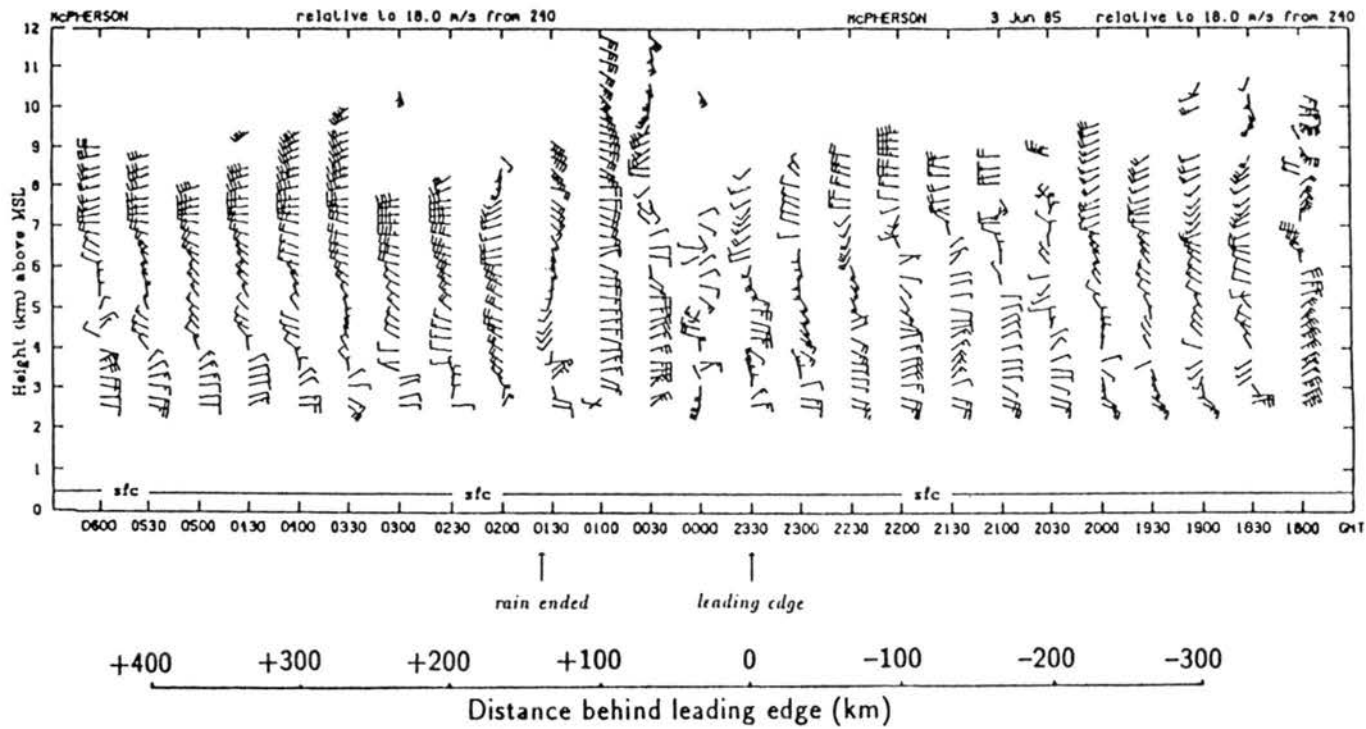


Figure 6.6: Same as 5.19 except for McPherson KS.

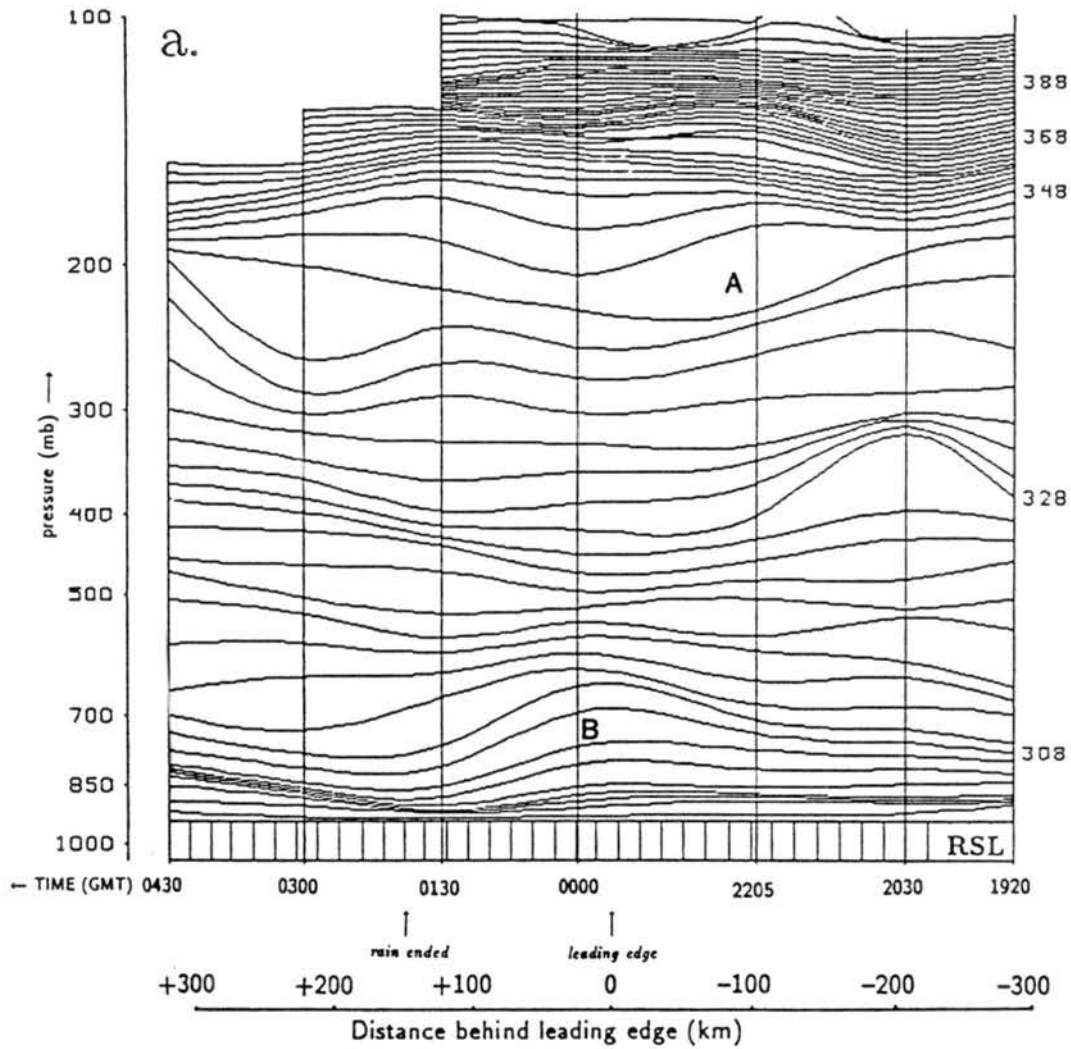


Figure 6.7: Time-height vertical cross section of potential temperature at: a) Russell KS (RSL); b) Enid OK (END). Contour intervals are 2K.

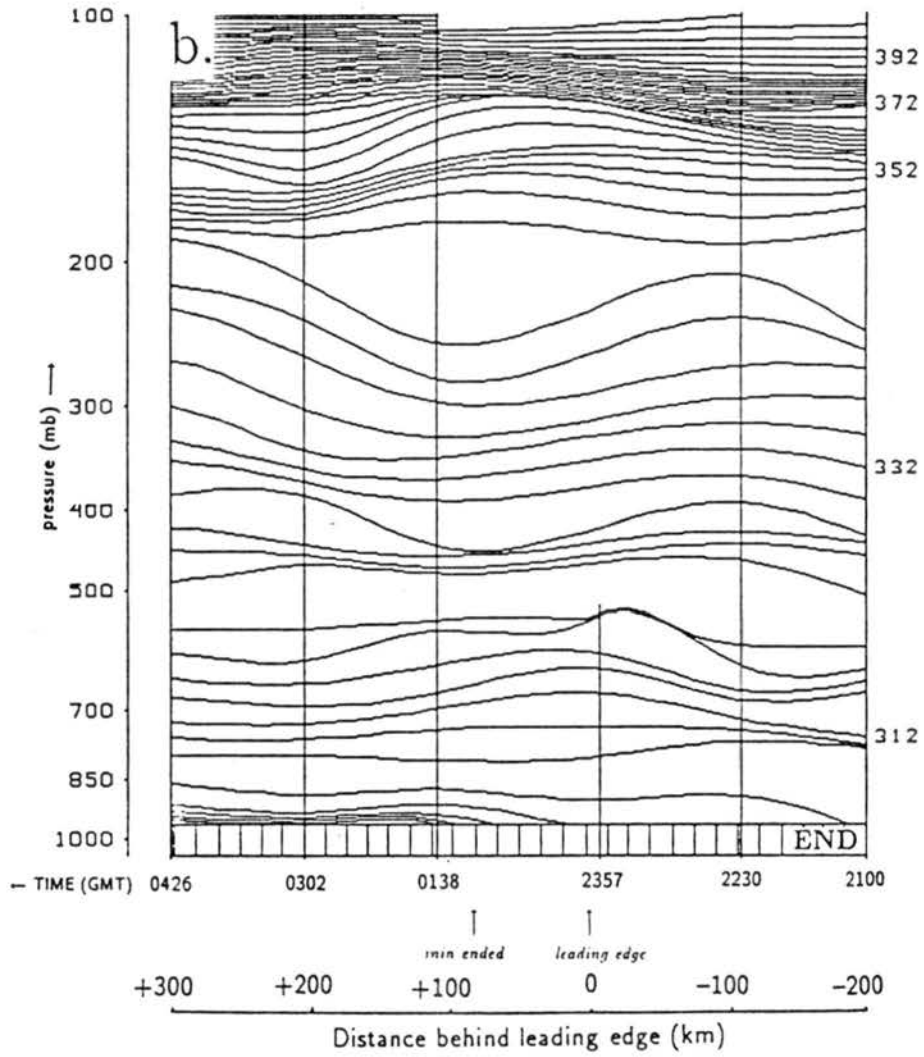


Figure 6.7: Continued.

Analysis of geopotential height perturbations at RSL (Fig. 6.8a), shows a pronounced minimum (mesolow) at 550 mb between 0000 and 0130 GMT. A mid-level mesolow is also evident at PTT and FRI (figures not shown), all three stations being in the northern segment of the MCS. A mid-level mesolow was also found (with a maximum amplitude at about 650 mb) by Johnson and Gallus (1988) and Rutledge *et al.* (1988) with the 10-11 June 1985 PRE-STORM squall line. Brown (1979), in a modeling study, found a mid-level mesolow in the stratiform region. Ogura and Liou (1980) also found pronounced convergence at 500 mb behind the convective updrafts of an Oklahoma squall line. Pressure gradients near the mesolow could be driving this convergence. The midlevel mesolow has been shown to be the result of the combined effects of evaporative cooling below the anvil cloud and latent heat release above it (Brown, 1979). Additional convergence may be due to the melting of snow at the freezing level [Leary and Houze (1979), Szeto *et al.* (1988)].

Near END, in the southern segment of the MCS, a mid-level mesolow to the rear of the system was not detected (Fig. 6.8b). The same was observed at WWR (figure not shown). A strong wake low was not observed in the southern segment of MCS2. Since a trailing anvil was not observed in the southern segment of MCS2, circulations typically associated with stratiform anvils are not found, namely the rear inflow jet, mid-level convergence, and a mid-level mesolow. These observations suggest that the circulations caused by the mesoscale upper level pressure fields present within stratiform anvils are probably the driving mechanism for the creation of a rear inflow jet and subsequently a surface wake low.

Other features observed on these cross sections include a strong mesohigh observed at 200 mb over the convective system (Fig. 6.8a,b). This feature is observed in both the northern and the southern segments of the MCS. This is related to the upper level heating and outflow at the top of the convective towers (Smull and Houze, 1987a). A strong low-level mesohigh is not apparent on Fig. 6.8a, probably because the highest surface pressures were observed to the south of RSL.

Pre-squall upper level mesolows were also observed. At RSL (Fig. 6.8a), one is located at 200 mb while at END (Fig. 6.8b) and WWR (figure not shown), one is found

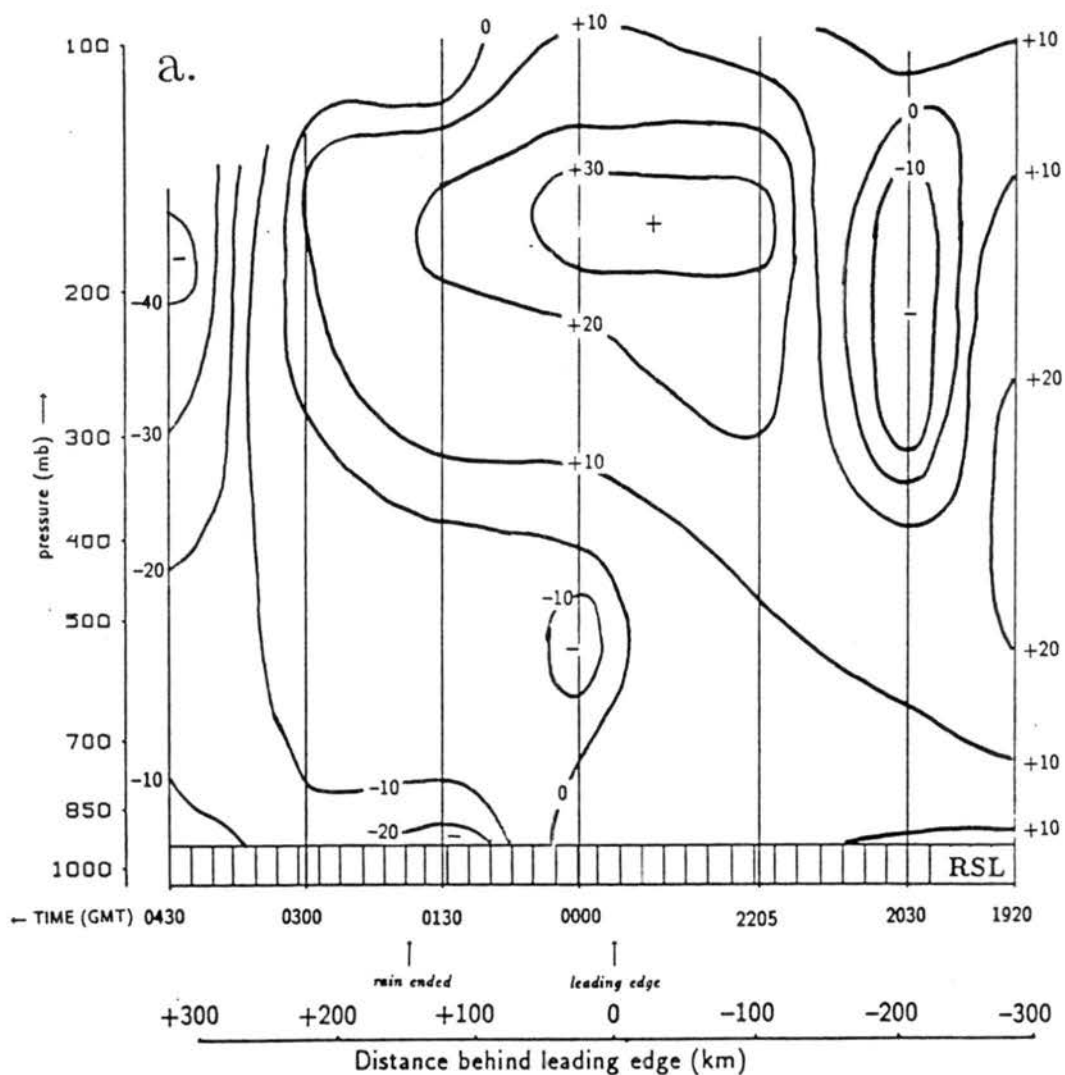


Figure 6.8: Time height vertical cross section of geopotential height perturbation for: a) Russell KS (RSL); b) Enid OK (END). Contour interval is 10 m (“+” indicates mesohigh, “-” indicates mesolow).

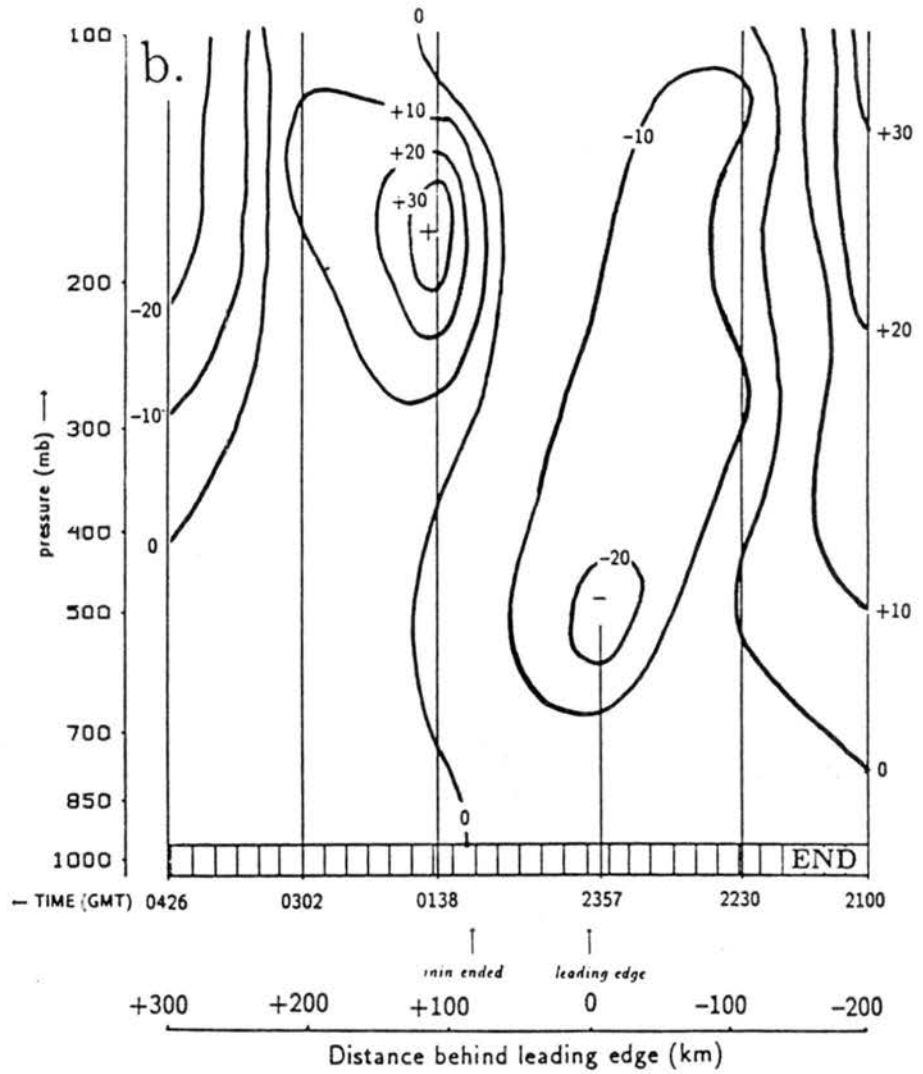


Figure 6.8: Continued.

at 500 mb. This mesolow was probably attributed to subsidence beneath the leading anvil (Hoxit *et al.*, 1976), leading to the formation of a surface pre-squall mesolow.

6.2 Internal flow structure of the mature MCS

In this section, several vertical and horizontal cross sections of dual Doppler wind and reflectivity data (kindly provided by Dr. Bradley Smull of NSSL/MRD) will be presented to investigate the detailed internal structure of the stratiform region. Figure 6.9 shows the two dual-Doppler analysis domains superimposed on the Wichita KS (IAB) radar reflectivity pattern at 0110 GMT. The heavy contour on this figure represents the first closed contour of the wake low at this time. The southwest analysis domain, which samples the stratiform area of the MCS, is presented in this section to detail the structure of the MCS wake on a smaller scale. The northern edge of the southwest analysis domain cuts through the southern end of the wake low center, however, a low pressure trough exists behind most of the stratiform rain in the northern segment of the MCS. For all winds shown, the mean motion of the MCS has been subtracted out.

Figure 6.10 depicts a Doppler radar east-west cross-section through an area just to the south of the wake low center at about 0110 GMT (line A-A' on Fig. 6.9). Contours on this figure represent radar reflectivity, and vectors depict the storm-relative flow. This storm relative flow depicts the along cross section component of the horizontal wind as well as the vertical component of the wind¹. The low-level shows a strong FTR flow associated with the moist cool outflow emanating from the rear of the system. At the edge of the stratiform rain on the surface (depicted by a heavy arrow), this low-level outflow extends to about 3 km AGL (~700 mb). Above this outflow and extending from the west edge of the domain is rear inflow with winds at about 12 m s^{-1} . This rear inflow is found at about 4.5 to 6.5 km (600 to 450 mb) along the bottom of the non- precipitating anvil².

¹The vertical wind component was calculated using a method similar to O'Brien (1970) by integrating the horizontal divergence fields using the continuity equation and assuming a zero upper boundary condition 0.5 km above the radar echo top (Smull, personal communication).

²Non-precipitating refers to that part of the anvil where falling rain is evaporated before reaching the ground (virga).

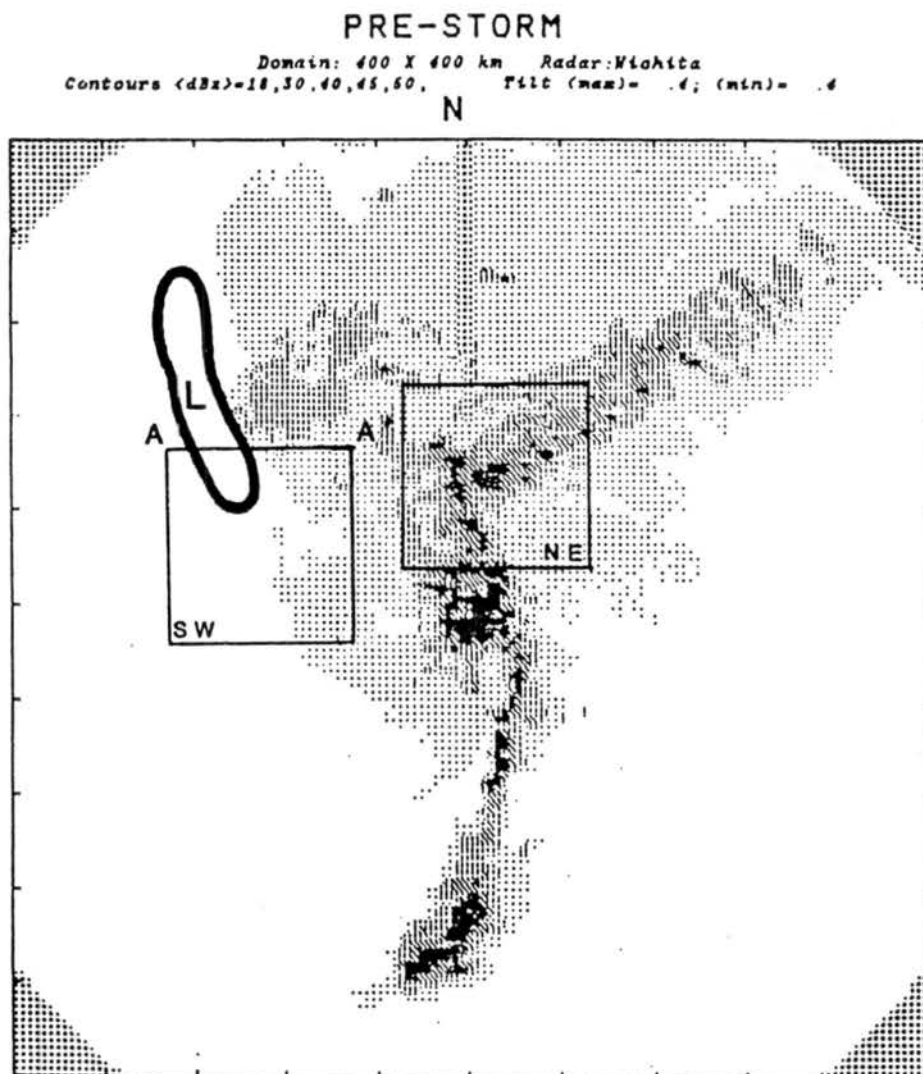


Figure 6.9: SW and NE analysis domains of the CP3 and CP4 dual-Doppler pair. Superimposed is the Wichita KS radar reflectivity field at 0105 GMT 4 June 1985. The heavy contour shows the 955 mb isobar of the wake low at 0110 GMT 4 June 1985. Line A-A' depicts the position of the vertical cross section in Fig. 6.10.

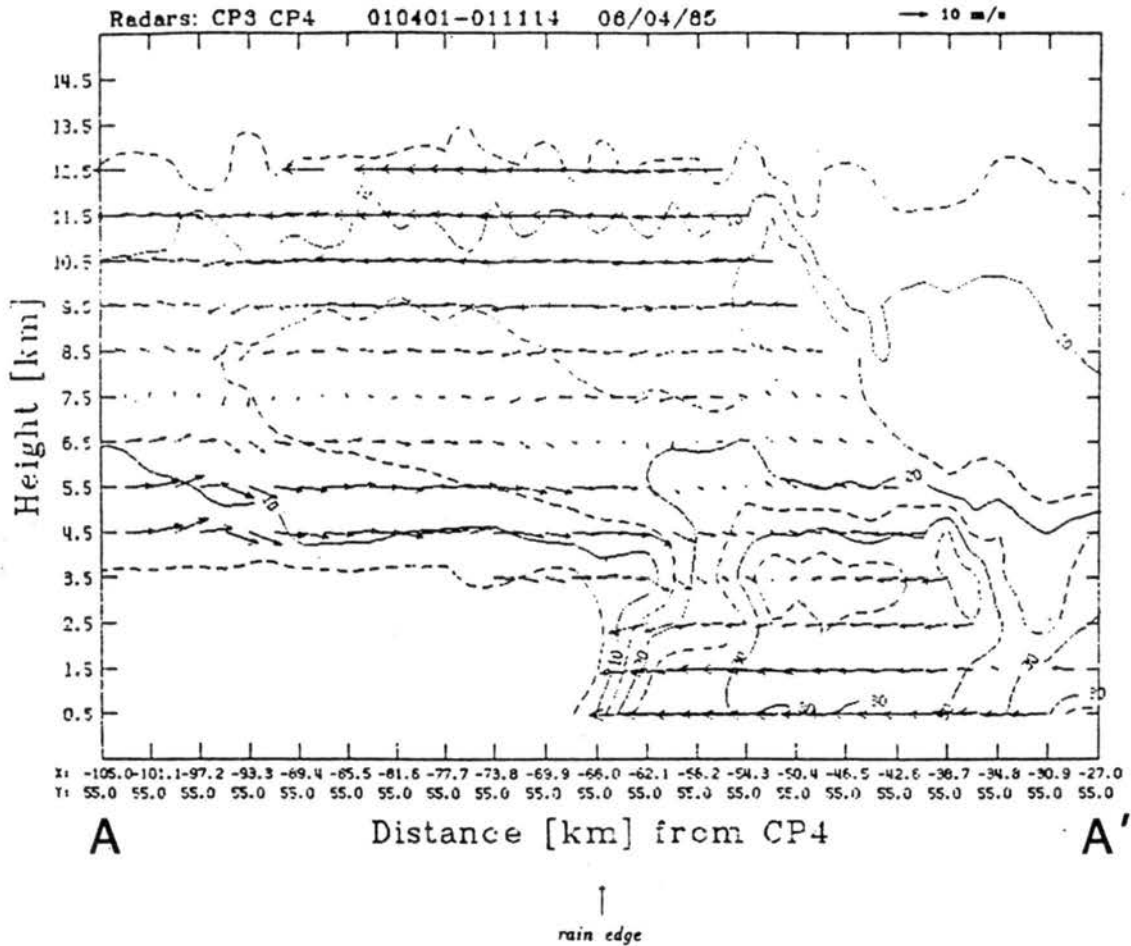


Figure 6.10: East-west vertical cross section of Doppler winds and reflectivity (see A-A' in Fig. 6.9). Wind vectors depict storm-relative flow. Reflectivity intervals are 10 dBz for solid contours. Dashed contours show 5 dBz intervals.

Since a radar target (such as rain or snow) must be present to measure the air speed using the Doppler radar, analysis of the wind flow below the non-precipitating anvil cannot be determined. It is possible that the rear inflow was present at a lower level than observed by Doppler in the trailing anvil. Since profiler data and supplemental sounding data showed that the rear inflow was not present well below the anvil cloud, it is believed that the strongest rear inflow did in fact line up along the base of the trailing anvil.

Note the mid-level convergence at 3.5 km AGL at $x=-50$ km. This convergence extends along a upward tilted line back to 7.5 km AGL at $x=-100$ km. This convergence coincides with a tilted 15 dBz reflectivity contour in the anvil. Mid-level convergence has also been observed to the rear of MCSs with trailing stratiform anvils [Ogura and Liou (1980), Smull and Houze (1987b), Johnson and Hamilton (1988), Johnson and Gallus (1988), Rutledge *et al.* (1988)]. The midlevel mesolow observed on the geopotential height cross section at RSL (Fig. 6.8a) may be forcing this convergence (Smull and Houze, 1987b).

A salient feature found at the rear edge of the stratiform rain is the cessation of the rear inflow jet. Rather than a smooth descent toward the leading edge of the MCS [as found by Smull and Houze (1987b) and Johnson and Hamilton (1988)], the jet appears to maintain a constant level and then converges with some opposing FTR flow at the rear edge of the stratiform rain. Referring back to Fig. 5.23a, strong convergence is found at the rear edge of the rain in the northern segment. Augustine and Howard (1988) noted that θ_e values at 500 mb are consistent with those found in a column down to the surface. Above 500 mb, θ_e values are greater. This implies that the air is descending in a mesoscale downdraft along the convergence at the rear edge of the stratiform rain. An extremely rapid descent of the air along this convergence suggests that strong evaporation and subsidence warming must be occurring along the rear edge of the precipitation. This strong subsidence, localized along a narrow strip under a non-precipitating anvil, could account for the extremely sharp pressure falls on the east side of the surface wake low.

Referring back to Fig. 5.6a, the wake low is found directly upstream from a localized maximum in the stratiform rain echo (≥ 35 dBz). Johnson and Hamilton (1988) speculate

that the intensity of a descending rear inflow jet is directly proportional to the intensity of the stratiform precipitation. If evaporation drives the sinking processes in the anvil region, then air encountering heavier precipitation would sink more rapidly and have the greatest vertical displacement (Zipser, 1977). Therefore, adiabatic warming and the subsequent hydrostatic lowering of the surface pressure should be maximized at the location where the stratiform rain is strongest.

The wake low is maximized at the rear edge of the stratiform rain because precipitation cooling neutralizes the adiabatic warming in the wake low (Johnson and Hamilton, 1988). Just outside the precipitation area, the precipitation cooling is insufficient to offset the warming and rapid surface pressure falls are found here.

A FTR flow is found above the rear inflow in the stratiform anvil (above 8.5 km in Fig. 6.10). It will be shown on horizontal Doppler analyses that this flow is directed predominantly to the northwest at midlevels rather than to the west-southwest which would be line normal FTR flow.

Figures. 6.11a-c show dual-Doppler horizontal wind fields in the southwest analysis domain represented in Fig. 6.9. The first level at 0.5 km AGL (Fig. 6.11a; the elevation of CP4 is 438 m which places this level at roughly 910 mb) shows the low-level FTR outflow at the rear of the system. This outflow extends to a 2.5 km AGL depth. At 3.5 km AGL (~ 660 mb; Fig. 6.11b), weak rear inflow is evident. Speed convergence is found along the right edge of the domain at about $x = -55$ km. Confluence is observed in the northern part of the domain. Since the northern part of the southwest analysis domain samples the southern portion of the wake low, it is possible that this convergence is responsible for a locally strong downdraft here accounting for the extreme hydrostatic surface pressure reduction. Note that winds here turn to the north-northwest parallel to the rear edge of the stratiform rain (also depicted on Fig. 5.23a). This was also observed by Rutledge *et al.* (1988). The rear inflow extends vertically up to 6.5 km AGL. Above that level, the winds back to the southeast at 9.5 km AGL (~ 280 mb; Fig. 6.11c). This level shows the weak relative FTR flow which is responsible for the hydrometeor transport into the relatively short trailing anvil. This southeasterly flow was also observed at 0130 GMT on

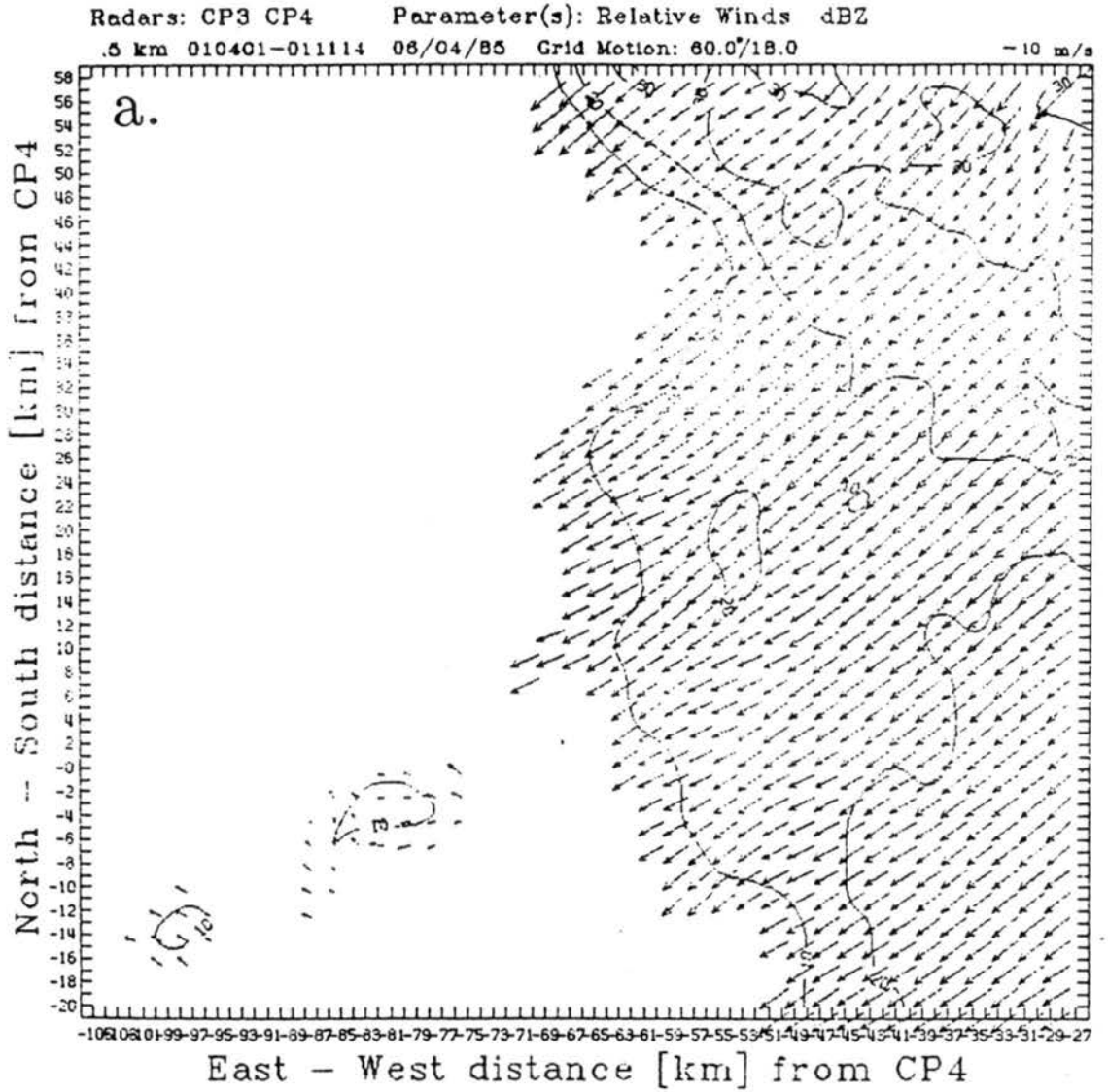


Figure 6.11: Dual-Doppler horizontal wind fields of storm-relative motion in the SW analysis domain for: a) 0110 GMT 4 June 1985 at 0.5 km AGL (above ground level for CP4.); b) 3.5 km AGL; c) 9.5 km AGL. Elevation of CP4 is 438 m. Reflectivity contours are the same as Fig. 6.10.

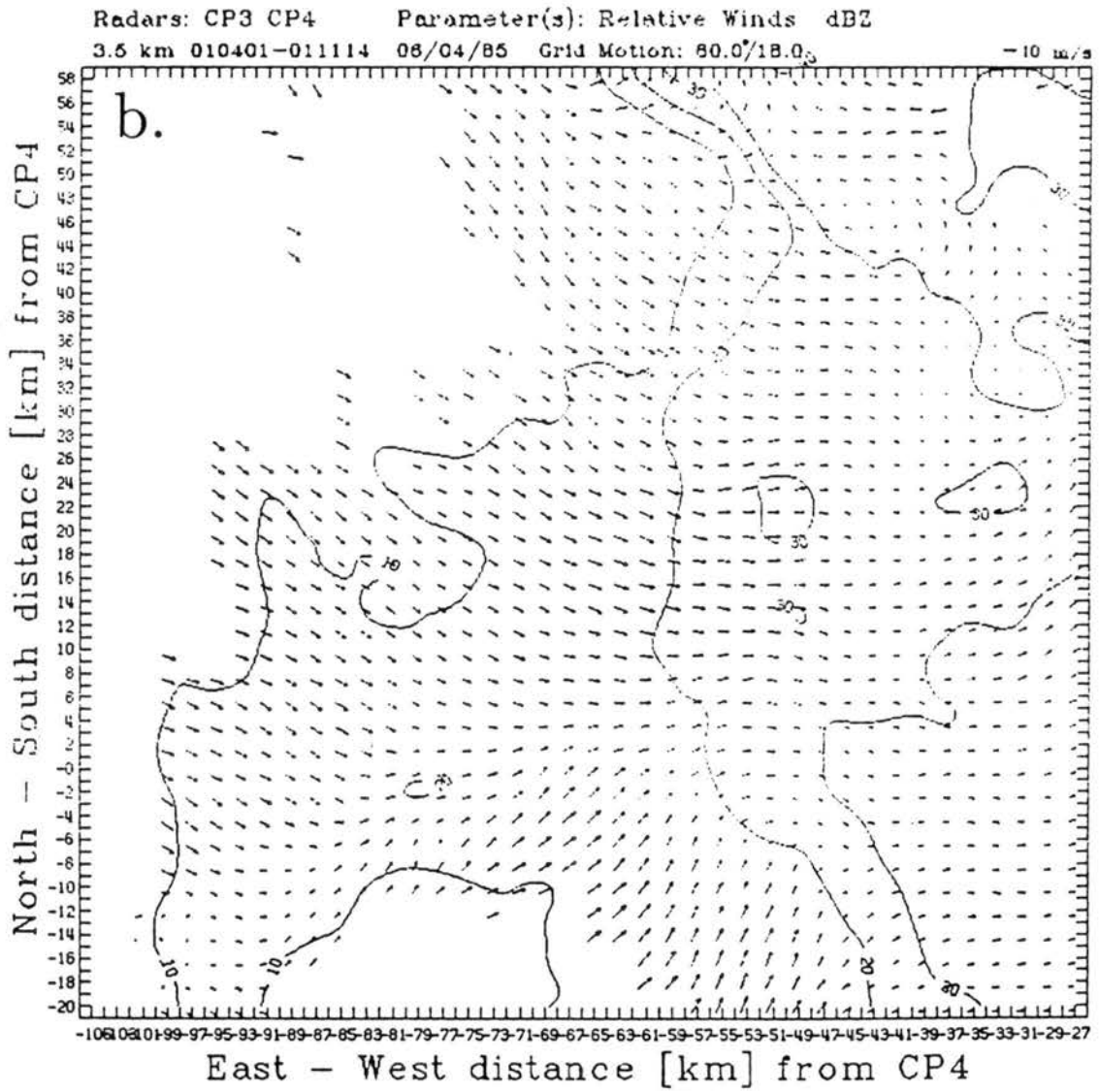


Figure 6.11: Continued.

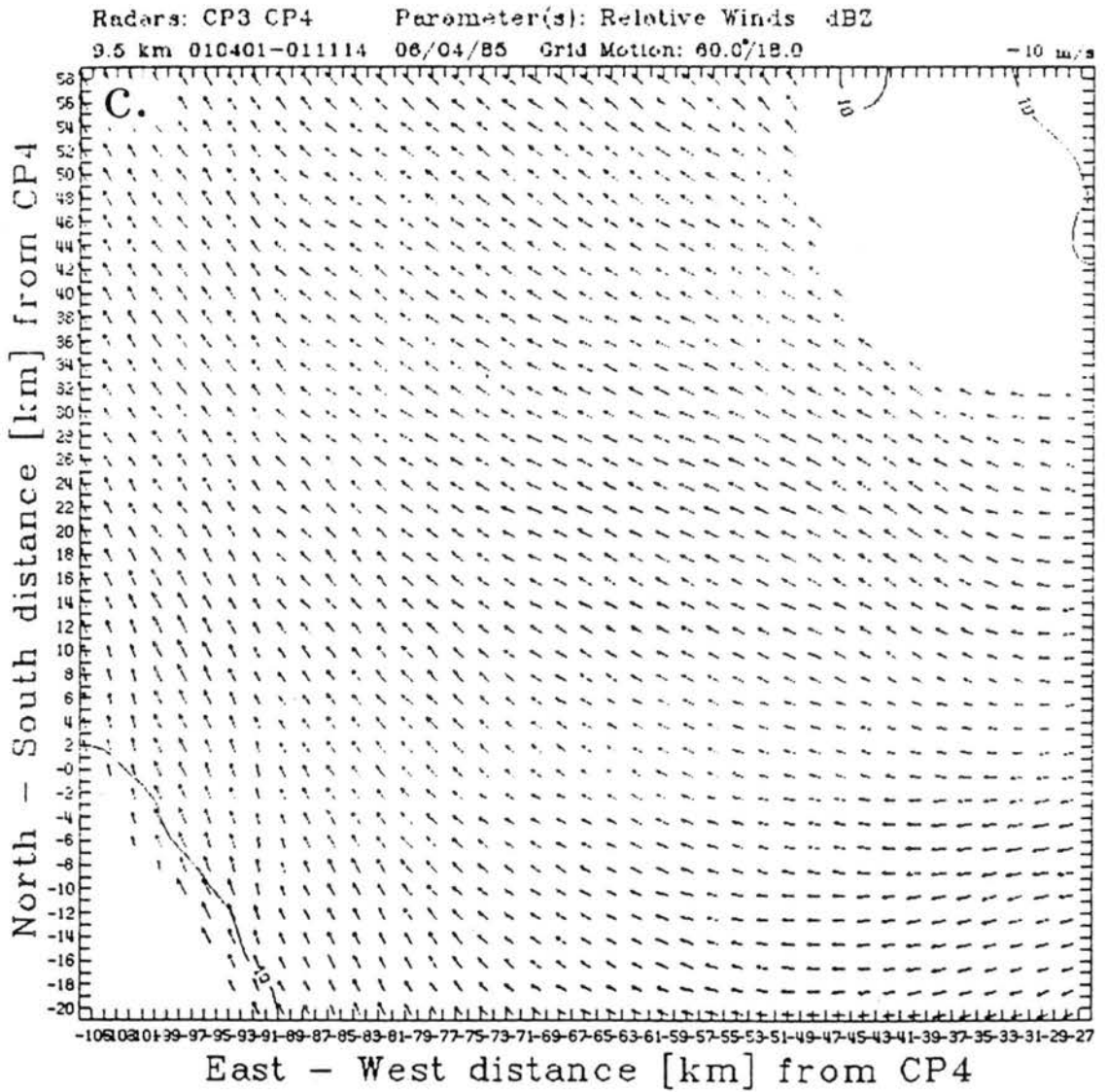


Figure 6.11: Continued.

the RSL cross section (Fig. 6.1a). Along the southwest corner of the domain (at the rear edge of the anvil indicated by the 10 dBz reflectivity contour), winds are more southerly.

6.3 Variations between wake low and mesohigh structure and north-south variations in wake low structure

Upper air sounding profiles in the wake low and the mesohigh are now shown to contrast the vertical structure in these regions. Figures 6.12a,b show two thermodynamic soundings taken in each region. The first (Fig. 6.12a) is taken at Fort Riley KS (FRI) at 0000 GMT. This sounding was taken within the northern precipitation area. This sounding is moist adiabatic from just above the surface to 300 mb. Relative humidities are above 80% up to 530 mb. A surface inversion is evident as well. The sounding at Russell KS (RSL; Fig. 6.12b) at 0130 GMT, sampled near the wake low, contrasts with the FRI sounding. There is a saturated surface layer associated with the low-level outflow behind the MCS. Above this is a dry deep mixed layer. This sounding is similar to the "onion" sounding (Zipser, 1977), however, a saturated layer in the mid-troposphere is not observed. Air above 450 mb (which was the approximate level of the rear inflow—see Fig. 6.1) is slightly less than saturated. Assuming that the trailing anvil was at the level, it is possible that rawinsonde instrumentation was being affected by ice leading to an inaccurate dewpoint measurement. An "onion" sounding was also observed at IAB (Fig. 6.12c). The top of the mixed layer in the IAB sounding is near the freezing level, which is at the base of the anvil.

The "onion" sounding has been observed by Zipser (1977), Ogura and Liou (1980), Leary and Rappaport (1987), and Hamilton and Johnson (1987). In a typical "onion", three distinct regions are found. One is the moist surface layer due to the rearward low-level outflow from the MCS. Second is the warm and dry mixed layer due to the mesoscale downdrafts found beneath the trailing anvil. Third is the moist layer beginning at the base of the anvil and continuing upward.

Computations of the hydrostatic surface pressure change due to the development of the warm dry mixed layer to the rear of the MCS were carried out and reported in Table 6.1. Using the mean virtual temperature in the warmed column, the change in the surface

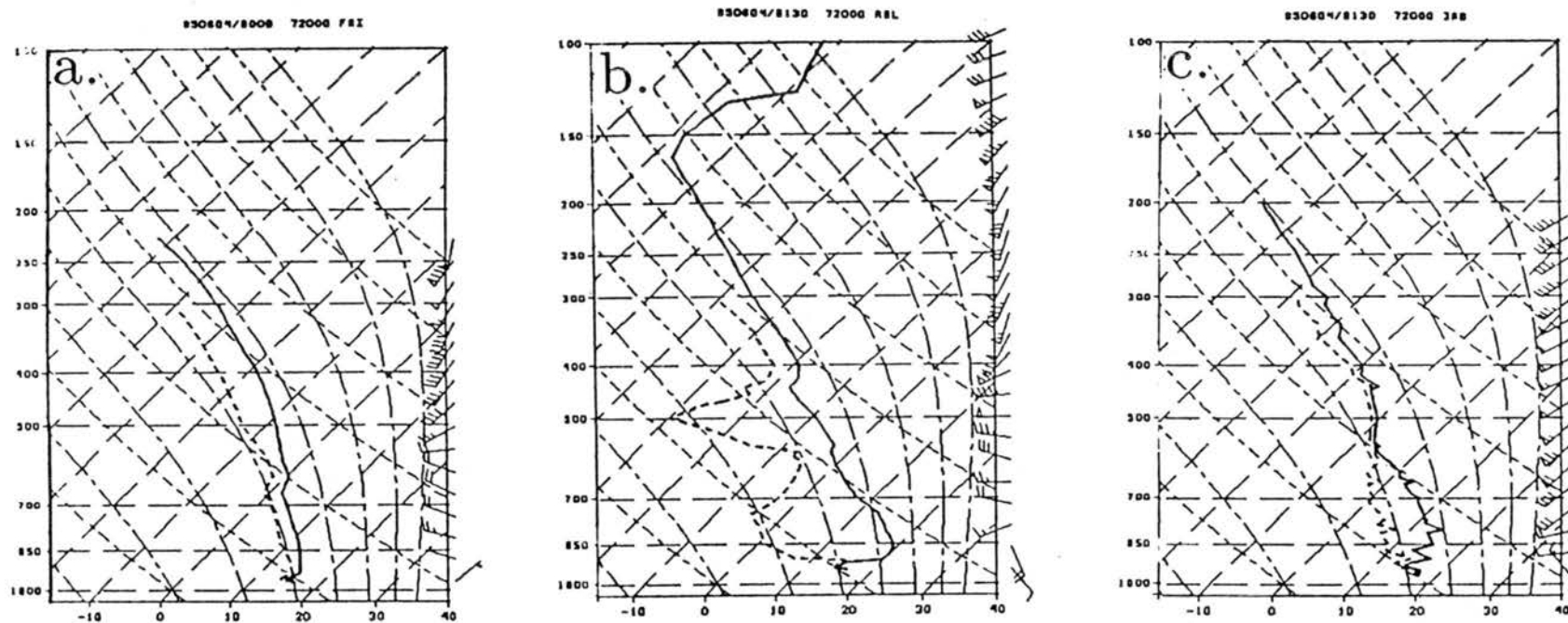


Figure 6.12: Same as 6.4 except for: a) 0000 GMT 4 June 1985 at Fort Riley KS (FRI);
 b) 0130 GMT 4 June 1985 at Russell KS (RSL); c) 0130 GMT 4 June 1985 at Wichita
 KS (IAB)

Table 6.1: CALCULATIONS OF HYDROSTATIC SURFACE PRESSURE CHANGE.

Station	Time period	p	Δz	$\Delta \bar{T}_v$	Δp_s
Russell, KS	0000 to 0130	600 mb	+ 5.31 m	+2.86 K	-4.66 mb
Pratt, KS	0000 to 0130	600 mb	+14.63 m	+3.99 K	-5.68 mb
Wichita, KS	0000 to 0130	600 mb	- 9.05 m	+2.41 K	-5.62 mb
Enid, OK	0130 to 0300	500 mb	-10.30 m	+0.55 K	-2.65 mb
Woodward, OK	2230 to 0000	600 mb	+14.05 m	+0.40 K	+0.95 mb
Woodward, OK	0000 to 0130	500 mb	+ 9.14 m	+1.03 K	-1.47 mb
Fort Riley, KS	2230 to 0000	600 mb	+35.91 m	-2.94 K	+9.98 mb

pressure associated with this warming is given as:

$$\Delta p = p(z) \left[\exp\left(\frac{gz}{R_d \bar{T}_v}\right)_f - \exp\left(\frac{gz}{R_d \bar{T}_v}\right)_i \right] \quad (6.1)$$

where the subscripts i and f refer to initial and final values. Hydrostatic surface pressure changes were carried out at a number of stations for various column depths above the ground. The pressure and height above the ground of the top of the column are given as $p(z)$ and z respectively.

One can see from Table 6.1 that the strongest calculated pressure falls are for the northern stations (RSL, PTT, and IAB). These calculated pressure falls agree very closely to what was observed at PAM stations in the vicinity of the sounding sites. For example, station P04, near RSL, experienced a 5.4 mb surface pressure fall from 0000 to 0130 GMT, and the surface pressure at P20 fell 6.0 mb from 0000 to 0130 GMT. By comparison, END and WWR show a smaller reduction in surface pressure, which also agrees quite well to observed pressure falls (see Fig. 5.10).

These results show that the majority of the warming aloft is found to the rear of the northern segment of the MCS in association with the trailing anvil. It is here that the strongest wake low was observed. Since a trailing anvil was not observed in the south, then the warming expected beneath such an anvil will not take place, and a strong wake low should not be observed.

From 2230 to 0000 GMT, the surface to 600 mb column at FRI experienced strong cooling associated with the precipitation filled downdraft of the northern rain area. The calculated hydrostatic pressure rise was almost 10 mb. Observed pressure rises were only as high as 6 mb. This discrepancy is probably due to the location of the sounding site which was outside the mesonet network of PAM stations. A larger surface pressure rise may have been experienced there. Also, hydrostatic changes aloft could have reduced the pressure rise.

Chapter 7

SUMMARY

Presented in this paper is an extensive overview of the meteorological conditions associated with the second MCS of the 3-4 June 1985 period which passed through the domain of the OK PRE-STORM field experiment. Surface and upper air data reveals the complex structure of the MCS.

The analyses presented in Section 5.1 illustrates the mesoscale surface pressure features observed with this system. Shown is the development of a strong mesohigh in the western section of the mesonet network. This mesohigh moved eastward with the centroid of the northern stratiform region throughout the MCS's mature phase. Coupled with the progression of the mesohigh across the PAM network was a wake low which followed the mesohigh, "hugging" the rear edge of the stratiform rain.

During the initial stage of the MCS, the convection was characterized as a "random" (Blanchard and Watson, 1986) conglomeration of heavy convective cells. As time went on, the convection became more stratiform, especially in the northern segment. Coupled with the development of this northern stratiform region was a mesohigh centered over the rain. Also, a pre-squall trough and mesolow were observed before the storm reached maturity.

As the MCS matured, it developed a surface precipitation pattern resembling an occluded wave cyclone (Blanchard and Watson, 1986) but on a much smaller scale. A strong convective line developed along a wind shift line to the south. The northern portion of the MCS was comprised of a stratiform rain area with some embedded convection. It was in the northern segment where the most dramatic pressure features were observed. A broad mesohigh was situated over the stratiform rain area and a strong wake low developed at the back edge of the northern stratiform rain area. An intense pressure

gradient was observed between the mesohigh and the wake low during the mature phase. Local gradients were close to 2 mb per 10 km, corresponding to a geostrophic wind speed of 190 m s^{-1} . The surface flow patterns observed in the vicinity of the intense pressure features resembled those found by Johnson and Hamilton (1988).

The mature phase of the MCS lasted only a few hours. Soon afterwards, reflectivity intensities decreased, and the southern convective line broke up. As the stratiform rain region left the northeast corner of the mesonet, it carried with it the mesohigh with its highest pressures recorded. The wake low lagged behind, but maintained its intensity.

What made this case so interesting is that a wake low/mesohigh couplet, typically observed with linear MCSs having trailing stratiform anvils, has been discovered with an MCS having a very complex storm structure. This case featured a stratiform anvil region which was predominantly north of the heaviest convective elements. The mid- to upper-tropospheric relative flow played an important role in determining the spreading of the stratiform anvil.

At mid-levels, a confluence axis stretched along the southern squall line north-northwestward along the back edge of the northern stratiform rain area. To the east of this confluence was southeast flow which spread some of the anvil rearward in the northern stratiform area. To the west of this line, cutting under the trailing anvil, was a rear inflow jet (Smull and Houze, 1987b). In the southern part of the MCS, the relative flow was predominantly along the line at midlevels, and a trailing anvil was not observed.

At upper levels, the relative flow was predominantly towards the northeast upstream of the MCS. Some of the flow diverged around the MCS, but the basic tendency was to blow the anvil "plume" to the northeast ahead of the MCS.

A small portion of the upper level flow was directed rearward in the northern segment of the MCS, and a relatively short ($\sim 50\text{-}100 \text{ km}$) non-precipitating trailing anvil was observed. Mesoscale circulations at the rear of the trailing anvil subsequently led to rapid surface pressure falls and the formation of a strong surface wake low. It is suggested that the wake low is attributable to subsidence warming at the back edge of the stratiform rain area [Williams (1963), Zipser (1977), Johnson and Hamilton (1988)]. The strongest

pressure falls were observed just outside the area where precipitation was reaching the ground, and the wake low "hugged" the back edge of the rain because precipitation cooling was insufficient to offset the subsidence warming. Also, a "heat burst" (Johnson, 1983) was observed beneath the trailing anvil, a manifestation of strong subsidence and dry downdrafts in that area.

The extreme pressure drops found at the rear edge of the mesohigh imply that a very strong mesoscale unsaturated downdraft was present in this region. It was shown in Chapter 6 that the rear inflow jet, which traveled along the bottom part of the trailing anvil, met up with the relative FTR flow at midlevels at the back edge of the surface rain. Johnson and Hamilton (1988) felt that the surface pressure falls were a manifestation of the descending rear inflow jet. It is felt that the rear inflow in our case descended sharply along the convergence at the rear edge of the rain, leading to the extreme surface pressure falls observed there [this downdraft idea was supported by the θ_e analyses of Augustine and Howard (1988)]. The wake low was observed adjacent to a maximum in the stratiform radar reflectivity suggesting that mesoscale unsaturated downdrafts are maximized at those locations (Johnson and Hamilton, 1988).

It was discovered that the strongest mesohigh and wake low were observed with the northern portion of the MCS. This portion had the large stratiform rain region, and it appears that the stratiform rain region played an important role in producing these features.

This study revealed that a stronger mesohigh was observed over the northern rain area compared to the southern squall line. The proportion of hydrostatic to non-hydrostatic effects of the pressure rise between the two segments of the MCS are in question. Hydrostatic computations of the surface pressure rise in the northern segment of the MCS showed that a large part of the mesohigh was due to cooling within the downdraft. Figure 5.10 showed that the duration of the mesohigh was longer on the northern segment, but the increase in pressure at the leading edge was much more abrupt in the southern segment. If the rainfall rates were much greater in the southern segment, why then was a cold pool and larger mesohigh not produced there? It is felt that saturated downdrafts

within the stratiform rain area produced the necessary widespread cooling to create a broad mesohigh. In the southern segment, where peak pressures observed were lower, and the rain was of a shorter duration, non-hydrostatic effects may have dominated the pressure rises. For example, 1 to 2 mb rises could be expected from precipitation loading (Nicholls *et al.*, 1988), which is close to what was observed there (see Fig. 5.10).

We found that a trailing anvil, a rear inflow jet, some midlevel FTR relative flow, midlevel convergence, and a midlevel mesolow were all present in the north and *not* in the south. Also, computations of hydrostatic pressure change due to temperature and height changes in a column showed that the greatest warming and subsequent surface pressure falls should have been observed in the north. Therefore, we feel that a stratiform anvil is fundamental in the production of a surface wake low, however the exact physical processes involved are not fully understood.

Boundary layer modification by MCS1 may have inhibited stronger convective cell development in the northern segment of MCS2. Previous to MCS2's mature phase, a frontal boundary existed along the Oklahoma-Kansas border. North of this front was an air mass modified by MCS1. But south of the front, the air had yet to experience convection that day. The available potential energy here had not been "tapped" for convection yet. The heaviest convection seemed to be in the area which was not modified by MCS1, namely the southern segment. Future work should be carried out to study how the boundary layer modifications in the wake of each MCS affected succeeding MCSs in the 3-4 June 1985 period or other PRE-STORM case periods.

Rotunno *et al.* (1988) modeled squall line circulations with varying combinations of low-level shear and cold pools produced by thunderstorm outflows. They found that the "optimal state" of the squall line is when the deep circulation of the cold pool is effectively countered by the circulation caused by the shear. It was shown that the relative flow in the mid-levels of MCS2 had a large along line component in the southern segment. In the north, the complex mid- to upper-tropospheric flow developed a stratiform rain area which created a large cold pool. This large cold pool coupled with a complex shear pattern may have inhibited strong convective updraft formation here. In the south, the squall line

only lasted a few hours. The absence of a cold pool here probably led to the collapse of this convection.

Further radar analysis should reveal more complexities about the structure of this MCS. Dual-Doppler analyses at different times throughout the storm history could detail the storm structure before and after the mature phase. The structure of the decaying stratiform anvil could be studied to see how long the rear inflow circulation persists, since the wake low is still observed and remains strong during dissipation.

REFERENCES

- Augustine, J. A., and K. W. Howard, 1988: Mesoscale convective complexes over the United States during 1985. *Mon. Wea. Rev.*, **116**, 685-701.
- Barnes, S. L., 1964: A technique for maximizing details in numerical weather map analysis. *J. Appl. Meteor.*, **3**, 396-409.
- Blanchard, D. O., and A. I. Watson, 1986: Modes of mesoscale convection observed during the PRE-STORM program. *Preprints, 23rd Conf. on Radar Meteor.*, Snowmass, Colorado, Amer. Meteor. Soc., J115-J118.
- Brown, J. M., 1979: Mesoscale unsaturated downdrafts driven by rainfall evaporation: A numerical study. *J. Atmos. Sci.*, **36**, 313-338.
- Brunk, I. W., 1949: The pressure pulsation of 11 April 1944. *J. Meteor.*, **6**, 181-187.
- Byers, H. R., and R. R. Braham, 1949: The thunderstorm. U. S. Weather Bureau, Washington, D. C., 287 pp.
- Chapman, S., and R. S. Lindzen, 1970: *Atmospheric Tides*. Riedel, Dordrecht, Netherlands.
- Cunning, J. B., 1986: The Oklahoma-Kansas Preliminary Regional Experiment for STORM-Central. *Bull. Amer. Meteor. Soc.*, **67**, 1478-1486.
- Cunning, J. B., and M. DeMaria, 1986: An investigation of the development of cumulonimbus systems over South Florida. Part I: Boundary Layer Interactions. *Mon. Wea. Rev.*, **114**, 5-24.
- Fankhauser, J. C., 1974: The derivation of consistent wind fields of wind and geopotential height from mesoscale rawinsonde data. *J. Appl. Meteor.*, **13**, 637-646.
- Fortune, M. A., and R. L. McAnelly, 1986: The evolution of two mesoscale convective complexes with different patterns of convective organization. *Preprints, 23rd Conf. on Radar Meteor.*, Snowmass, Colorado, Amer. Meteor. Soc., J175-J178.

- Fritsch, J. M., and C. G. Chappell, 1980: Numerical prediction of convectively driven mesoscale pressure systems. Part II: Mesoscale model. *J. Atmos. Sci.*, **37**, 1734-1762.
- Fujita, T. T., 1955: Results of detailed synoptic studies of squall lines. *Tellus*, **7**, 405-436.
- Fujita, T. T., 1959: Precipitation and cold air production in mesoscale thunderstorm systems. *J. Meteor.*, **16**, 454-466.
- Fujita, T. T., 1963: Analytical Mesometeorology. A review. *Met. Monogr.*, **5**, 77-125.
- Fujita, T. T., 1981: Tornadoes and downbursts in the context of generalized planetary scales. *J. Atmos. Sci.*, **38**, 1511-1534.
- Gamache, J. F., and R. A. Houze, 1982: Mesoscale air motions associated with a tropical squall line. *Mon. Wea. Rev.*, **110**, 118-135.
- Garratt, J. R., and W. L. Physick, 1983: Low-level wind response to mesoscale pressure systems. *Bound.-Layer Meteor.*, **27**, 69-87.
- Hamilton, P. J., and R. H. Johnson, 1987: Observations of a midlatitude squall line boundary layer wake. Atmospheric Science Paper No. 414, Colorado State University, Dept. of Atmos. Sci., Fort Collins, Colorado, 93 pp.
- Hoskins, B. J., I. Draghici, and H. C. Davies, 1978: A new look at the ω -equation. *Quart. J. Roy. Meteor. Soc.*, **104**, 31-38.
- Hoxit, L. R., C. F. Chappell, and J. M. Fritsch, 1976: Formation of mesolows or pressure troughs in advance of cumulonimbus clouds. *Mon. Wea. Rev.*, **104**, 1419-1428.
- Johnson, B. C., 1983: The heat burst of 29 May 1976. *Mon. Wea. Rev.*, **111**, 1776-1792.
- Johnson, R. H., and W. A. Gallus, 1988: The wake structure of an intense midlatitude squall line in OK PRE-STORM. *Preprints, 15th Conf. on Severe Local Storms*, Baltimore, Maryland, Amer. Meteor. Soc., 229-232.
- Johnson, R. H., and P. J. Hamilton, 1988: The relationship of surface pressure features to the precipitation and air flow structure of an intense midlatitude squall line. *Mon. Wea. Rev.*, **116**, 1444-1472.

- Johnson, R. H., and M. E. Nicholls, 1983: A composite analysis of the boundary layer accompanying a tropical squall line. *Mon. Wea. Rev.*, **111**, 308-319.
- Johnson, R. H., and J. J. Toth, 1986: Preliminary data quality analysis for May-June 1985 Oklahoma-Kansas PRE-STORM PAM II mesonetwork. Atmospheric Science Paper No. 407, Colorado State University, Dept. of Atmos. Sci., Fort Collins, Colorado, 41 pp.
- Johnson, R. H., J. J. Toth, and S. Chen, 1988: Circulations associated with a mature-to-decaying midlatitude mesoscale convective system. Part I: Surface features—heat bursts and mesolow development. *Mon. Wea. Rev.*, (in press).
- Koch, S. E., and J. McCarthy, 1982: The evolution of an Oklahoma dryline. Part II: Boundary-layer forcing of mesoconvective systems. *J. Atmos. Sci.*, **39**, 237-257.
- Leary, C. A., and R. A. Houze, 1979: Melting and evaporation of hydrometeors in precipitation from the anvil clouds of deep tropical convection. *J. Atmos. Sci.*, **36**, 669-679.
- Leary, C. A., and E. N. Rappaport, 1987: The life cycle and internal structure of a mesoscale convective complex. *Mon. Wea. Rev.*, **115**, 1503-1527.
- Maddox, R. A., 1980: Mesoscale convective complexes. *Bull. Amer. Meteor. Soc.*, **61**, 1374-1387.
- Meitin, J. G., and J. B. Cuning, 1985: The Oklahoma-Kansas preliminary regional experiment for STORM-Central (OK PRE-STORM), Volume I. Daily operations summary. NOAA Tech. Memo. ERL ESG-20, Dept. of Commerce, Weather Research Program, Boulder, Colorado, 313 pp.
- Meitin, J. G., and A. I. Watson, 1986: The mesoscale convective complex of 3-4 June 1985, Part I: Kinematic structure and precipitation characteristics. *Preprints, 3rd Conf. on Mesoscale Processes*, Vancouver, Canada, Amer. Meteor. Soc., p. 33.
- Miller, M. J., and A. K. Betts, 1977: Traveling convective systems over Venezuela. *Mon. Wea. Rev.*, **105**, 883-848.

- NCAR (National Center for Atmospheric Research), 1984: The national STORM program; STORM-Central phase, preliminary program design. Boulder, Colorado, 247 pp.
- Newton, C. W., 1966: Circulations in large sheared cumulonimbus. *Tellus*, **4**, 699-712.
- Newton, C. W., and J. C. Fankhauser, 1964: On the movements of convective storms, with emphasis on size distribution in relation to water-budget requirements. *J. Appl. Meteor.*, **3**, 651-668.
- Nicholls, M. E., R. H. Johnson, and W. R. Cotton, 1988: The sensitivity of two-dimensional simulations of tropical squall lines to environmental profiles. *J. Atmos. Sci.*, (in press).
- O'Brien, J. J., 1970: Alternative solutions to the classical vertical velocity problem. *J. Appl. Meteor.*, **9**, 197-203.
- Ogura, Y., and M.-T. Liou, 1980: The structure of a midlatitude squall line: A case study. *J. Atmos. Sci.*, **37**, 553-567.
- Pedgley, D. E., 1962: A meso-synoptic analysis of the thunderstorms on 28 August 1958. Brit. Meteor. Off., Geophys. Mem., No. 106, 74 pp.
- Pruppacher, H. R., and J. D. Klett, 1978: *Microphysics of clouds and precipitation*. D. Reidel Publ. Co., Dordrecht-Boston-London, 714 pp.
- Rotunno, R., J. B. Klemp, and M. L. Weisman, 1988: A theory for strong, long-lived squall lines. *J. Atmos. Sci.*, **45**, 463-485.
- Rutledge, S. A., and R. A. Houze, 1987: A diagnostic study of the trailing stratiform region of a midlatitude squall line. *J. Atmos. Sci.*, **44**, 2640-2656.
- Rutledge, S. A., R. A. Houze, M. I. Biggerstaff, and T. Matejka, 1988: The Oklahoma-Kansas mesoscale convective system of 10-11 June 1985: Precipitation structure and single-Doppler radar analysis. *Mon. Wea. Rev.*, **116**, 1409-1430.
- Sangster, W. E., 1987: An improved technique for computing the horizontal pressure-gradient force at the earth's surface. *Mon. Wea. Rev.*, **115**, 1358-1369.
- Schaefer, J. T., L. R. Hoxit, and C. F. Chappell, 1985: Thunderstorms and their mesoscale environment. In *Thunderstorm Morphology and Dynamics* (Edwin Kessler, Ed.), 113-130.

- Smull, B. F., and R. A. Houze, 1985: A midlatitude squall line with a trailing region of stratiform rain: Radar and satellite observations. *Mon. Wea. Rev.*, **113**, 117-133.
- Smull, B. F., and R. A. Houze, 1986: The rear inflow jet in mesoscale convective systems. *Preprints, 23rd Conf. on Radar Meteorology*, Snowmass, Colorado, Amer. Meteor. Soc., J163-J166.
- Smull, B. F., and R. A. Houze, 1987: Dual-Doppler radar analysis of a midlatitude squall line with a trailing region of stratiform rain. *J. Atmos. Sci.*, **44**, 2128-2148.
- Smull, B. F., and R. A. Houze, 1987: Rear inflow in squall lines with trailing stratiform precipitation. *Mon. Wea. Rev.*, **115**, 2869-2889.
- Smull, B. F., and D. P. Jorgensen, 1986: The mesoscale convective complex of 3-4 June 1985, Part II: Internal structure shown by dual-Doppler radar. *Preprints, 3rd Conf. on Mesoscale Processes*, Vancouver, Canada, Amer. Meteor. Soc., p. 34.
- Srivastava, R. C., T. J. Matejka, and T. J. Lorello, 1986: Doppler radar study of the trailing anvil region associated with a squall line. *J. Atmos. Sci.*, **43**, 356-377.
- Stumpf, G. J., and W. A. Gallus, 1989: An examination of new convective development with a PRE-STORM squall line case. *Preprints, 24th Conf. on Radar Meteorology*, Tallahassee, Florida, Amer. Meteor. Soc., (in press).
- Stumpf, G. J., and R. H. Johnson, 1988: Lower tropospheric profiling needs in relation to the initiation of mesoscale convective systems. *Symposium on Lower Tropospheric Profiling: Needs and Technologies*, Boulder, Colorado, Amer. Meteor. Soc., 29-30.
- Szeto, K. K., R. E. Stewart, and C. A. Lin, 1988: Mesoscale circulations forced by melting snow. Part II: Application to meteorological features. *J. Atmos. Sci.*, **45**, 1642-1650.
- Tepper, M., 1950: A proposed mechanism of squall lines: The pressure jump line. *J. Meteor.*, **7**, 21-29.
- Trenberth, K. E., 1978: On the interpretation of the diagnostic quasi-geostrophic omega equation. *Mon. Wea. Rev.*, **106**, 131-137.
- Uccellini, L. W., and D. R. Johnson, 1979: The coupling of upper and lower tropospheric jet streaks and implications for the development of severe convective storms. *Mon. Wea. Rev.*, **107**, 682-703.

- Vonder Haar, T. H., C. F. Shih, D. L. Randel, J. J. Toth, D. N. Allen, R. A. Pielke, and R. Green, 1987: The prototype digital weather laboratory at Colorado State University. *Bull. Amer. Meteor. Soc.*, **68**, 230-236.
- Wakimoto, R. M., 1982: The life cycle of thunderstorm gust fronts as viewed with Doppler radar and rawinsonde data. *Mon. Wea. Rev.*, **110**, 1060-1082.
- Williams, D. T., 1948: A surface micro-study of squall-line thunderstorms. *Mon. Wea. Rev.*, **76**, 239-246.
- Williams, D. T., 1953: Pressure wave observations in the central Midwest, 1952. *Mon. Wea. Rev.*, **81**, 278-298.
- Williams, D. T., 1954: A surface study of a depression-type pressure wave. *Mon. Wea. Rev.*, **82**, 289-295.
- Williams, D. T., 1963: The thunderstorm wake of May 4, 1961. Nat. Severe Storms Project Rep. No. 18, U. S. Dept. of Commerce, Washington D. C., 23 pp. [NTIS PB 168223].
- Zipser, E. J., 1977: Mesoscale and convective-scale downdrafts as distinct components of squall-line structure. *Mon. Wea. Rev.*, **105**, 1568-1589.

APPENDIX A

Removal of the atmospheric tide from pressure data

Diurnal variations of heating due to absorption of solar ultraviolet radiation by water vapor and ozone in the upper atmosphere give rise to daily oscillations of temperature called the atmospheric tide. These stratospheric temperature changes force waves which propagate to the ground and show up as surface pressure fluctuations. The tide is composed of two main wave numbers, the diurnal and semidiurnal components. The diurnal component has a 24-hour period, and the semidiurnal component has a 12-hour period with a larger (1 mb) and more regular oscillation than the diurnal part. For a discussion of the atmospheric tidal theory in greater detail, see Chapman and Lindzen (1970).

To determine the variation of tidal oscillation of surface pressure, data from selected PAM stations (P04, P17, P20, P24, and P36) were averaged for each 5-minute interval over the entire PRE-STORM data collection period (1 May to 27 June 1985). Deviations from the mean surface pressure for each of the five stations were calculated at each 5 minute interval and plotted on pressure vs. time-of-day curves. Next, the data on these curves were averaged for the five stations, and the final curve was smoothed. This curve is shown in Fig. A.1. One can see that the curve has a diurnal as well as a semidiurnal oscillation with maxima at 0510 GMT (0.26 mb) and 1450 GMT (1.04 mb). Minima are at 0845 GMT (-0.23 mb) and 2345 GMT (-1.28 mb). The values along this twenty-four hour curve are removed from the surface pressure data so that the pressure changes shown in the analyses are purely meteorological.

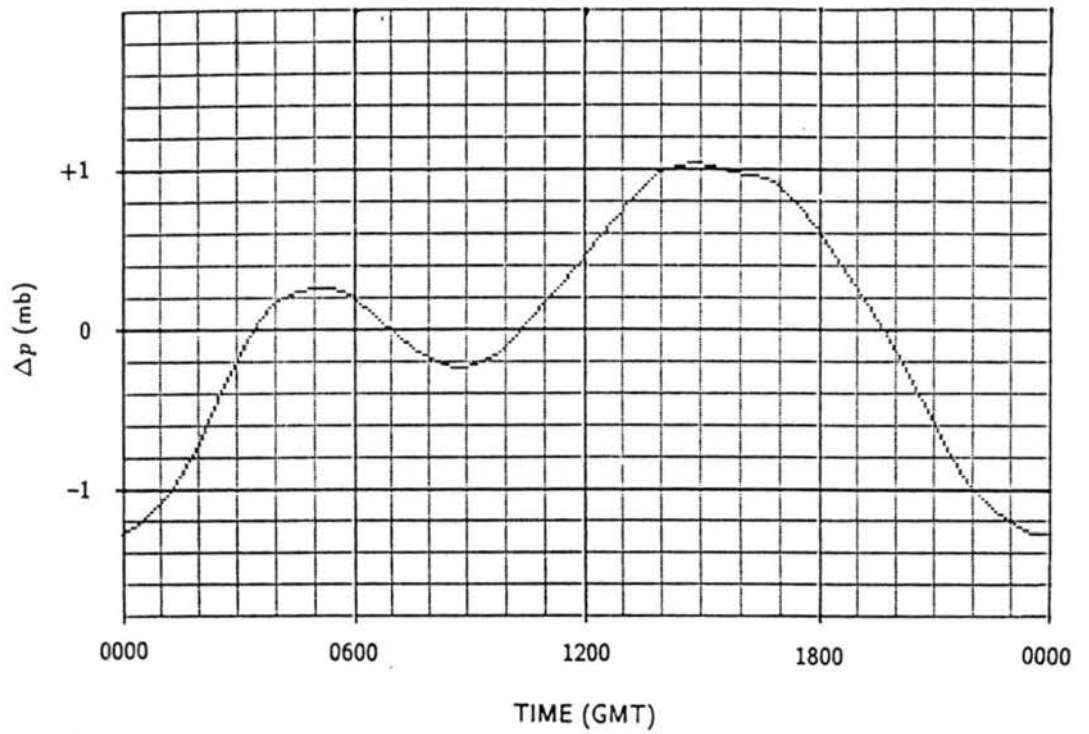


Figure A.1: The diurnal tide curve. Units are in mb. Time is GMT. Values shown on the curve were subtracted from the pressure data as a function of time.

APPENDIX B

Removal of instrument bias from the pressure data

Analyses of surface pressure fields with mesoscale phenomena require nearly precise readings of pressure. Calibration checks into the PAM data revealed that errors existed with some of the pressure instrumentation. Also, these errors sometimes drifted in time throughout the experiment. Johnson and Toth (1986) carried out an extensive data quality check of the PAM mesonet network and developed a set of pressure corrections for the PAMs based on sensor calibration records and smooth subjective analyses of mean pressure of the individual stations for 10- and 20-day periods. Pressure corrections were not carried out by Johnson and Toth (1986) for the SAM stations. However, Johnson and Hamilton (1988) did compile a set of corrections to the SAM stations which involved an intercomparison of the mesonet network data with NWS data for an undisturbed period prior to the squall line case on 10-11 June 1985. These sets of corrections for the PAM and SAM were used in the initial analyses of surface pressure for the case studied in this paper, but were found somewhat inaccurate for 3-4 June.

Instead, a method was chosen which emphasized the intercomparison of PAM and SAM data with NWS data for a few undisturbed periods prior to the case study period. The undisturbed period used occurred a couple of days prior to the passage of the MCSs on 3-4 June 1985, namely 2100 GMT 31 May, 0000 GMT 1 June, and 0100 GMT 1 June, 1985. Pressure across the mesonet network varied only by about 2.5 mb and no major convective systems were affecting the area at those times. Intercomparisons were made for these three periods of mesonet network data to the surrounding NWS stations (NWS data were considered to be of higher quality because daily calibrations of NWS pressure sensors were maintained). Hydrostatically adjusted NWS pressure data [to 480 m; see Eq. (3.1)] were objectively analyzed on a one-half degree latitude/longitude grid using a method similar to Barnes (1964) for each of the three times. Next, a "reverse" objective analysis

scheme was used to determine the pressure values to be expected at the location of each of the PAM and SAM stations on each of the three grids. Finally, these values were then compared to the actual values recorded by the mesonet network instrumentation (adjusted to 480 m), and the differences were tabulated. For each station, the correction values were averaged over the three times to result in an initial set of pressure corrections for each of the 84 stations. Next, mesonet network pressures (adjusted to 480 m) were averaged for a 33 hour period (1100 GMT 3 June to 1900 GMT 4 June 1985) for each station and subjectively analyzed with the initial set of corrections applied (see Fig. B.1). This initial pressure field was not very smooth (some biases still existed with some of the stations). This initial field was then subjectively smoothed, aided by sensor calibration records, Johnson and Toth's (1986) PAM corrections, and Johnson and Hamilton's (1988) SAM corrections. This smoothed pressure field is shown in Fig. B.2. Finally, the smoothed pressure field was compared station by station to the initial non-smoothed field and those additional corrections were added to the initial corrections calculated using NWS intercomparisons. The final list of pressure corrections, considered valid for the 3-4 June 1985 period only, are listed in Table B.1¹.

As a result of the pressure corrections described above and analysis of time-series traces of pressure for the mesonet network stations, the SAM pressure data appear to be of a less superior quality than the PAM data. Numerous data gaps were found in the SAM data, and no SAM calibration records were available.

An example of the difference in data quality can perhaps be best illustrated by comparing the pressure time-series plots for two of the collocated mesonet network stations, P41 and S38 (Fig. B.3). Note the SAM trace is more erratic, and it appears that the sensor "got stuck" several times which resulted in flat traces between gaps.

¹This final set of corrections is felt to be acceptable for the 3-4 June 1985 period, and should not be used for other study periods in PRE-STORM. The method described above, however, is highly recommended for other study periods in PRE-STORM, given that an undisturbed period exists within a few days of the study period.

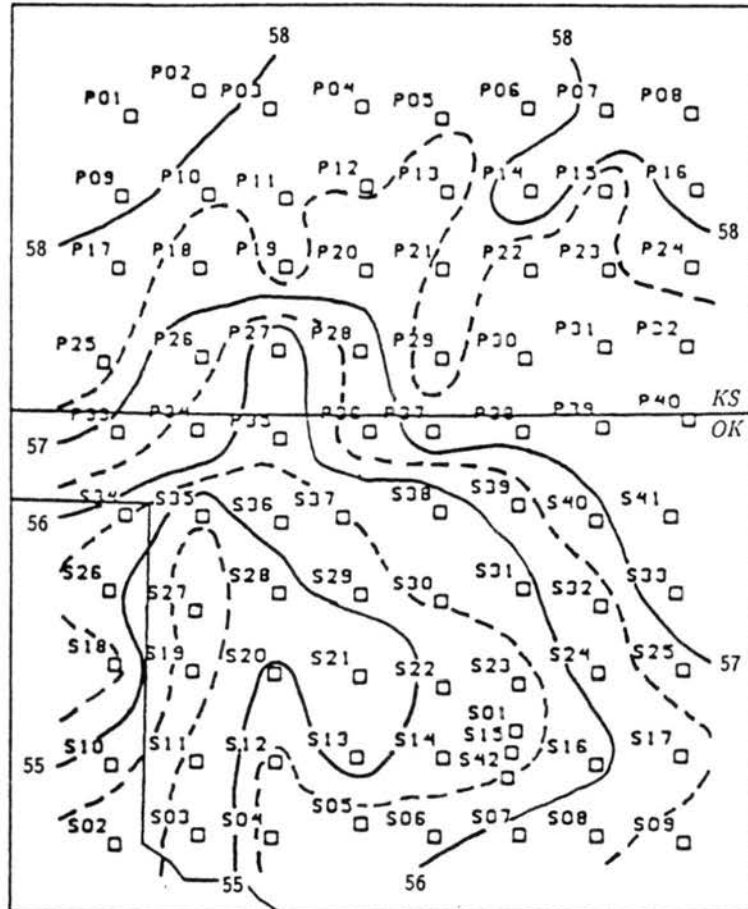


Figure B.1: Non-smoothed analysis of average pressure (e.g., 59 = 959 mb) with first corrections.

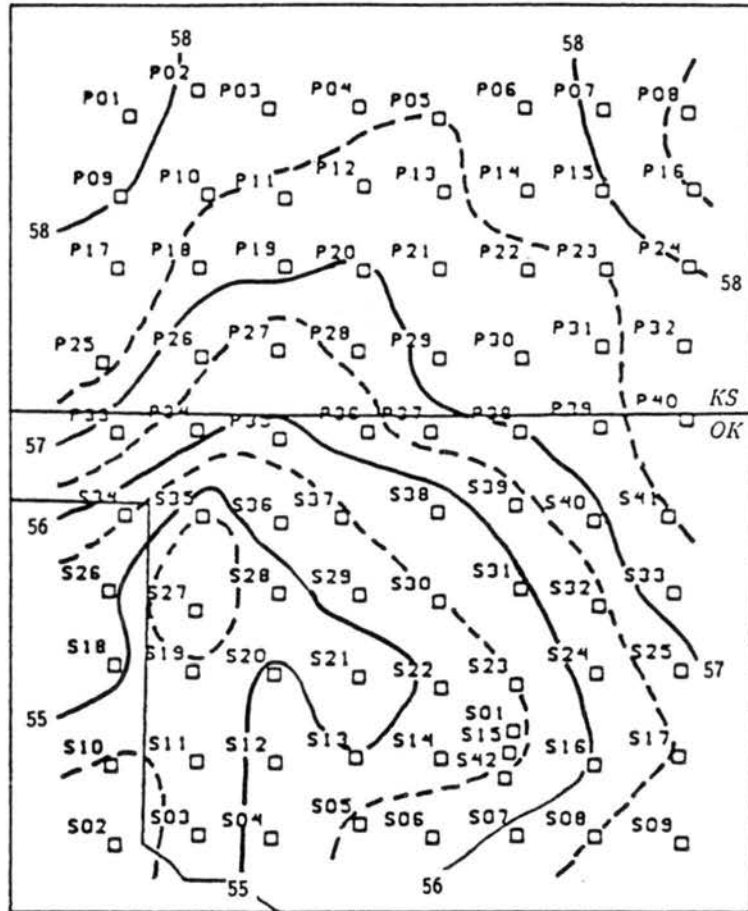


Figure B.2: Smoothed analysis of average pressure in mb (e.g., 59 = 959 mb) with final corrections.

Table B.1: PAM AND SAM PRESSURE CORRECTIONS.

Station	Adjustment (mb)	Station	Adjustment (mb)
P01	1.17	S01	-0.23
P02	1.06	S02	0.71
P03	-0.38	S03	2.02
P04	-1.14	S04	1.87
P05	-0.35	S05	0.70
P06	-0.55	S06	1.14
P07	0.43	S07	0.11
P08	-0.59	S08	0.24
P09	0.09	S09	-0.19
P10	-0.26	S10	M
P11	0.03	S11	M
P12	1.31	S12	1.92
P13	0.64	S13	1.26
P14	-2.53	S14	M
P15	1.03	S15	0.03
P16	0.05	S16	-0.60
P17	-0.16	S17	-0.57
P18	0.03	S18	0.33
P19	0.41	S19	M
P20	-0.16	S20	0.97
P21	0.53	S21	-1.08
P22	-0.71	S22	0.41
P23	0.08	S23	0.06
P24	-1.09	S24	M
P25	0.75	S25	0.17
P26	0.14	S26	0.99
P27	-0.17	S27	0.18
S28	-1.09	S28	0.50
P29	1.80	S29	0.87
P30	0.80	S30	-0.29
P31	1.27	S31	0.84
P32	-1.94	S32	0.08
P33	0.30	S33	-0.18
P34	0.49	S34	0.80
P35	0.05	S35	0.58
P36	0.29	S36	0.57
P37	0.80	S37	0.76
P38	0.23	S38	1.57
P39	2.11	S39	0.81
P40	0.54	S40	1.02
P41	-0.70	S41	E 2.30
P42	-0.09	S42	-0.37

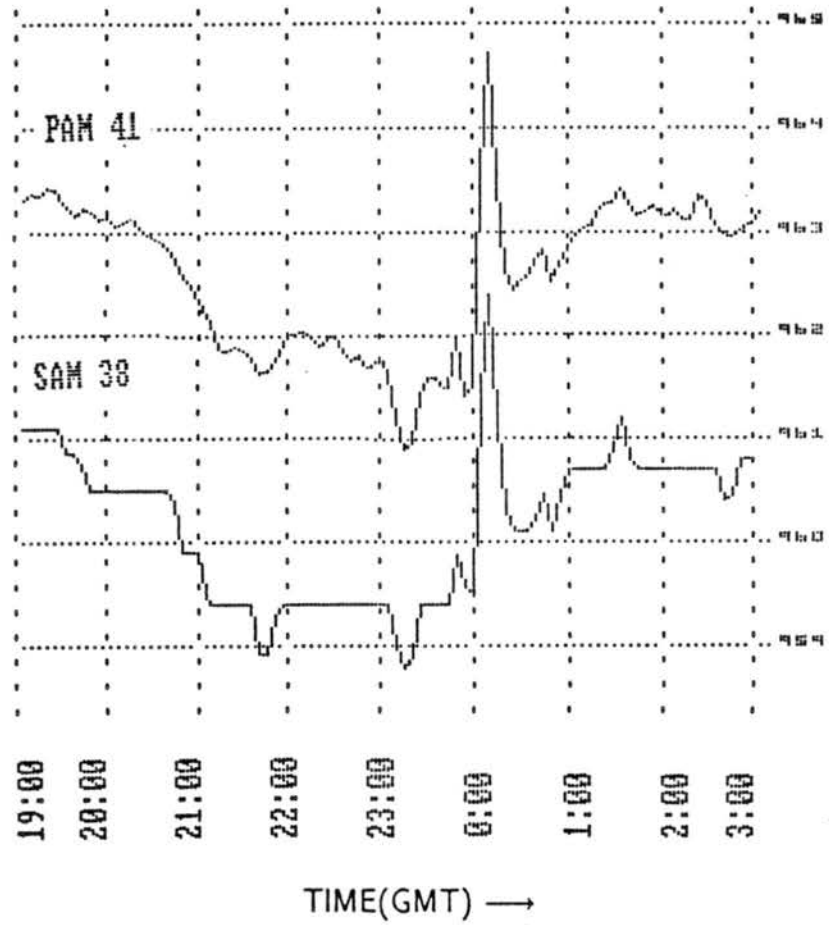


Figure B.3: Surface pressure traces at P41 and S38. Units are in mb. Time increases to the right and is GMT. No adjustments were made to remove tidal oscillation or instrument bias.

APPENDIX C

The heat burst at station P19

Figure C.1 depicts the meteorological conditions associated with the minor heat burst (Johnson, 1983) observed at station P19 at 0020 GMT 4 June. In a roughly 30-minute period, the temperature rose and then fell about 1.4°C. Correspondingly, the dewpoint fell and then rose about 0.6°C. The heat burst occurred about 20 minutes following the rapid pressure drop from the mesohigh to the wake low. During the heat burst, the pressure was fluctuating by about 1 mb, and the winds experienced a minimum. The heat burst occurred in the wake region of the MCS immediately following the cessation of the stratiform rain at P19.

The heat burst observed in Fig. C.1 had a smaller magnitude than those observed by Johnson (1983) and Johnson *et al.* (1988), however, its duration does compare with some of the heat bursts found by Johnson *et al.* (1988). Fig. C.2 shows the sounding taken at PTT at 0000 GMT, which was very near station P19. A low-level inversion is evident with a shallow mixed layer above it. Above 800 mb, the air is close to saturation and is probably the base of the anvil cloud. This sounding somewhat resembles the "onion" sounding (Zipser, 1977) but with a shallower and less dry mixed layer².

Johnson (1983) hypothesizes that the heat burst mechanism is similar to the mechanism which produces microbursts. Heat bursts develop as the trailing anvil introduces precipitation aloft which evaporates in the subsaturated environment below the anvil. The cool air parcel which develops upon evaporation becomes negatively buoyant and accelerates downward. In a typical microburst, a low-level inversion does not exist, and the cool parcel impacts on the ground resulting in surface cooling and a localized pressure

²Later at 0130 GMT (figure not shown), the mixed layer grew to 600 mb and the air became much warmer and drier within it.

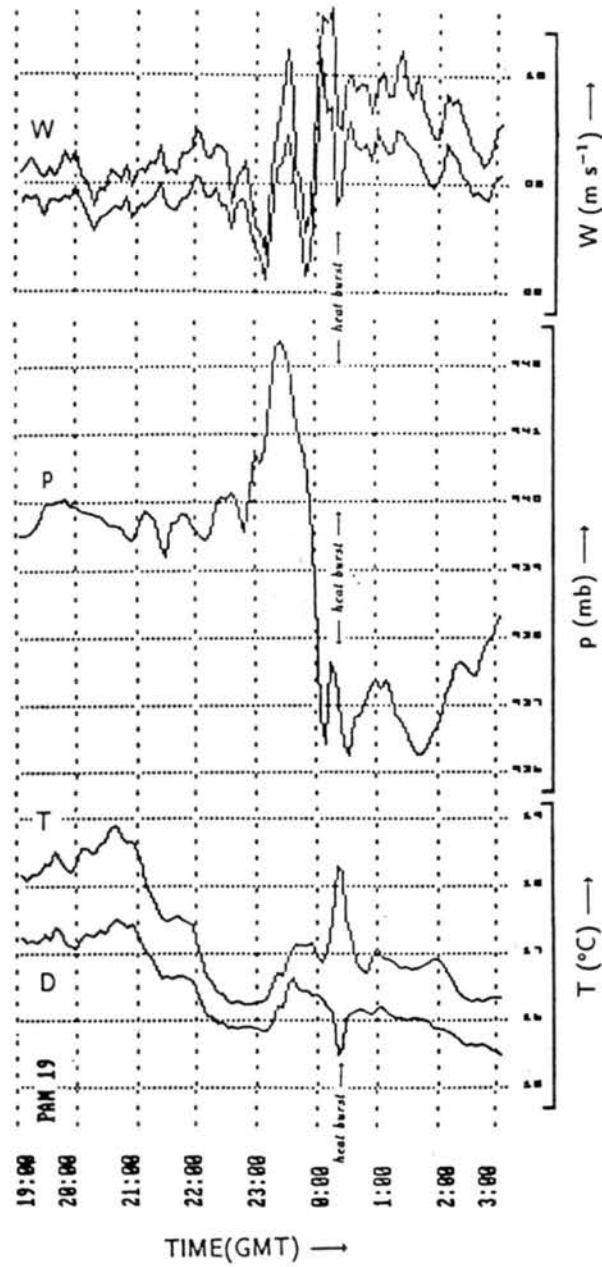


Figure C.1: Time series plots of temperature (T), dewpoint (D), station pressure (p), and wind speed and gust (W) during heat burst at station P19. Time increases to the right and is GMT. Temperature is °C, pressure is mb, and wind is m s⁻¹.

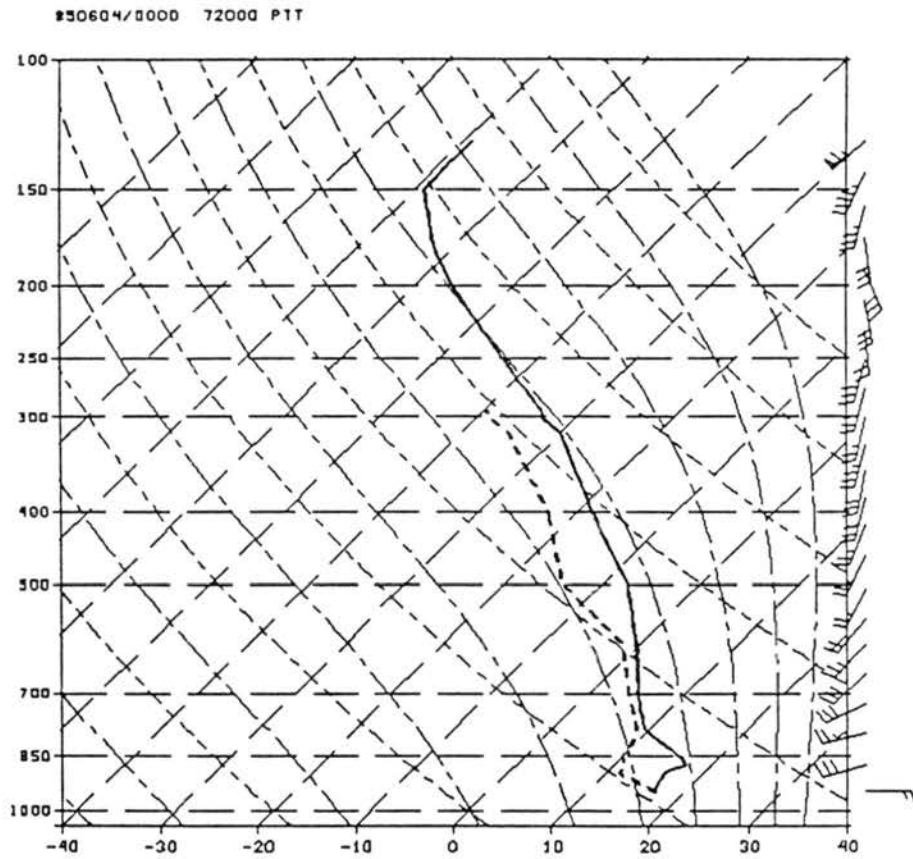


Figure C.2: Same as 6.4 except at 0000 GMT 4 June 1985 for Pratt KS (PTT).

rise. However, in the presence of a strong low-level inversion, the downdraft must penetrate the stable layer to reach the ground. Typically, the downdraft will lose its buoyancy upon penetration of the surface layer, and generally will not reach the surface. Instead, they can deform the top of the mixed layer (Zipser, 1977, Johnson *et al.*, 1988). If the downdraft has enough momentum and/or the surface inversion is not strong enough, then these microbursts can reach the surface in the form of a heat burst (Johnson *et al.*, 1988). The downdraft parcel, originally cooler than the environment in the mixed layer, is now warmer and drier than the stable layer. Figure C.3, adapted from Johnson *et al.* (1988) shows a schematic of a penetrating and non-penetrating heat burst. In the heat burst case observed at P19, the magnitude of the temperature and dewpoint changes were much less than observed by Johnson and Hamilton (1988) suggesting that the downdraft did not significantly warm adiabatically upon descent.

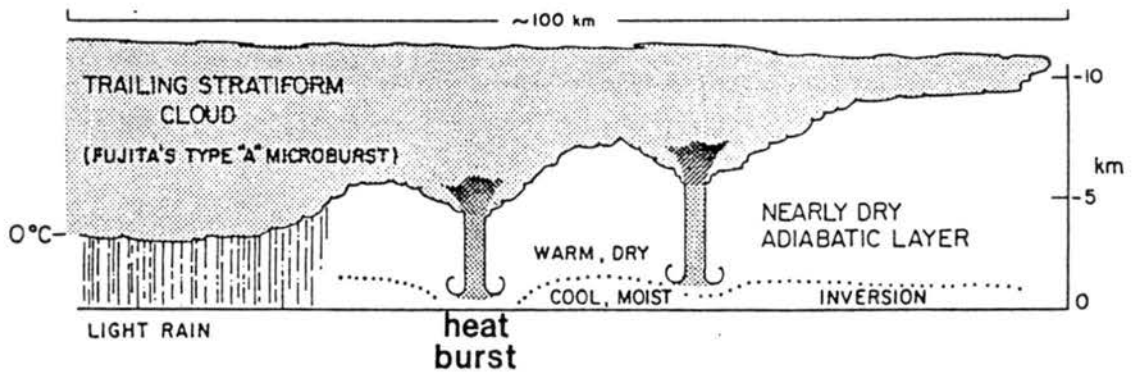


Figure C.3: Schematic of heat burst mechanism (after Johnson *et al.*, 1988).